Nitrous oxide and hydroxylamine in the eastern tropical Atlantic and Pacific Oceans

Dissertation zur Erlangung des Doktorgrades

der mathematisch-naturwissenschaftlichen Fakultät der

Christian-Albrechts-Universität zu Kiel

vorgelegt von Annette Kock

Kiel, im Dezember 2011

Referent/in: Dr. Hermann W. Bange

Koreferent/in: Prof. Dr. Arne Körtzinger

Tag der mündlichen Prüfung: 27.01.2012

Zum Druck genehmigt: 27.01.2012

gez. Prof. Dr. rer. nat. Lutz Kipp

Dekan

Eidesstattliche Erklärung

Ich versichere an Eides statt, dass ich die von mir vorgelegte Dissertation – abgesehen von der Beratung durch meine Betreuer – selbstständig und ohne unerlaubte Hilfe angefertigt und alle benutzten Quellen und Hilfsmittel vollständig angegeben habe. Ich erkläre, dass die vorliegende Arbeit gemäß der Grundsätze zur Sicherung guter wissenschaftlicher Praxis der Deutschen Forschungsgemeinschaft erstellt wurde.

Ich versichere ferner, dass weder diese noch eine ähnliche Arbeit zur Erlangung eines Doktorgrades bereits an anderer Stelle eingereicht worden ist.

Kiel, den 2. Dezember 2011 _____

(Annette Kock)

parvis imbutus tentabis grandia tutus

This thesis is based on the following manuscripts:

Kock, A., Freing, A., Bange, H. W., Nitrous oxide distribution in the eastern tropical Atlantic and Pacific Oceans (ms in preparation for Marine Chemistry).

Author Contribution: Annette Kock took most of the samples, measured and analyzed most of the depth profiles and wrote the manuscript. Alina Freing and Hermann Bange sampled, measured and analyzed part of the data, and Hermann Bange reviewed the manuscript.

Kock, A., Schafstall, J., Dengler, M., Brandt, P., and Bange, H. W.: Sea-to-air and diapycnal nitrous oxide fluxes in the eastern tropical North Atlantic Ocean, Biogeosciences Discuss., 8, 10229-10246, 10.5194/bgd-8-10229-2011, 2011.

Author Contribution: Annette Kock took the samples and measured most of the N_2O depth profiles, calculated the N_2O concentrations and the sea-to-air fluxes of N_2O and wrote the paper. J. Schafstall and M. Dengler measured the microstructure profiles and calculated the diapycnal N_2O fluxes. Peter Brandt and Hermann Bange assisted with inputs to the manuscript and its revisions.

Löscher, C. R., **Kock, A.**, Könneke, M., LaRoche, J., Bange, H. W., Schmitz, R. A., Production of oceanic nitrous oxide by ammonia-oxidizing archaea, 2011(ms submitted to Biogeosciences).

Author Contribution: Annette Kock took the N_2O samples and measured N_2O depth profiles, calculated the N_2O concentrations and ΔN_2O values. Carolin Löscher took and analyzed DNA samples, designed and performed the culture and incubation experiments, analyzed the data and wrote the paper. Hermann Bange, Julie LaRoche and Ruth Schmitz-Streit assisted with inputs to the manuscript and its revisions.

Ryabenko, E., **Kock, A.**, Bange, H. W., Altabet, M. A., and Wallace, D. W. R.: Contrasting biogeochemistry of nitrogen in the Atlantic and Pacific oxygen minimum zones, Biogeosciences Discuss., 8, 8001-8039, 10.5194/bgd-8-8001-2011, 2011.

Author Contribution: Annette Kock took the N_2O samples and measured and calculated the N_2O concentrations and ΔN_2O values. Evgeniya Ryabenko sampled and measured δ^{15}N-Nitrate and Nitrite profiles, did the analysis and wrote the paper. Douglas Wallace, Mark Altabet and Hermann Bange assisted with the writing of the manuscript and its revision.

Kock A. and Bange H., An improved method for measurements of dissolved hydroxylamine in seawater, (ms in preparation for Limnology and Oceanography - Methods).

Author Contribution: Annette Kock did the field sampling, designed and performed the experiments, analyzed the data and wrote the manuscript. Hermann Bange assisted with inputs to the experimental design and reviewed the manuscript.

Table of Contents

Summary

Our view on the oceanic nitrogen cycle has recently been challenged by a number of findings such as the central role of archaea during nitrification and the detection of anaearobic ammonium oxidation (anammox) and euphotic zone nitrification, which also affect our understanding of N_2O production pathways in the ocean. This thesis compiles different studies that help to identify where, how and by whom N_2O is produced in the ocean.

A mixed layer budget of N_2O in the Mauritanian upwelling revealed large discrepancies between the sea-to-air flux out of the mixed layer and the N_2O supply from below via diapycnal mixing and vertical advection. To close the discrepancy, N_2O production from nitrification within the mixed layer was suggested earlier in several studies. However, in our study, the biological production would have to be unrealistically high: Calculated potential N_2O production rates in the mixed layer exceed the maximum subsurface N_2O production rates by far. Therefore, other processes, most likely a reduced sea-to-air flux by surfactants, have to be investigated as possible explanation for an unbalance in the mixed layer budget, too.

Due to the different oxygen concentrations in both regions, the comparison of the oxygen minimum zones (OMZs) in the eastern tropical North Atlantic (ETNA) Ocean with minimum oxygen concentrations of >30µmol L^{-1} and the eastern tropical South Pacific (ETSP) Ocean with minimum oxygen concentrations <5 µmol L^{-1} reveals significant differences in the nitrogen cycling of both regions, which is reflected in N_2O concentrations as well as measurements of $\delta^{15}N\text{-}NO_3^-$. Strong signals of N-loss processes are found in the southern part of the South Pacific OMZ, with N_2O depletion and increase in $\delta^{15}N\text{-}NO_3^-$ in the core of the oxygen minimum zone. Both findings are consistent with the activity of canonical denitrification in the centre of the OMZ. A threshold oxygen concentration of 5µmol L^{-1} was found for the onset of N-loss processes throughout the area. Waters with oxygen concentrations >5 µmol L^{-1} did not show signs of active N-loss. A linear correlation of ΔN_2O vs. AOU was found for waters with oxygen concentrations >50 µmol L^{-1} that showed the same slope in the ETNA and ETSP for the upper oxycline, suggesting a nitrification source. Oxygen concentrations far below 50 µmol L^{-1} were found only in the ETSP, and a significant increase in the ΔN_2O/AOU slope was observed for oxygen concentrations between 5 and 50 µmol L^{-1}.

Evidence for N_2O production of archaea is found from field studies as well as from culture experiments: It could be shown in laboratory studies with the cultured ammonium oxidizing archaeon *Nitrosopumilus maritimus* that archaea have the potential for N_2O production. The

dominance of archaeal over bacterial *amoA* gene abundances and their correlation with N_2O concentrations on the one hand and the reduction of N_2O production by addition of a selective inhibitor for archaea in incubation experiments on the other hand give evidence that archaea are the main producers of N_2O in the water column of the tropical ocean. Moreover, it could be shown that similar to N_2O production during bacterial nitrification, N_2O production by *N. maritimus* increased with decreasing oxygen concentrations.

Hydroxylamine is known as an intermediate during bacterial nitrification and could thus be an indicator for sites of active nitrification. However, the role of hydroxylamine during archaeal nitrification is still unknown. In this work it could be shown that measurements of hydroxylamine in seawater using the method by Butler and Gordon (1986a) can significantly be biased by ambient concentrations of nitrite in the samples. This problem can be overcome by the addition of sulfanilamide before the application of the method by Butler and Gordon (1986a). This modified method is a new tool to elucidate the role of hydroxylamine in nitrogen transformations. First applications of the modified method at a coastal time series station and in the water column of the equatorial Atlantic Ocean showed relatively low concentrations of hydroxylamine. While hydroxylamine was below or close to the detection limit in the equatorial Atlantic, at the coastal time series station hydroxylamine was detectable during several months, showing high spatial and temporal variability. No simple correlation with other parameters was found at the coastal site, and additional measurements of hydroxylamine in the water column as well as in incubation experiments are required to understand the dynamics of hydroxylamine production and consumption in the ocean.

Zusammenfassung

Neue Erkenntnisse wie die zentrale Rolle von Archaeen für die Nitrifizierung, die Entdeckung der anaeroben Ammoniumoxidation (anammox) und der Nitrifizierung in der euphotischen Zone haben unser Bild des marinen Stickstoffkreislauf in den letzten Jahren verändert, was auch unser Verständnis der N_2O-Produktion im Ozean verändert. In dieser Dissertation sind mehrere Arbeiten zusammengefasst, die dazu beitragen, zu identifizieren, wo, von wem und auf welche Weise N_2O im Ozean produziert wird:

Eine Berechnung von N_2O-Flüssen für die Deckschicht des Auftriebsgebiets vor Mauretanien zeigte eine große Diskrepanz zwischen dem Gasaustausch-Fluss von N_2O aus dem Ozean in die Atmosphäre und dem Nachschub an N_2O von unterhalb der Deckschicht durch diapyknische Vermischung und vertikale Advektion. N_2O Produktion durch Nitrifizierung innerhalb der Deckschicht wurde in einigen früheren Studien als Möglichkeit vorgeschlagen, diesen Unterschied auszugleichen. Im Mauretanischen Auftrieb müsste diese Produktion jedoch unrealistisch hoch sein: Die berechneten Produktionsraten übersteigen Produktionsraten in der Tiefe bei weitem. Andere Prozesse, darunter vor allem die Reduktion des Gasaustauschs durch Oberflächenfilme, sollten daher als Erklärung für das Missverhältnis der Flüsse untersucht werden.

Bedingt durch die unterschiedlichen Sauerstoffkonzentrationen in beiden Regionen zeigte ein Vergleich der Sauerstoffminimumzonen im tropischen Nordostatlantik (eastern tropical North Atlantic, ETNA), wo Sauerstoffkonzentrationen oberhalb von $30\,\mu mol\,L^{-1}$ liegen, und im tropischen Südostpazifik (eastern tropical South Pacific, ETSP) mit Sauerstoffkonzentrationen bis unterhalb von $5\mu mol\,L^{-1}$ bedeutende Unterschiede im Stickstoffkreislauf beider Regionen, was sowohl N_2O Konzentrationen als auch Messungen von $\delta^{15}N\text{-}NO_3^-$ widerspiegeln. Im südlichen Teil der südpazifischen Sauerstoffminimumzone wurden starke Anzeichen für Stickstoffzehrungsprozesse gefunden, die zum Abbau von N_2O und einem Anstieg der $\delta^{15}N\text{-}NO_3^-$-Werte im Kern der Sauerstoffminimumzone führen. Beide Beobachtungen lassen sich durch aktive kanonische Denitrifizierung in der Sauerstoffminimumzone erklären. Im gesamten Gebiet lag die Obergrenze der Sauerstoffkonzentrationen, bei denen Stickstoffzehrung auftrat, bei $5\mu mol\,L^{-1}$. In Wassermassen mit Sauerstoffkonzentrationen oberhalb von $5\mu mol\,L^{-1}$ konnte keine aktive Stickstoffzehrung beobachtet werden. Eine lineare Korrelation zwischen ΔN_2O und AOU konnte für Sauerstoffkonzentrationen $>50\mu mol\,L^{-1}$ gefunden werden, mit der gleichen Steigung im ETNA und ETSP für die obere Oxykline, was für Nitrifikation als N_2O-Quelle spricht. Ein starker Anstieg der ΔN_2O/ Steigung konnte bei Sauerstoffkonzentrationen zwischen 5 und $50\,\mu mol\,L^{-1}$ festgestellt werden.

N_2O Produktion durch nitrifizierende Archaeen konnte in Feldstudien sowie in Kultur-experimenten gezeigt werden: In Laborexperimenten mit Kulturen des ammoniumoxidierenden Archaeon *Nitrosopumilus maritimus* wurde nachgewiesen, dass N_2O von Archaeen produziert werden kann. Weiterhin zeigen einerseits die Dominanz der Archeen-*amoA* über bakterielle *amoA* und die Korrelation zwischen N_2O und *amoA*-Verteilung und andererseits eine Reduktion der N_2O-Produktion nach Zugabe eines Archaeen-Inhibitors, dass Archaeen wahrscheinlich den größten Anteil der N_2O-Produktion im tropischen Ozean ausmachen. Darüberhinaus konnte gezeigt werden, dass wie bei der N_2O Produktion durch bakterielle Nitrifikation die Ausbeute von N_2O mit abnehmenden Sauerstoffkonzentrationen anstieg.

Hydroxylamin ist ein Zwischenprodukt bakterieller Nitrifikation und kann deshalb als Indikator für aktive Nitrifizierung. Die Rolle Hydroxylamins in der Nitrfizierung durch Archaeen ist jedoch noch unbekannt. In dieser Arbeit konnte gezeigt werden, dass Messungen von Hydroxylamin in Seewasser nach der Methode von Butler und Gordon (1986a) durch die Anwesenheit von natürlichen Konzentrationen von Nitrit gestört werden können, was durch die Zugabe von Sulfanilamid vor der Anwendung des Nachweises von Butler and Gordon (1986a) überwunden werden kann. Diese so modifizierte Methode stellt ein neues Werkzeug dar, um die Rolle von Hydroxylamin in Stickstofftransformationen zu bestimmen. Erste Messungen von Hydroxylamin nach der modifizierten Methode an einer küstennahen Zeitserienstation und im äquatorialen Atlantik zeigten relativ niedrige Hydroxylamin-Konzentrationen. Während Konzentrationen im äquatorialen Atlantik nah am oder unterhalb des Detektionslimits der Messungen lagen, konnte Hydroxylamin in einigen Monaten an der Zeitserienstation gemessen werden. Die Konzentrationen zeigten eine große räumliche und zeitliche Variabilität, und es konnte keine einfache Korrelation mit anderen Parametern identifiziert werden. Um die Zusammenhänge von Produktion und Zehrung von Hydroxylamin im Ozean zu verstehen, braucht es weitere Messungen von Hydroxylamin in der Wassersäule sowie in Inkubationsexperimenten.

1 Introduction

The marine nitrogen cycle as source of nitrous oxide

Although nitrogen (N) is abundant in large amounts as molecular nitrogen (N_2) in the Earth's atmosphere, it is often a limiting factor for biological growth as it cannot be taken up as molecular nitrogen by most organisms. The recycling of fixed nitrogen (i.e. bioavailable inorganic N compounds such as nitrate, NO_3^- and ammonium, NH_4^+) within both the oceanic and terrestrial environment is therefore an essential factor to maintain biological productivity on Earth (Gruber, 2008).

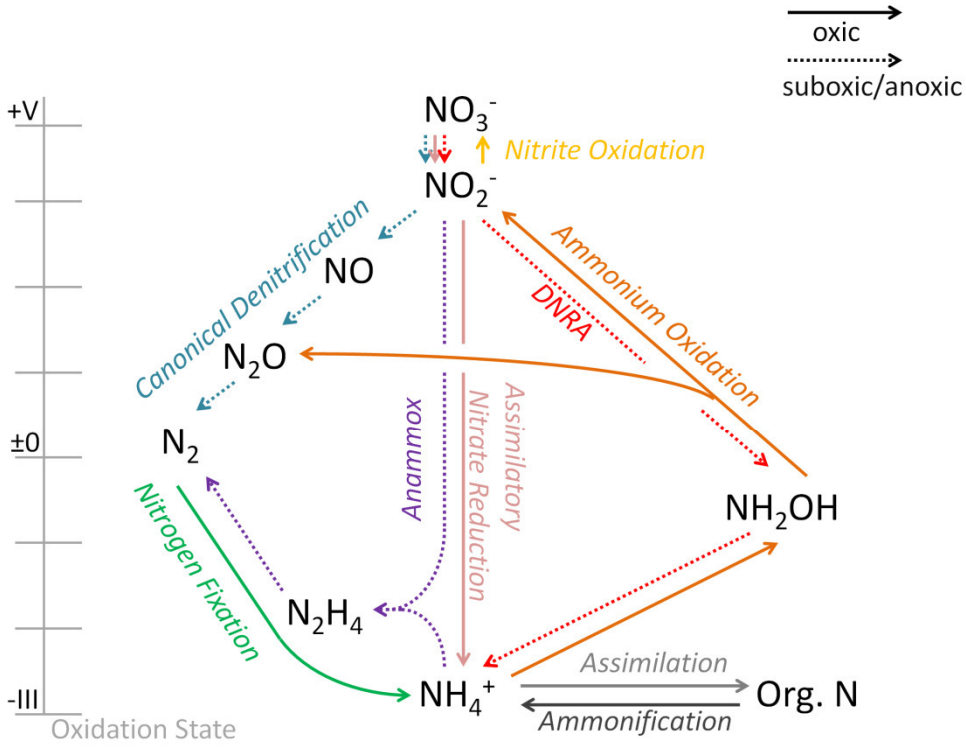

Figure 1: Major redox transformations in the nitrogen cycle. Solid arrows indicate nitrogen transformations taking place under oxic conditions; dashed arrows indicate transformations under suboxic/anoxic conditions. DNRA stands for dissimilatory nitrate reduction to ammonia.

Nitrogenous compounds occur in the ocean in a number of oxidation states, and therefore nitrogen cycling mainly involves redox transformations between nitrogen species with different oxidation states, all of them being microbially mediated (Fig. 1). Transformations within the N cycle serve either the incorporation of nitrogen into organic molecules (assimilatory processes) or the yield of energy (dissimilatory processes).

One major control parameter of the nitrogen transformations within the oceanic N cycle is the prevailing ambient oxygen (O_2) concentration. Under oxic conditions, nitrogen transformations involve the assimilation of inorganic nitrogen by incorporation of ammonium or assimilatory nitrate reduction and the remineralization (nitrification, $NH_4^+ \rightarrow NO_3^-$) of organic nitrogen. Nitrification produces hydroxylamine (NH_2OH) as an intermediate, whereas nitrous oxide (N_2O) evolves as a by-product that accumulates in the subsurface and deep layers of the water column where the exchange of the waters with the overlying atmosphere is restricted (Bange, 2008).

Under anoxic conditions respiration of nitrogen by denitrification and anammox becomes dominant (Canfield et al., 2010). During both processes, fixed nitrogen is respired to N_2, with different pathways for both processes. Canonical denitrification is the reduction of NO_3^- to N_2 (Fig. 1) with N_2O as an intermediate which can be released to the water column from this process (Ferguson, 1994). In the anammox process ammonium and nitrite (NO_2^-) react in a comproportionation reaction to N_2, with hydrazine (N_2H_4) as characteristic intermediate. Significant N_2O production from anammox has not been detected so far (Kartal et al., 2007). The question of the dominance of denitrification or anammox in oceanic environments is subject of ongoing discussion (e.g. Lam et al. (2009), Voss and Montoya (2009), Ward et al. (2009)).

The biogeochemical consequences of both processes are similar, though: denitrification and anammox lead to significant loss of fixed N from oceanic environments (Gruber and Sarmiento, 1997). Nitrogen fixation, along with atmospheric and riverine deposition of fixed nitrogen, compensates the oceanic nitrogen loss, and a regional coupling of nitrogen fixation and nitrogen respiration has been proposed (Deutsch et al., 2007). There is some evidence that the oceanic nitrogen budget is currently not at steady-state, with denitrification outbalancing the supply of fixed nitrogen by nitrification and riverine and atmospheric deposition (Canfield et al., 2010;Codispoti, 2007).

The threshold concentration of oxygen for the transition from the oxic to anoxic N cycling is not well defined, yet. Several studies found a co-occurrence of nitrification and denitrification/ anammox under suboxic conditions (Bange et al., 2005;Farias et al., 2009). Evidence for nitrogen respiration is provided by a substantial nitrogen deficit which has been observed to evolve at oxygen concentrations below 5 µmol L^{-1} (Bange et al., 2005).

The ocean as a source of atmospheric N_2O

Although N_2O plays only a minor role in the nitrogen turnover, its role as a potent greenhouse gas in the Earth's atmosphere (Forster et al., 2007) has driven some attention to nitrous oxide production within the N cycle. Moreover, due to its long lifetime of about 114 years, N_2O is is mixed from the troposphere into the stratosphere where it is involved in the stratospheric ozone depletion cycle (Prather, 1998;Ravishankara et al., 2009). Nitrification and denitrification are the main processes of N_2O production in marine (Suntharalingam and Sarmiento, 2000) as well as terrestrial environments (Bouwman, 1996) (Fig.1), and the large additions of industrially fixed nitrogen to the natural inventory of bioavailable N has fuelled an increase in nitrogen turnover as well as N_2O production (Gruber and Galloway, 2008), which, among other anthropogenic sources, has been increasing the atmospheric N_2O inventory. Current N_2O mixing ratios in the atmosphere of 322 ppb are about 19% higher than in preindustrial times (~270 ppb), and N_2O is constantly increasing at a rate of 0.7 ppb yr^{-1} (Montzka et al., 2011).

The ocean is the second largest natural source of atmospheric N_2O (Fig. 2), with the major contribution from the open ocean (Nevison et al., 1995), but disproportionally high contributions from coastal waters (Bange et al., 1996).

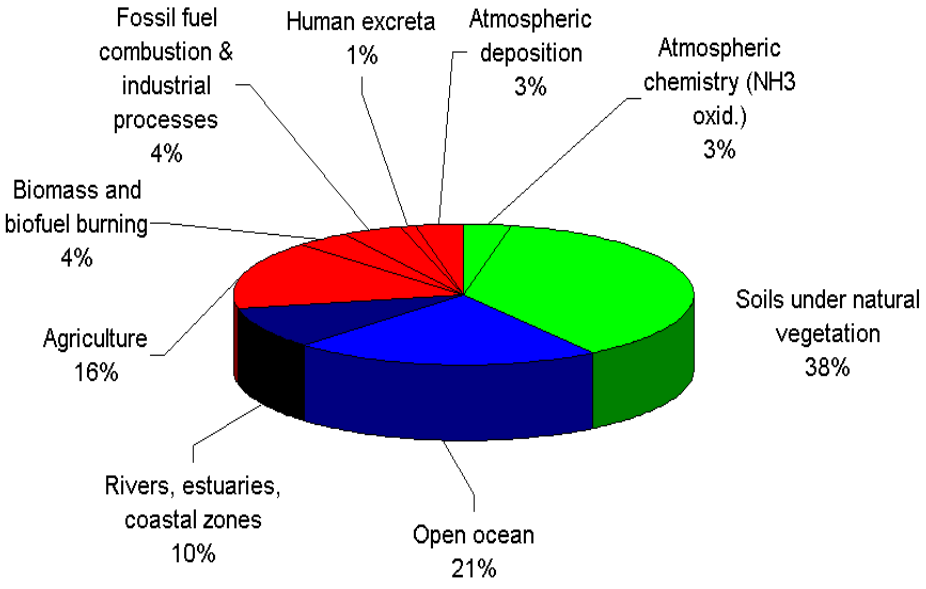

Figure 2: Sources for atmospheric N_2O (Denman et al., 2007).

Nitrification and denitrification in the ocean take place under different conditions and have different effects on N_2O distributions. The current view on oceanic nitrous oxide production can be summarized as follows:

1) Under oxic conditions, N_2O is produced by nitrifying organisms, while N_2O consumption is not observed (Bange et al., 2010b) and N_2O thus accumulates in the subsurface and deep water column. N_2O production under oxic conditions involves two possible pathways, the "classical" nitrification pathway, and nitrifier-denitrification. It is likely that both processes can be carried out by nitrifying organisms (Wrage et al., 2001). During "classical" bacterial nitrification, N_2O evolves as a by-product during the oxidation of hydroxylamine to nitrite by the enzyme hydroxylamine oxidoreductase (HAO), however, the exact pathway of N_2O formation is still unclear (Arp and Stein, 2003). During nitrifier-denitrification N_2O is produced from nitrite in a similar pathway to that of canonical denitrification which involves nitric oxide as intermediate (Arp and Stein, 2003) (Fig. 3).

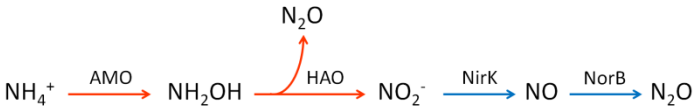

Figure 3: N_2O production pathways in ammonia-oxidizing bacteria. The classical nitrification pathway is marked in red, the nitrifier-denitrification pathway in blue. Involved enzymes are: ammonium monooxygenase (AMO), hydroxylamine oxidoreductase (HAO), nitrite reductase (NirK), nitric oxide reductase (NorB).

The distinction between classical nitrification and nitrifier-denitrification relies on the different isotopic composition of the N_2O produced: N_2O production from oxidation of hydroxylamine yields low $\delta^{15}N$ and $\delta^{18}O$ signatures, and produces a distinct site preference ($SP=\delta^{15}N_\alpha - \delta^{15}N_\beta$) , whereas N_2O production from nitrite reduction yields a site preference close to zero and higher $\delta^{18}O$ signatures as the two oxygen atoms incorporated into the nitrite molecule stem from different sources (Sutka et al, 2006;Ostrom et al., 2000). A large variability of the isotopic composition of N_2O has been found not only in suboxic, but also in oxygenated waters and has been explained by a shift from nitrification to nitrifier-denitrification with decreasing oxygen concentrations (Ostrom et al., 2000;Popp et al., 2002).

Archaeal N_2O production during nitrification has only recently been detected (Santoro et al., 2011). Given the large dominance of archaeal over bacterial gene copy numbers in a

number of marine environments and the similarities in the distribution of nitrification rates and abundances of archaeal ammonium monooxygenase genes (Beman et al., 2008) it was concluded that ammonium oxidizing archaea (AOA) are responsible for the majority of water column nitrification and N_2O production (Molina et al., 2010;Santoro et al., 2010). N_2O production by enrichment cultures of marine AOA has been demonstrated recently (Santoro et al., 2011). Little is known about the pathway of ammonium oxidation carried out by archaea, but some evidence has been found that AOA can grow at lower substrate concentrations than AOB (Martens-Habbena et al., 2009), and unlike AOB, a set of genes encoding the hydroxylamine oxidoreductase has not been identified in AOA yet (Walker et al., 2010), suggesting a different metabolic pathway for ammonium oxidation in AOA. This also revives the question of N_2O production pathways and their controlling mechanisms in the ocean.

2) N_2O production and consumption by denitrification is known to become dominant as oxygen concentrations decrease to values close to zero (Codispoti et al., 1992). Water column suboxia and anoxia in the oceans are known only for a few habitats which include sporadic suboxic and anoxic events in coastal areas, the Baltic Sea and the Black Sea, and the OMZs in the eastern tropical Pacific Ocean and the Arabian Sea (Naqvi et al., 2010). However, these habitats show different behavior of N_2O accumulation and consumption (Fig. 4): Although rapid N_2O consumption is typically observed with a drop of oxygen concentrations below 5 $\mu mol\ L^{-1}$ (Bange, 2008), accumulation of N_2O is much more variable. While the OMZs in the Arabian Sea and the ETSP show a characteristic double-peak structure with accumulation of N_2O in the upper and lower oxycline (Bange et al., 2001;Cohen and Gordon, 1978), in the Baltic Sea and the Black Sea, where a sharp decrease in oxygen concentrations towards anoxia is characteristic, no N_2O accumulation is observed (Walter et al, 2006a).

Large short-term accumulations of N_2O have been observed during episodically occurring anoxic events at continental shelves and they may contribute significantly to oceanic N_2O emissions when ventilated to the atmosphere (Naqvi et al., 2000; Codispoti, 2010). They have been explained by dynamic shifts in the denitrification sequence that leads to the temporary accumulation of N_2O (Naqvi et al., 2000). The influence of oxygen on N_2O production and consumption pathways during denitrification is not well understood, yet. It is known that the enzymes responsible for the reduction of nitric oxide to N_2O and of N_2O to N_2 show different tolerances to low levels of oxygen (Korner and Zumft, 1989;Ferguson, 1994), however, the limiting oxygen concentrations are yet unknown and leave the question of the onset of N_2O production by denitrification unanswered.

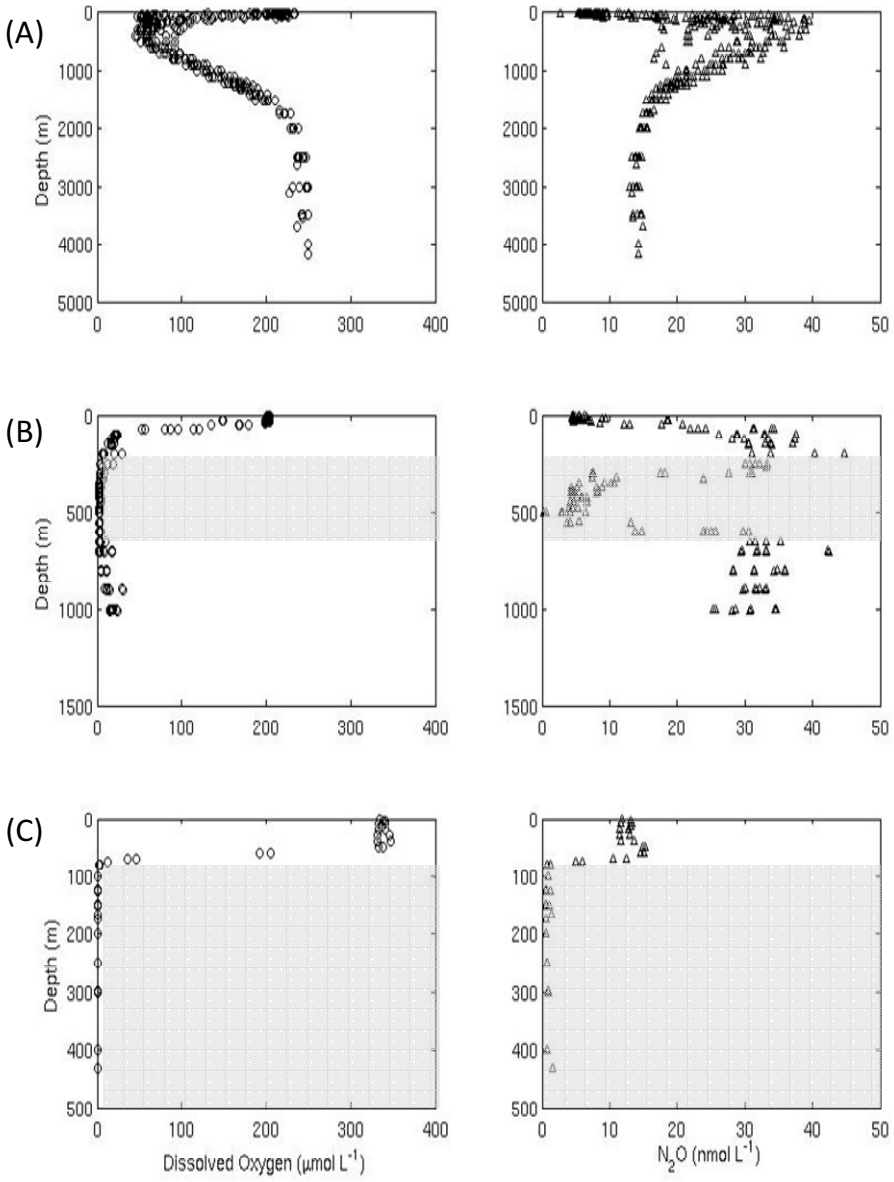

Figure 4: Oxygen and N_2O profiles from different environments, showing different patterns of accumulation and consumption of N_2O at different oxygen conditions within the OMZ. A) Tropical North Atlantic Ocean, oxic conditions B) Costa Rica Dome, suboxic conditions, C) Baltic Sea, anoxic conditions. From Bange et al. (2010b).

3) Although euphotic zone nitrification has been shown to be light-inhibited in a number of culture experiments (Guerrero and Jones, 1996;Horrigan et al., 1981), field measurements of nitrification rates provide evidence for euphotic zone nitrification in a magnitude that is large enough to substantially contribute to nutrient recycling in the surface layer (Yool et al., 2007, Dore and Karl, 1996;Diaz and Raimbault, 2000;Raimbault and Garcia, 2008). Accordingly, it was suggested that N_2O production may not only take place in the

subsurface and deep ocean but also in the oceanic mixed layer and may contribute significantly to oceanic N_2O emissions to the atmosphere (see e.g. Dore and Karl, 1996). However, unlike for nitrification, direct measurements of nitrous oxide production rates in the mixed layer are (currently) not possible as current N_2O analysis methods do not provide sufficient sensitivity to measure the changes in the N_2O inventory attributed to in-situ production: To measure detectable changes in the N_2O inventory, production rates would need to be as high as several nmol L^{-1} d^{-1}, whereas maximum N_2O production rates, calculated for the deep ocean, did not exceed 5 nmol L^{-1} yr^{-1} (Freing, 2009). Indirect mixed layer budget calculations, however, using sea-to-air flux calculations and estimates of the diapycnal N_2O flux into the mixed layer, indicate a potentially large contribution of surface N_2O production (Morell et al., 2001;Santoro et al., 2010;Dore and Karl, 1996;Charpentier et al., 2010).

The role of hydroxylamine in the N cycle

In contrast to N_2O, hydroxylamine is an intermediate during microbial nitrification (Arp and Stein, 2003) that can be produced and consumed in this process. It is labile in aquaeous solutions under neutral to alkaline conditions, reacting rapidly with ambient oxygen (Hughes and Nicklin, 1967, 1971), while under acidic conditions, protonization of the free electrons of the nitrogen atom stabilizes the molecule and prevents its oxidation (Butler and Gordon, 1986a). It can furthermore be photooxidized by ultraviolet radiation at wavelengths <260 nm (Behar et al., 1972), which, however, are negligible in oceanic envrionments.

In the marine N cycle, hydroxylamine evolves as a short-term intermediate in bacterial nitrification and DNRA: Nitrification is the enzymatic oxidation of ammonium to nitrate, a two-step process with each step carried out by different organisms: oxidation of ammonium to nitrite can be carried out by AOB or AOA while the further oxidation of nitrite to nitrate is known to be performed by nitrite oxidizing bacteria (NOB) (Ward, 2008).While the reaction mechanism in the second step does not involve hydroxylamine, it was identified as an intermediate and a precursor for nitrous oxide in the first step of bacterial nitrification (Arp and Stein, 2003). The recent detection that ammonium oxidizing archaea may outcompete ammonium oxidizing bacteria in large parts of the oceans (Wuchter et al., 2006; Martens-Habbena et al., 2009) requires new investigations on the metabolic pathway of archaeal ammonium oxidation, particularly as a recent study found indications for a different pathway that may not involve hydroxylamine as an intermediate (Walker et al., 2010).

Although the reaction products of DNRA are very similar to that of nitrate assimilation, its purpose and abundance in the water column are very distinct: Unlike in the assimilatory process, the nitrogen during DNRA is primarily used as an electron acceptor and nitrogen is not incorporated by the organisms. Furthermore, DNRA is a strictly anaerobic process that can only occur in suboxic to anoxic environments (Yordy and Ruoff, 1981). Nevertheless, DNRA has been identified in suboxic zones of lakes and oceans and has been suggested as supply mechanism for ammonium required for anaerobic ammonium oxidation (Lam et al., 2009). During DNRA, hydroxylamine evolves as an enzyme-bound intermediate during reduction of nitrite (Einsle et al., 2002) which may be released only under acidic conditions.

Early ideas that NH_2OH occurs as an intermediate during the anammox process (van de Graaf et al., 1997) could not be verified (Kartal et al., 2011;Jetten, 2009).

Hydrographic settings in the eastern tropical Atlantic and Pacific Oceans

The nitrous oxide distributions in the eastern tropical Atlantic and Pacific Oceans are strongly controlled by the hydrographic settings of these regions: the tropical oceans between 30 °N and 30 °S lie in the trade wind zone which largely influences the hydrographic and biogeochemical settings of this region (Longhurst et al., 1995). On the one hand, the wind field distribution leads to the formation of basin-scale anticyclonic gyres (subtropical gyres). They are characterized by downwelling in the centre of the gyres leading to the formation of a stable thermocline which, in turn, largely inhibits the exchange of dissolved compounds (e.g. nutrients and trace gases) between the mixed layer and the subsurface ocean (Tomczak and Godfrey, 2002). The subtropical gyres are therefore known as the most oligotrophic areas in the world's ocean (Morel et al., 2010).

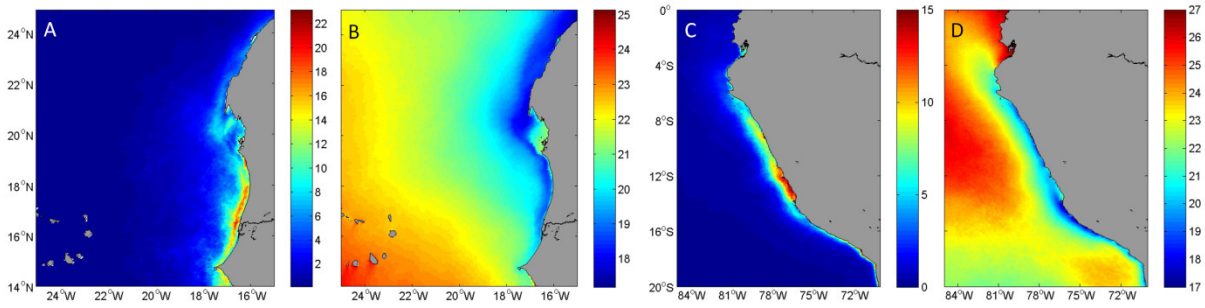

Figure 5: Chla (A, C) and SST (B, D) in winter/spring from 2002 to 2010 in the ETNA and ETSP. Data were obtained from MODIS Aqua SST and chlorophyll a images.

Coastal upwelling, on the other hand, fuels high biological productivity along the eastern boundaries of the basins, where alongshore trade winds cause offshore Ekman transport of surface waters. These waters are replaced with cold, nutrient-rich subsurface waters, leading to high primary productivity (Fig. 5). Coastal upwelling areas are among the most productive oceanic areas and carry among the most abundant fish stocks in the oceans (Chavez and Messie, 2009). Additionally, they are known as hot-spots for the emissions of climate-active gases (Nevison et al., 2004;Paulmier et al., 2008). Adjacent to the upwelling areas, the high primary productivity and slow ventilation of the subsurface waters lead to the formation of oxygen-deficient zones. Oxygen concentrations in the eastern Pacific Ocean are considerably lower than in the Atlantic Ocean mainly due to the different water mass age of the waters within the OMZ (Karstensen et al., 2008). A detailed description of the individual hydrographic settings of the eastern tropical North Atlantic and the eastern tropical South Pacific Ocean is given in Chapter 2.

Thesis outline

The recent detection of new processes and organisms that play a significant role in nitrogen cycling of the world's oceans have some implications on our current picture of oceanic N_2O production: If archaeal and not bacterial ammonium oxidizers produce the majority of the oceanic N_2O, we are faced with the fact that the pathways of the production of large amounts of N_2O in the ocean are largely unknown. Hydroxylamine has only been found as an intermediate during bacterial ammonium oxidation, and it role in ammonium oxidation by archaea has to be determined, yet. Furthermore, a potentially large contribution of surface N_2O production during nitrification within the euphotic zone/mixed layer would have far-reaching consequences for the interpretation of oceanic N_2O emissions to the atmosphere. If significant amounts of oceanic N_2O are produced in the mixed layer, they can be directly ventilated to the atmosphere. However, oxygen concentrations in the mixed layer are close to saturation, and thus not favorable for a pronounced N_2O production. If there is indeed a significant surface N_2O production, other factors than O_2 may influence the N_2O production in the mixed layer. This thesis compiles a number of studies based on a large dataset of nitrous oxide and hydroxylamine measurements that investigate the oceanic N_2O and hydroxylamine production pathways.

An analysis of the N_2O distribution and $\Delta N_2O/AOU$ and $\Delta N_2O/NO_3^-$ relationships in the eastern tropical North Atlantic and the eastern tropical South Pacific Oceans is presented in chapter 2.

In chapter 3, nitrous oxide measurements are combined with microstructure measurements to calculate a mixed layer budget of N_2O for the highly productive upwelling region off Mauritania. The potential N_2O production in the mixed layer was estimated and other processes that can lead to the observed N_2O mixed layer deficit are discussed.

In chapter 4, N_2O and $\delta^{15}N$-nitrate measurements are used to compare the different nitrogen cycles in the oxygen minimum zones of the eastern tropical North Atlantic and the eastern tropical South Pacific Oceans.

N_2O production by archaeal ammonium oxidation is shown in chapter 5 in a combined approach using field data as well as culture and incubation experiments. Archaeal N_2O production is indicated in a correlation between N_2O distribution and archaeal *amoA* abundance on one hand and N_2O production from a cultured archaeon and inhibitor experiments on the other hand.

In chapter 6, an improved the method for measurements of hydroxylamine in seawater is described. Measurements of hydroxylamine at the Boknis Eck Coastal Time Series Station and first measurements from four stations in the equatorial Atlantic Ocean using the improved method are presented.

2 Nitrous oxide distribution in the eastern tropical Atlantic and Pacific Oceans

Introduction

Nitrous oxide (N_2O) is a potent greenhouse gas (Denman et al., 2007) in the Earth's troposphere and acts as an ozone depleting compound in the Earth's stratosphere (Isaksen and Stordal, 1986;Ravishankara et al., 2009). Emissions to the atmosphere have been increasing since the end of the 18th century due to human activities (Khalil et al., 2002a). A number of anthropogenic and natural sources for atmospheric N_2O have been identified (Kroeze, 1994), with oceanic production making up for about 30 % of all natural N_2O emissions (Denman et al., 2007). Although it is known that N_2O production and, in suboxic to anoxic areas, consumption in the ocean is controlled by nitrification and denitrification (Bange, 2008), the exact N_2O production pathways and their controlling factors are still unclear: The classical view of nitrification and its role in N_2O production have recently been fundamentally changed by the detection of archaeal nitrification (Wuchter et al., 2006) and its potential of dominating N_2O production (Santoro et al., 2011). Similarly, the detection of anammox as a potentially large contributor to N loss processes in marine oxygen minimum zones (Kuypers et al., 2005) has thrown into question the role of denitrification and its role for N_2O production and consumption in these regions (Lam et al., 2009).

ΔN_2O/AOU relationship

The majority of the ocean interior can be parameterized relatively well from its oxygen and nitrate contents: A close relationship between N_2O and oxygen concentrations has been identified by a large number of investigators and has widely been interpreted as an indirect evidence for N_2O production via nitrification (Yoshinari, 1976; Yoshida et al., 1989; Nevison et al. 2004). The relationship between N_2O and oxygen concentrations is usually examined by correlating ΔN_2O with the apparent oxygen utilization (AOU). AOU and ΔN_2O are defined as follows:

$$AOU = [O_2]_{equilibrium} - [O_2]_{in-situ} \quad (1)$$

$$\Delta N_2O = [N_2O]_{in-situ} - [N_2O]_{equilibrium} \quad (2)$$

$[N_2O]_{equilibrium}$ (see equations 3 and 4 below) and $[O_2]_{equilibrium}$ (calculated according to Weiss (1970)) are traditionally calculated using the contemporary N_2O and O_2 mole fractions in the atmosphere. This methodology implicitly introduces some bias in the ΔN_2O calculations as the contemporary atmospheric mole fraction of N_2O has been increasing since the beginning of the industrial revolution from pre-industrial values of 270 ppb to contemporary (2011) 323 ppb (Khalil et al., 2002b;Forster et al., 2007). Thus, $[N_2O]_{equilibrium}$ can be currently overestimated to up to 19% (Freing et al., 2009), which may lead to an underestimation of ΔN_2O in old water masses. To calculate the corrected ΔN_2O (N_2O_{excess}), the knowledge of the age of the respective water mass is necessary, which is often not the case. Most of the published ΔN_2O/AOU relationships calculated using the conventional method are therefore biased and make direct comparison questionable.

Linear ΔN_2O/AOU relationships were found in a large number of studies, reflecting that the yield of N_2O during O_2 consumption is relatively constant (Yoshinari, 1976;Elkins et al., 1978;Walter et al., 2006b). Similarly, a linear relationship between ΔN_2O and nitrate has been interpreted as an additional indirect evidence for N_2O production during nitrification (Yoshida et al., 1989). Both relationships, however, have been shown to vary between water masses and with depth (Nevison et al., 2003), which complicates the interpretation of ΔN_2O/AOU relationships as a result of constant N_2O yields during nitrification. Moreover, it has been shown that a linear ΔN_2O/AOU relationship could also result from mixing of waters with different ΔN_2O/AOU ratios (Yamagishi et al., 2007;Nevison et al., 2003).

Parameterizations of N_2O in the water column mainly rely on an exponential relationship between N_2O yields during nitrification and decreasing oxygen concentrations. This relationship was first introduced by Goreau et al. (1980) as a result of culture experiments with marine nitrifying bacteria. A conceptual model of the relationship between N_2O production and oxygen concentrations, including N_2O production from nitrification and production and consumption from denitrification at decreasing oxygen concentrations, was introduced by Codispoti et al. (1992) and had some applications in modeling (Suntharalingam et al., 2000). Nevison et al. (2003) used the results of Goreau et al. (1980) to derive an oxygen-dependent parameterization for N_2O from field data which applies for oxic environments only, however.

Freing et al. (2009) used the transient time distribution (TTD) approach (Haine et al. 2002) to calculate N_2O production rates (N_2OPR) and apparent oxygen utilization rates (AOUR) from

tracer distributions. N_2O concentrations in the water column were then calculated by multiplying the N_2OPR with the mean age of the water mass. The difference between this method and the traditionally used ΔN_2O/AOU relationships described above is that TTD-derived N_2OPR are not directly parameterized from oxygen concentrations, but from oxygen consumption rates instead, which can differ greatly from oxygen and nitrous oxide distributions. Similarly to the relationships found between ΔN_2O and AOU, N_2OPR correlates linearly with AOUR. This, however, is not necessarily contradictory to the laboratory studies if the majority of the N_2O production takes place at similar oxygen concentrations.

N_2O measurements in the ETNA and ETSP

Nitrous Oxide was measured on five cruises to the oxygen minimum zone of the eastern tropical North Atlantic Ocean (ETNA) between 2006 and 2010 and on one cruise to the eastern tropical South Pacific Ocean (ETSP) in early 2009 (Fig. 1). The cruises were part of the German BMBF joint project SOPRAN (**S**urface **O**cean **Pr**ocesses in the **An**thropocene, www.sopran.pangaea.de) and the German Research Foundation collaborative research project SFB-754 (www.sfb754.de). In combination with turbulence measurements, metagenomic analyses and isotopic measurements, these data are the basis for a number of studies investigating the transport and production pathways of N_2O in eastern tropical oceans (see chapters 3-5).

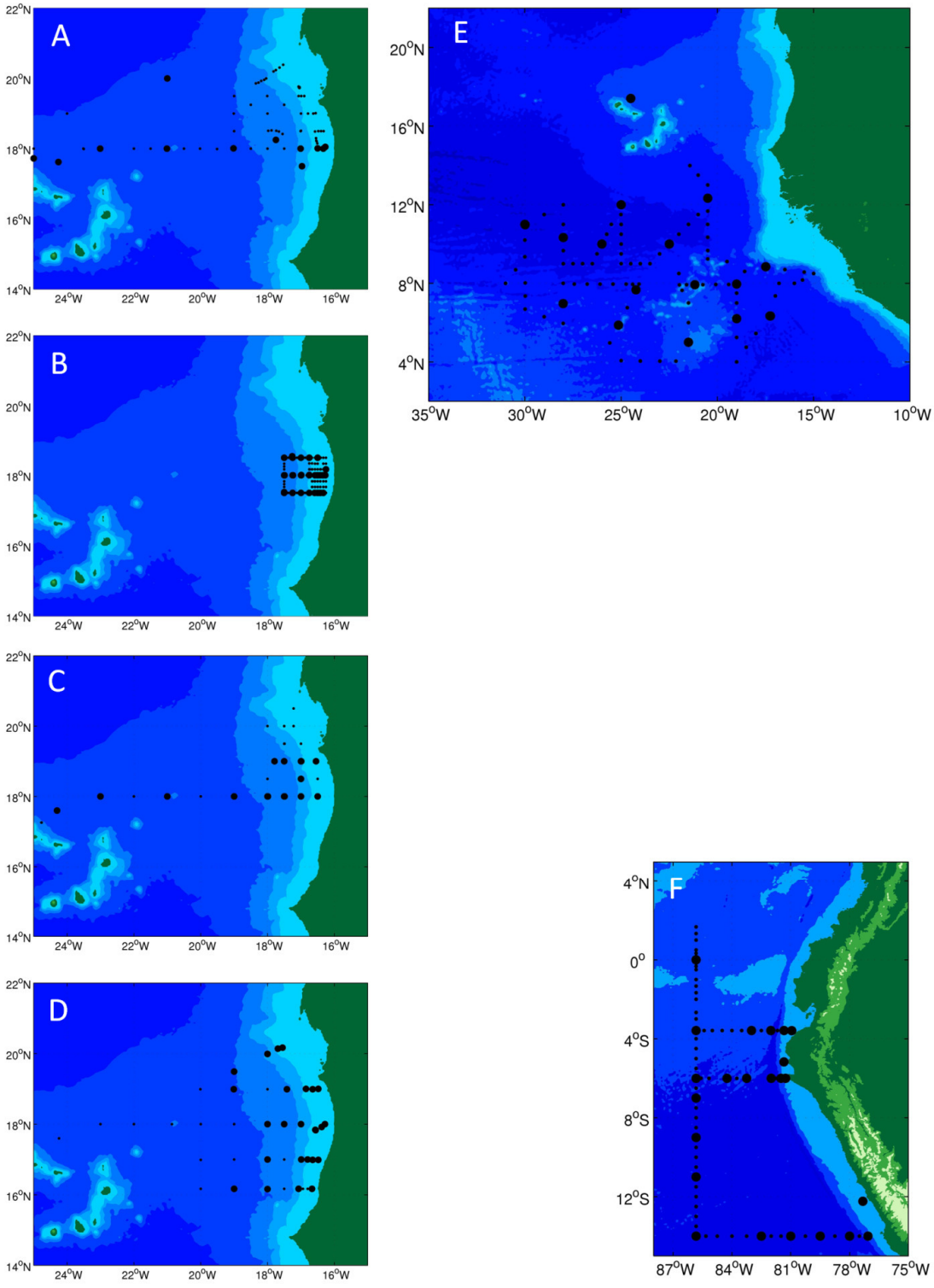

Figure 1: Station maps from cruises to the ETNA and ETSP: Meteor 68-3, July/August 2006 (A), Poseidon 347, January 2007 (B), Poseidon 348, February 2007 (C) and L'Atalante 3, February 2008 (D) to the Mauritanian upwelling; Meteor 80-2, November/December 2009 (E) to the region south of Cape Verde and Meteor 77-4 January/February 2009 (F) to the ETSP. Stations that were sampled for N_2O are highlighted.

Study Sites

Eastern tropical North Atlantic Ocean (ETNA)

Four cruises to the ETNA covered the region between the Cape Verde islands and the Mauritanian coast (R/V Meteor Cruise M68-3, July-August 2006; R/V Poseidon Cruise P348, February 2007; R/V L'Atalante Cruise ATA3, February 2008) and one cruise covered the region south of the Cape Verde islands (R/V Meteor Cruise M80-2) (Fig. 1A-E). The region east of the Cape Verde islands is largely influenced by coastal upwelling off the Mauritanian coast (Mittelstaedt, 1983) which denotes the southern part of the Canary Current upwelling system, one of the four major eastern boundary upwelling systems (Chavez and Messié, 2009). This system is dominated by a strong seasonality that is determined by seasonality of the north- and southward movement of the intertropical convergence zone (ITCZ) (Schemainda et al., 1975;Messie et al., 2009). In the region between Cap Blanc (21°N) and Cap Vert (15°N) this is reflected in the length of the upwelling period: At Cap Blanc, upwelling conditions are prevalent throughout the year while upwelling conditions at Cap Vert dominate only during winter with an upwelling period of about six months (Schemainda et al., 1975). However, the occurrence and intensity of the coastal upwelling is determined by the individual wind conditions, which leads to a large spatiotemporal variability in the upwelling (Wittke et al., 2010) building an eddy-dominated flow field with the occurrence of upwelling filaments that can be advected offshore over several hundreds of kilometers. In the northern region, for example, the exposed geography of the coast and the year round upwelling-favourable conditions lead to the existence of the "Giant Cape Blanc Filament", a persistent upwelling filament found throughout the year between 20 °N and 22 °N (Fischer et al., 2009). Compared to other OMZs adjacent to eastern boundary upwelling systems, oxygen concentrations are relatively high, with minimum concentrations of about 30µmol L^{-1} south of the Cape Verde islands and 40 µmol L^{-1} in the region off Mauritania (Stramma et al., 2008a). The center of the oxygen minimum zone is collocated with a weak upwelling field called the "Guinea Dome" south of the Cape Verde islands (Siedler et al., 1992).

Two water masses dominate the density range of the OMZ waters with the mixing front located at ~20 °N in the ETNA: In the southern region the older South Atlantic Central Water (SACW) is dominant, which is reflected in lower oxygen and higher nutrient concentrations than the North Atlantic Central Water (NACW) which is prevalent north of 21°N. The upwelling region off Mauritania is strongly affected by the mixing of these two waters and causes some spatial and temporal variability in oxygen and nutrients in this area (Minas et al., 1982;Hagen, 2001).

Eastern tropical South Pacific Ocean (ETSP)

The oxygen concentrations in the ETSP are among the lowest concentrations measured in the oceans, with large volumes reaching oxygen concentrations well below 20 µmol L^{-1} (Fuenzalida et al., 2009). Oxygen concentrations below 5 µmol L^{-1} reveal substantial differences in the nitrogen cycling with N-loss processes (denitrification and anammox) becoming dominant (Bange et al., 2005;Devol, 2008). Unlike in the ETNA, where the centre of the OMZ is uncoupled from the coastal upwelling system, in the ETSP a permanent OMZ with oxygen concentrations below 5 µmol L^{-1} is found off the Peruvian coast centered at ~10 °S (Karstensen et al., 2008) with a maximum vertical extension of up to 700 m between 100 and 800 m (Fuenzalida et al., 2009). This very shallow oxygen minimum is closely coupled to the coastal upwelling along the Peruvian coast which enables the emissions of large amounts of greenhouse gases (N_2O, CO_2) to the atmosphere (Paulmier et al., 2008). The very low oxygen content of the waters off Peru can be explained by the co-occurrence of strong remineralization in the coastal upwelling area and a limited oxygen supply by adjacent waters (Czeschel et al., 2011), with the main oxygen supply route to the ETSP coming from the equatorial region with its zonal current system (Stramma et al., 2010a). Moreover, strong remineralization rates drive oxygen concentrations to suboxic and episodically anoxic conditions (Helly and Levin, 2004; Reichart et al, 1998).

N_2O Analysis

Discrete samples of nitrous oxide were measured on board using two GC/ECD systems (Hewlett Packard 5890 II during cruises M68-3, ATA3, M80-2 and M77-4; Carlo Erba HRGC 5160 Mega Series during cruises P347 and P348). The GCs were equipped with a 6' 1/8" stainless steel column packed with molecular sieve (5Å) (W. R. Grace & Co.-Conn., Columbia, MY) and operated at a constant oven temperature of 190 °C (HP 5890II) and 220 °C (Carlo Erba HRGC 5160). Argon-methane (95/5, 5.0, AirLiquide, Düsseldorf, Germany) was used as carrier gas at a flow rate of 30 mL min^{-1}.

Samples were analyzed for N_2O using a static equilibration method. Triplicates of bubble free samples were drawn from 10L Niskin bottles mounted on a CTD/rosette, poisoned with mercuric chloride or measured within 24 h after sampling. For analysis, a 10 mL helium headspace was added to each sample using a gas-tight syringe (VICI Precision Sampling, Baton Rouge, LA). A 9 to 9.5 mL subsample of the headspace was analyzed for nitrous oxide after an equilibration time of minimum 2 h. The GC was calibrated on a daily basis using at least two different standard gas

mixtures (Deuste Steininger GmbH, Mühlheim, Germany) to account for potential drift of the detector.

The mole fraction x_{N_2O} of N_2O in the headspace was calculated from the Peakarea PA using a linear fit for $x_{N_2O} > 312$ ppb and a quadratic fit for $x_{N_2O} \leq 312$ ppb:

$$x_{N_2O_{linear}} = \frac{PA-b}{a} \quad (1)$$

$$x_{N_2O_{quadratic}} = -\frac{b}{2a} \pm \sqrt{\left(\frac{b}{2a}\right)^2 + \frac{PA}{a}} \quad (2)$$

The N_2O concentration was calculated from the measured mole fraction x_{N_2O} in the headspace according to:

$$[N_2O] = \frac{pVx_{N_2O}}{RT}\frac{V_{Hs}}{V_W} + \beta x_{N_2O} p' \quad (3)$$

with the ambient air pressure p in Pascal and p' in atmospheres, air temperature T in Kelvin, and the universal gas constant R. The factor $\frac{V_{Hs}}{V_W}$ is the volume ratio of the headspace and water phase. The Bunsen solubility β of N_2O in seawater is calculated according to the solubility function by Weiss and Price (Weiss and Price, 1980):

$$\beta = exp\left(A_1 + A_2\left(\frac{100}{T}\right) + A_3 ln\left(\frac{T}{100}\right) + A_4\left(\frac{T}{100}\right)^2 + S\left(B_1 + B_2\left(\frac{T}{100}\right) + B_3\left(\frac{T}{100}\right)^2\right)\right) \quad (4)$$

A_1 to B_3 are gas specific coefficients. For N_2O, these coefficients are given in Table 2.

Table 2: Coefficients for the Bunsen solubility of N_2O. From Weiss and Price (Weiss and Price, 1980).

A_1	A_2	A_3	A_4	B_1	B_2	B_3
-165.8806	+222.8743	+92.0792	-1.48425	-0.056235	+0.031619	-0.0048472

The uncertainty of the measurements was calculated from the standard deviation as defined by David (1951) of the triplicate measurements. Samples with a standard deviation > ± 10 % were not taken into account for analysis. Samples from the P347 cruise showed high standard deviations in the OMZ which were excluded from the analysis probably due to the fact that samples were stored for several weeks before analysis during the following cruise track (P348) and partly at IFM-GEOMAR. Due to the limitation of this dataset to water depths above and below the OMZ, N_2O data from this cruise were not included in the analysis of the N_2O distribution in this chapter. Samples from above and below the OMZ were in good agreement

with N_2O measurements from the P348, however, and were therefore used in chapter 3 to calculate diapycnal and sea-to-air fluxes of N_2O. Average standard deviation of the remaining measurements was ± 0.8 nmol L^{-1}.

N_2O in the ETNA

N_2O distribution in the North Atlantic Ocean

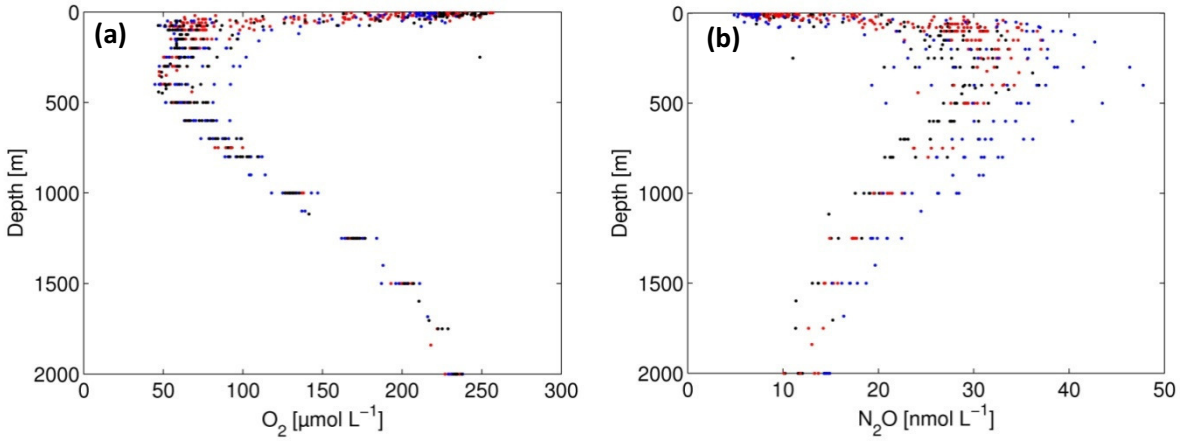

Figure 2: Oxygen (a) and nitrous oxide (b) depth profiles from the upwelling region off Mauritania, measured during M68-3 (blue), P348 (black) and ATA3 (red).

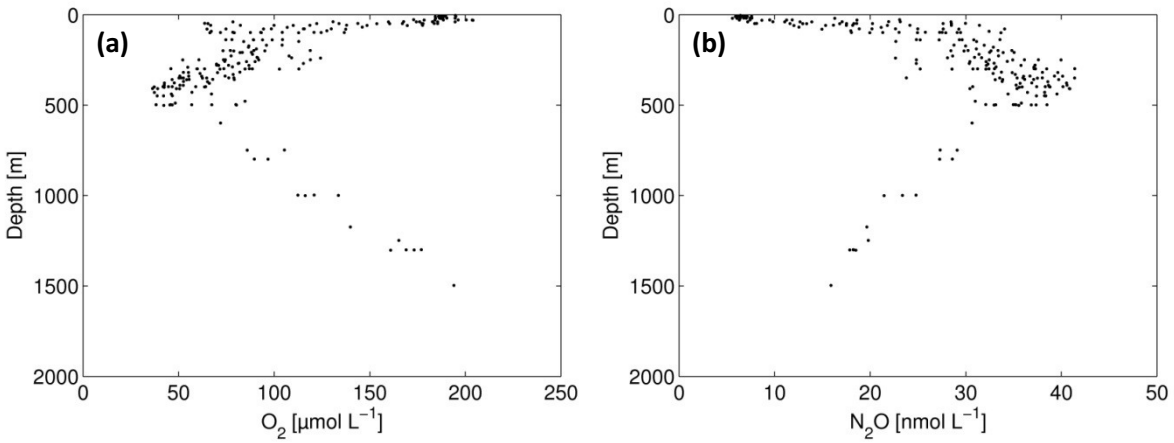

Figure 3: Oxygen (a) and nitrous oxide (b) depth profiles from the Guinea Dome region south of Cape Verde; samples from Meteor Cruise 80-2.

Nitrous oxide profiles in the ETNA were rather uniform and showed a broad and pronounced subsurface maximum which coincided with the oxygen minimum between 100 and 500 m (Fig. 2 & 3). Oxygen concentrations were below 100 µmol L^{-1} in the water depths between 100 and 700 m, and showed a primary oxygen minimum at about 100 m and a broader minimum around 500 m. These two minima were not resolved in the N_2O profiles due to the larger

variability of the N_2O data, especially in the depth range of the oxygen minimum. In the region south of Cape Verde, the two-peak structure of the oxygen profiles was more pronounced, with oxygen concentrations reaching down to about 60 µmol L^{-1} in the shallow minimum and 40 µmol L^{-1} in the deep minimum (Fig. 3). Again, this double-peak structure was less pronounced in the N_2O profiles. This can be an indication for some variability in the ΔN_2O/AOU yield in different water masses but may be disguised by the large variability in the ΔN_2O values.

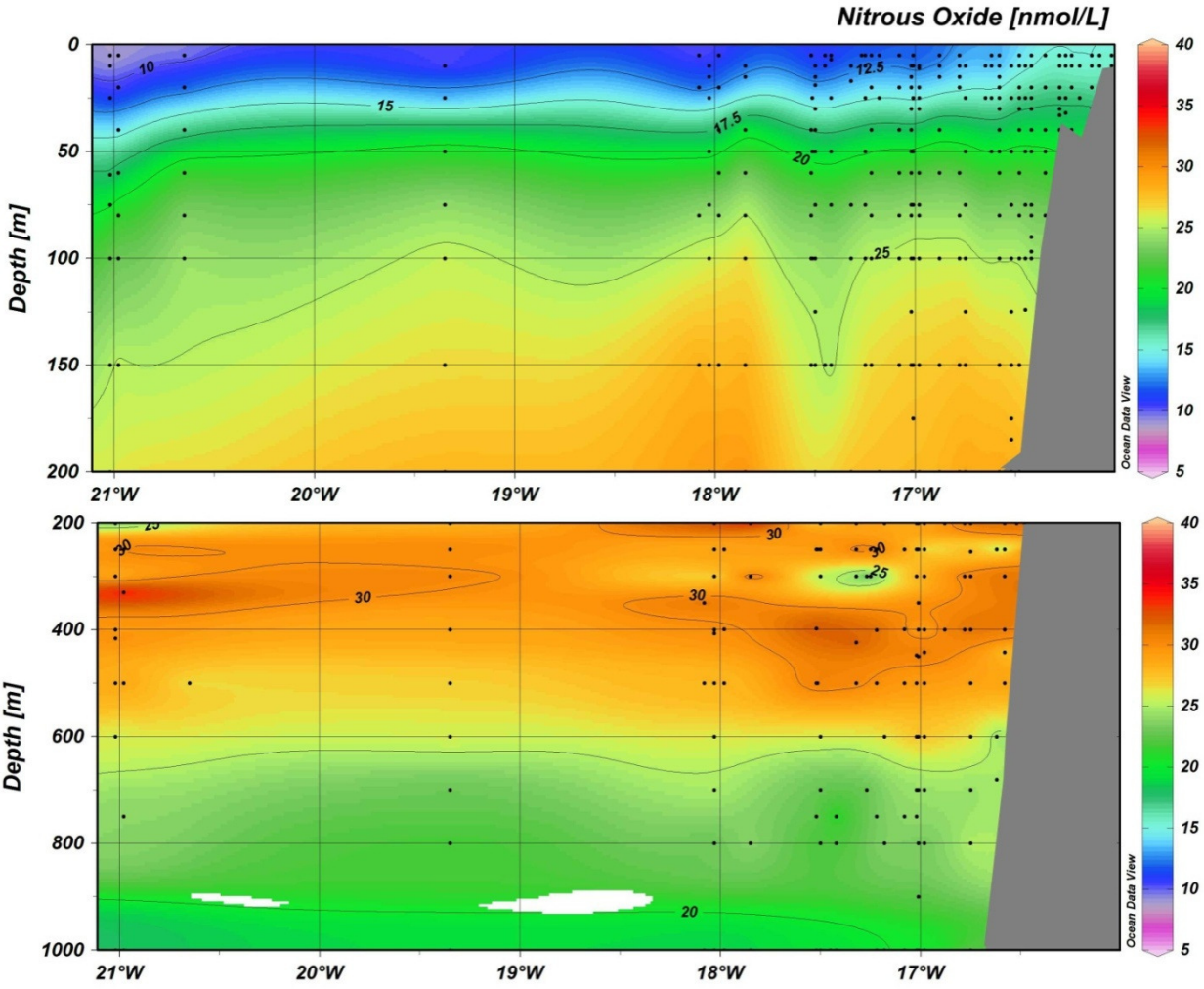

Figure 4: Composed section along 18°N of O_2 and N_2O in the ETNA from the upwelling season (P348 and ATA3): surface to 200 m (upper panel) and 200 to 1000 m (lower panel). Stations north and south of 18 °N were projected to 18 °N according to their distance from the 400 m isobath.

While N_2O concentrations in the subsurface ocean were rather unaffected by coastal upwelling (Fig. 2), surface concentrations at the Mauritanian coast were elevated up to 20.7 nmol L^{-1} (250 % supersaturation) during P348 and ATA3 (Fig. 4, upwelling season), while they stayed close to equilibrium during M68-3 (non-upwelling season). N_2O concentrations in the open ocean were

generally close to equilibrium with an average supersaturation of 105 %, which is in agreement with previous measurements from the tropical Atlantic ocean (Walter et al., 2004).

Influence of different water masses

Mixing of NACW and SACW in the ETNA has been shown to introduce some variability in both the nutrient and oxygen content of the OMZ (Minas et al., 1982;Hagen, 2001), which may also be reflected in the N_2O distribution. The temperature and salinity characteristics of the waters with highest N_2O concentrations lie between the SACW and NACW characteristics (Fig. 5), therefore, some of the variability of the N_2O data may be explained by mixing.

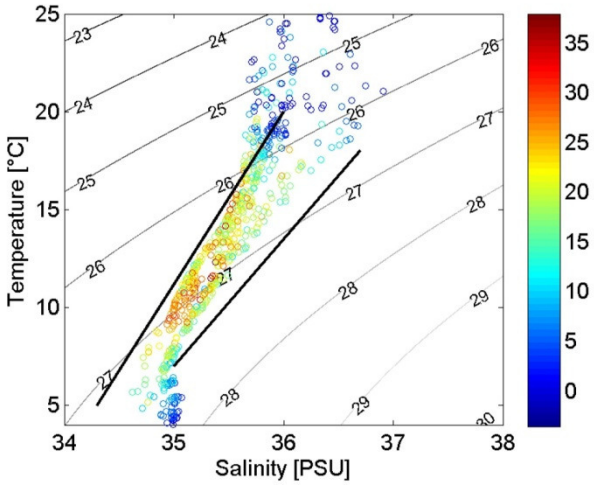

Figure 5: TS-diagram of the waters in the ETNA, with ΔN_2O as color code. The black lines denote the characteristics of the two water masses SACW (left line) and NACW (right line).

As a measure for the mixing of SACW and NACW, the fraction of NACW (xNACW) was calculated from isopycnal mixing with the characteristics of NACW and SACW as mixing endmembers (Tomczak and Godfrey, 2002) for the density range between 26.6 and 27.1 (Fig.7). This is a rather simplified approach as diapycnal mixing between SACW and NACW also contributes to the mixing process (Klein and Tomczak, 1994), but is still sufficient to give a qualitative estimate of this effect.

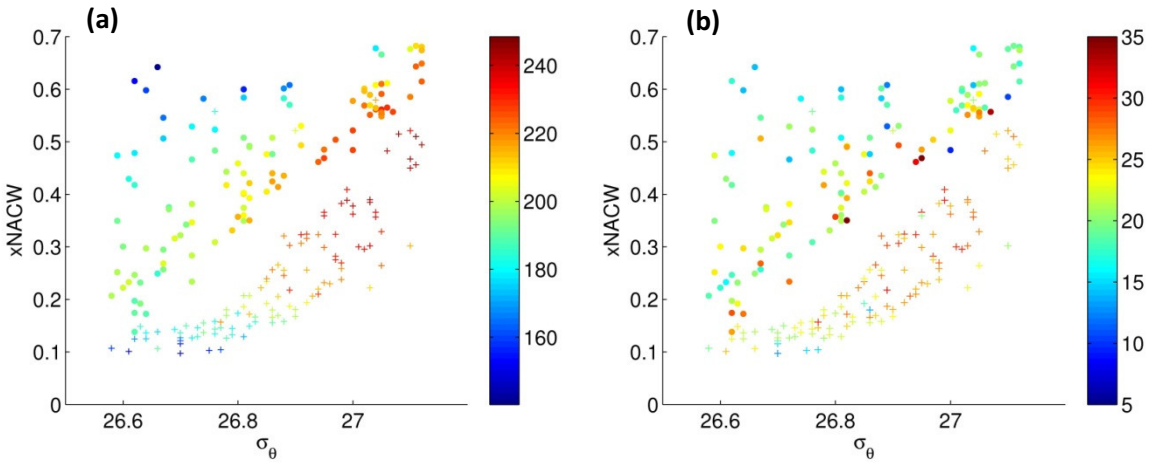

Figure 6: AOU (a) and ΔN_2O (b) dependence on potential density and fraction of NACW, calculated for the cruises to the Mauritanian upwelling (●) and for M80-2 (+).

Between the three cruises to the Mauritanian upwelling and the cruise south of Cape Verde, significant differences in the water mass distribution can be observed: samples from the southern region carry a lower fraction of NACW, with an increase in NACW content with increasing density. In the Mauritanian upwelling region the NACW fraction was close to 0.6 at high densities and showed an increasing variability with decreasing density, with the NACW fraction ranging from 0.1 to 0.6 at σ_θ=26.6. While for the Mauritanian upwelling region AOU and ΔN_2O increase with decreasing NACW content and decreasing density, the opposite trend is observed in the M80 dataset. However, these data show little variability in xNACW and the decrease in AOU and ΔN_2O with decreasing NACW is likely to be explained by the decrease in density. ΔN_2O values show a considerably larger variability than the AOU values. It can be concluded that the mixing of NACW and SACW has an influence on AOU and ΔN_2O levels, but it does not explain the larger variability in the N_2O concentrations compared to oxygen.

ΔN_2O vs. AOU and ΔN_2O vs. NO_3^- relationship

ΔN_2O/AOU and $\Delta N_2O/NO_3^-$ relationships in the Mauritanian upwelling did not show significant differences to the data from south of the Cape Verde islands; all data from the ETNA were thus merged for regression analysis (Fig. 7), ΔN_2O increased linearly with increasing AOU and nitrate concentrations, showing different linear relationships for the upper and lower oxycline. This has been observed in earlier studies (e.g. Cohen and Gordon (1979); Walter et al. (2006b); Nevison et al. (2003)) and was attributed to either a depth or temperature dependence of N_2O yields or mixing effects (Walter et al., 2006b;Nevison et al., 2003). Similarly, a linear relationship between ΔN_2O and NO_3^- has been interpreted as an indirect evidence for N_2O production by nitrification (Walter et al., 2006b).

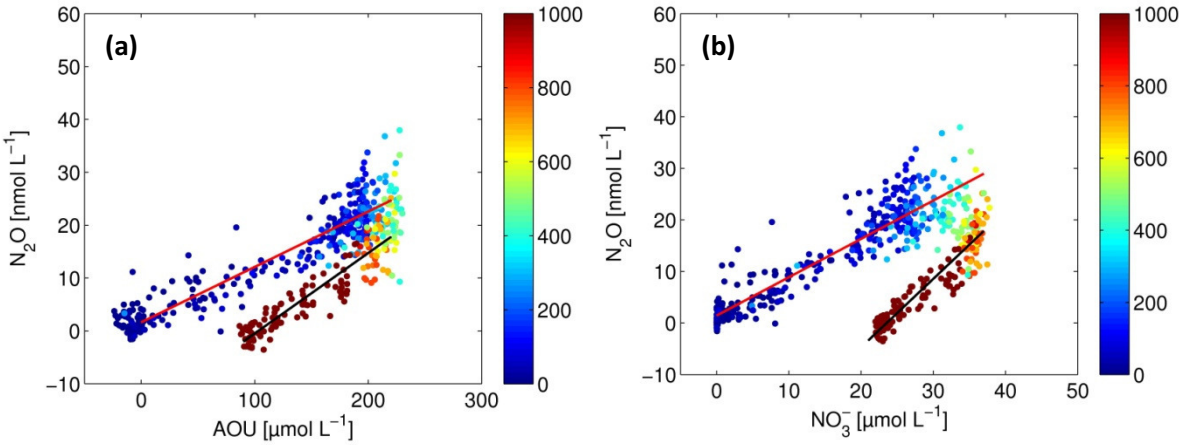

Figure 7: a) ΔN_2O/AOU relationships from the ETNA. Regression parameters are: y=0.10(±0.0016)x+1.64(±0.25) for water depths >500 m, r^2=0.88; y=0.15(±0.0049)x-15.7(±0.83) for water depths >500 m, r^2=0.85. b) $\Delta N_2O/NO_3^-$ relationship. Regression parameters are: y=0.74(±0.015)x+1.43(±0.31) for water depths <500 m, r^2=0.85; y=1.33(±0.047)x-31.27(±1.42) for water depths >500 m, r^2=0.84.

ΔN_2O/AOU relationships in the ETNA reported here are comparable to those reported in previous studies (Walter et al., 2006b;Rees et al., 2011;Forster et al., 2009) for the tropical Atlantic Ocean. ΔN_2O/AOU slopes were 0.10 nmol µmol^{-1} for the upper oxycline and 0.15 nmol µmol^{-1} in the lower oxycline, which is in reasonable agreement with the findings by Walter et al. (2006b) and Forster et al. (2009). Rees et al. (2011) observed a significant slope change in ΔN_2O/AOU at AOU levels of 50 to 100 µmol L^{-1} in the Mauritanian upwelling region with a significantly lower slope for AOU levels <100 µmol L^{-1}. These differences may be explained by the fact that Rees et al. (2011) exclusively sampled two upwelling filaments where the high biological productivity may affect additional processes that influence ΔN_2O and AOU differently. $\Delta N_2O/NO_3^-$ ratios from the ETNA reported by Walter et al. (2006b) were slightly lower than the ones reported here, but the data set by Walter et al. (2006b) included a number of data from the western basin of the Atlantic which introduces some more variability.

N_2O in the ETSP

N_2O distribution in the ETSP

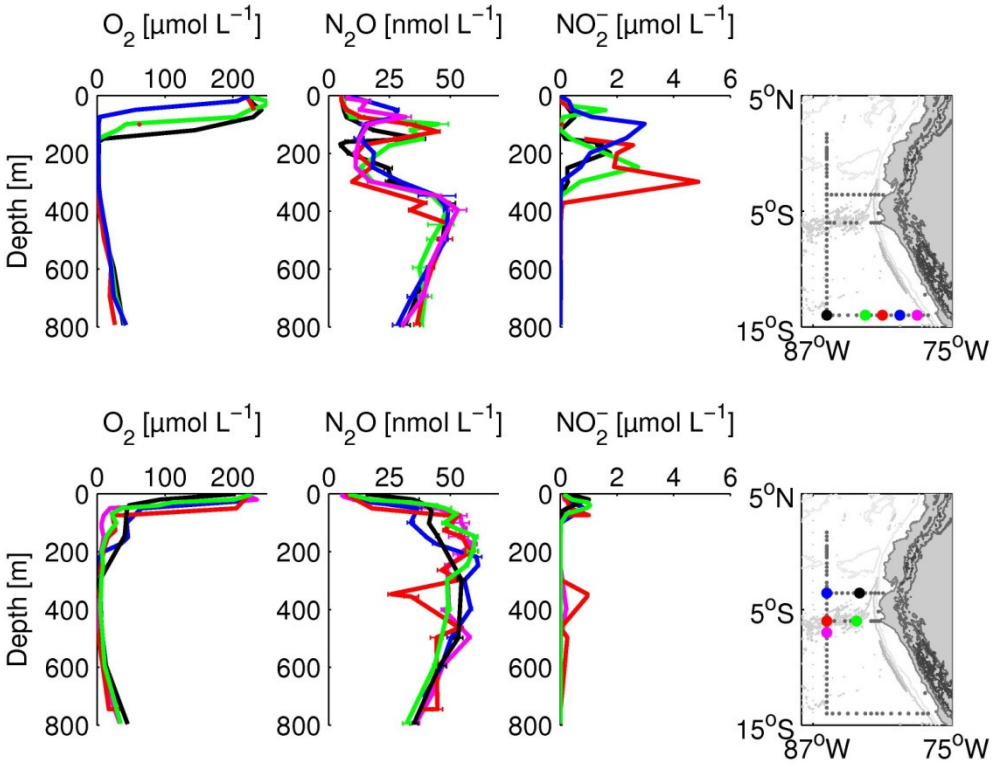

Figure 8: Selected depth profiles from M77-4 from southern stations (upper panel) and northern stations (lower panel).

Compared to the N_2O profiles in the Atlantic Ocean, the profiles in the ETSP show much larger variability: while profiles towards the equator showed a broad maximum in N_2O at the oxygen minimum similar to observations in the ETNA, N_2O depletion was observed within the OMZ in the southern part of the investigated area with two narrow N_2O maxima within the upper and lower oxycline (Fig. 8). N_2O depletion coincided with the accumulation of nitrite within the OMZ, which is characteristic for regions with denitrification processes dominating the N cycle (Codispoti et al., 1986).

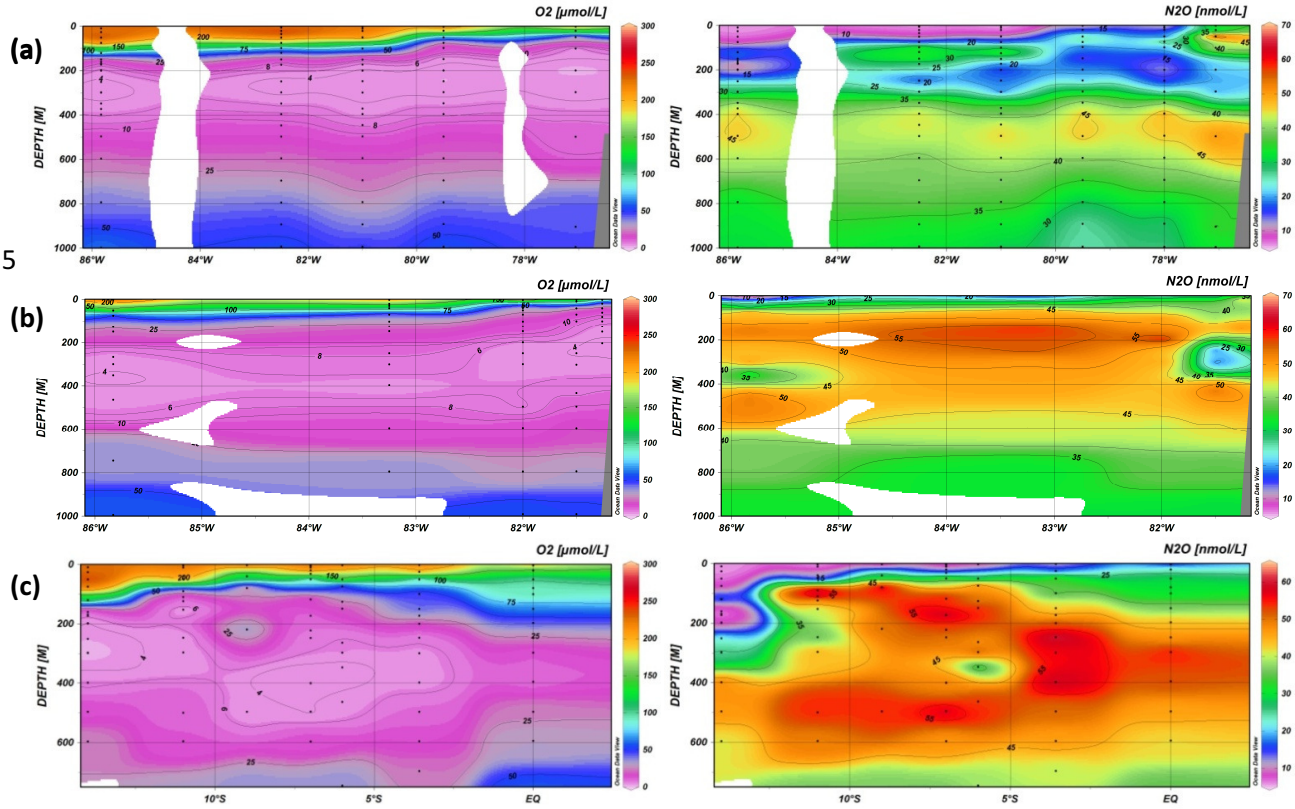

Figure 9: Oxygen (left) and N_2O (right) during M77-4, from 14 °S (a), 3 °S (b) and 86 °W (c).

The regional distribution of N_2O in the ETSP reflects the sensitivity of N_2O production and consumption to the oxygen supply in this area: the transition from double-peak structure of the profiles to single-peak profiles is closely linked to the oxygen concentrations, with the tipping point between N_2O production and depletion lying at oxygen concentrations of about 5 µmol L^{-1}. In the southern part of the investigated area N_2O depletion could be observed at depths between 100 and 400 m, coinciding with the lowest oxygen concentrations (Fig. 9a, c). In the northern part oxygen concentrations that allow N_2O depletion are confined to a narrow region at the coastal boundary, while offshore profiles show N_2O accumulation in the oxygen minimum (Fig. 9b). In the 86 °W section the transition from N_2O depletion to N_2O accumulation is observed between 10 °S and 5 °S, and can be associated with an increase in oxygen from below 4 µmol L^{-1} at 14 °S to 20 µmol L^{-1} at the equator.

A shift of the primary N_2O maximum towards shallower depths and N_2O surface supersaturation at the coast can be explained by coastal upwelling that leads to the lifiting of the thermocline towards the coast (Fig. 8). This phenomenon was observed at all zonal sections, with maximum surface concentrations of up to 40 µmol L^{-1} (saturation >500 %). This value was observed at the coast along the 14 °S section where a sharp and very shallow peak of N_2O accumulation in the upper oxycline was observed and most likely fueled the surface supersaturation.

ΔN_2O/AOU relationship in the ETSP

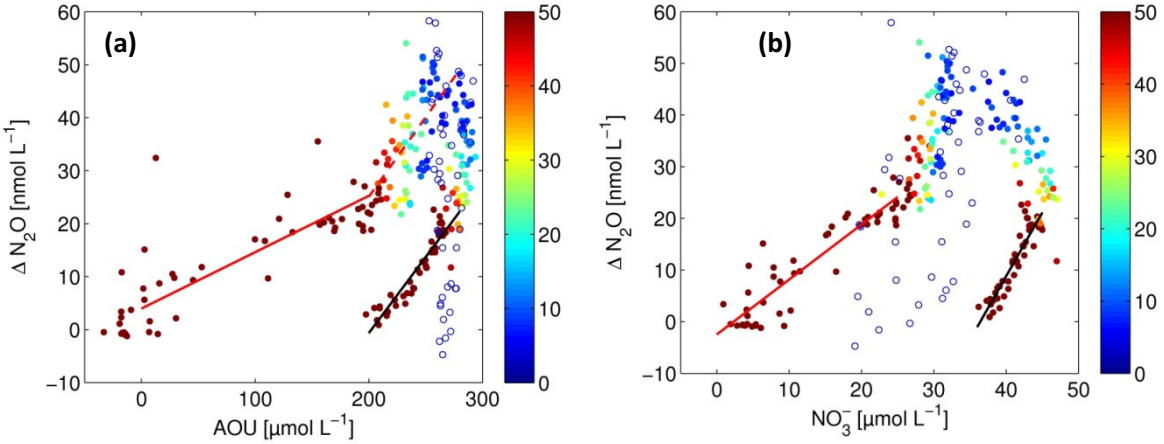

Figure 10: a) ΔN_2O/AOU relationships from the ETSP, with oxygen concentration as color code. Filled circles: samples with oxygen concentrations >5 µmol L^{-1}; open circles: samples with oxygen concentrations <5 µmol L^{-1}. Regression parameters are:
y=0.10(±0.009)x+4.81(±1.07) for water depths <350 m and oxygen >50 µmol L^{-1} (red solid line), r^2=0.70;
y=0.30(±0.050)x-35.5(±11.9) for water depths <350 m and 5 µmol L^{-1}< oxygen <50µmol L^{-1}, r^2=0.35;
y=0.29(±0.017)x-58.0(±4.03) for water depths >350 m (black line), r^2=0.88.
b) $\Delta N_2O/NO_3^-$ relationship. Regression parameters, calculated for oxygen concentrations <50µmol L^{-1}, are:
y=1.06(±0.064)x-2.47(±1.06) for water depths <350 m and oxygen >50 µmol L^{-1} (red line), r^2=0.84;
y=2.68(±0.298)x-96.3(±12.7) for water depths >350 m (black line), r^2=0.54.

In the ETSP samples can be separated into a number of regimes showing different behavior for ΔN_2O/AOU and $\Delta N_2O/NO_3^-$ (Fig. 10): 1) At oxygen concentrations <5 µmol L^{-1} ΔN_2O did not correlate with neither AOU nor NO_3^-, which is consistent with N_2O consumption at very low oxygen concentrations which leads to the breakdown of the ΔN_2O/AOU relationship.2) A linear relationship between ΔN_2O and AOU similar to the one found in the ETNA is observed only for oxygen concentrations >50 µmol L^{-1} in the upper oxycline at depths shallower than 350 m. This relationship compares well to the results from the ETNA for water depths <500 m. $\Delta N_2O/NO_3^-$ as well showed a linear relationship, but with considerably higher slope than in the Atlantic. 3) For water depths >350 m the ΔN_2O/AOU regression slope was two times larger in the ETSP than in the ETNA, however, AOU levels in the deep waters of the ETSP were considerably higher than in the ETNA and thus may carry higher ΔN_2O/AOU yields. This applies for $\Delta N_2O/NO_3^-$, too. 4) At oxygen concentrations below 50 µmol L^{-1} a significant change in the ΔN_2O/AOU slope was observed, with a ΔN_2O/AOU ratio of 0.30 nmol μmol^{-1}, which is about three times larger than at oxygen concentrations >50 µmol L^{-1}. An analogous increase in the ΔN_2O/AOU slope with increasing AOU has been reported for the Arabian Sea (Law and Owens, 1990) at similar AOU

levels, while Upstill-Goddard et al. (1999) found a quadratic parameterization to better fit their ΔN_2O/AOU data from the Arabian Sea. For the M77-4 data set, a quadratic parameterization was also applied for depths shallower than 350 m and oxygen concentrations >5 µmol L^{-1}, but the bilinear parameterization provided a better fit.

It can be argued that the abrupt change in the ΔN_2O/AOU slope is an artifact from the biased ΔN_2O calculations due to the use of the contemporary atmospheric mole fraction of N_2O, resulting in a larger bias for the ΔN_2O values from waters with lower oxygen concentrations, as these waters are also the oldest (Freing, 2009). To test for this effect on the shape of the ΔN_2O/AOU relationship, a simple model calculation was performed: ΔN_2O values were calculated with the preindustrial mole fraction for all samples with oxygen concentrations below 100 µmol L^{-1} as under these conditions the maximum change in the ΔN_2O/AOU shape would be expected. However, the bilinear parameterization still provided a better fit to the "corrected" ΔN_2O/AOU relationship than the quadratic parameterization.

An increase in ΔN_2O/AOU has been attributed to increasing N_2O production from denitrification (Upstill-Goddard et al., 1999) with decreasing oxygen concentrations, but can also result from an increased N_2O yield during nitrification. Farias et al. (2009) found active N_2O production and consumption by denitrification to take place in the upper oxycline of the ETSP OMZ, indicating that incomplete denitrification is responsible for N_2O accumulation. An abrupt slope change in ΔN_2O/AOU ratios may be an indicator for a change in the N_2O production pathway rather than the progressive onset of additional production or the progressive increase of the N_2O yield during nitrification and may indicate a change in the N_2O production mechanism as was suggested from the isotopic composition of N_2O (Ostrom et al., 2000;Popp et al., 2002). The sensitivity of denitrification processes to oxygen is still unclear (Ferguson, 1994), however, substantial nitrogen loss was only observed at oxygen concentrations <5 µmol L^{-1} in the ETSP.

Summary

The nitrous oxide measurements from five cruises to the ETNA and one cruise to the ETSP provide a substantial new data set and allow an intensive evaluation of the processes responsible for N_2O production and transport. N_2O distributions compare well to the results of earlier study for both the Atlantic and the Pacific OMZ. In the ETNA, N_2O profiles showed a broad maximum at the depth of the oxygen minimum, while surface concentrations stayed close to equilibrium in the open ocean and were moderately supersaturated during coastal upwelling at the Mauritanian coast. Mixing between North and South Atlantic Central Water was responsible for some

variability in the oxygen and N_2O distribution but did not explain the variability in ΔN_2O/AOU ratios. ΔN_2O/AOU and $\Delta N_2O/NO_3^-$ were similar to results from previous studies and showed a linear increase with increasing AOU and NO_3^- and indicated nitrification as main source of N_2O.

In the ETSP, N_2O depletion was observed to the south of the investigated area and was associated with oxygen concentrations below 5 µmol L^{-1}, whereas towards the north N_2O accumulation was observed in the oxygen minimum, oxygen concentrations being above 5 µmol L^{-1}. Surface supersaturation values of up to 500 % were observed at the coast, showing substantial outgassing of N_2O due to coastal upwelling. ΔN_2O/AOU showed a significant slope increase at oxygen concentrations below 50 µmol L^{-1} which may be an indication for a change in the N_2O production pathway rather than a progressive increase in N_2O yields with decreasing oxygen concentrations. One possible explanation could be the shift from N_2O production via nitrification to nitrifier-denitrification (Popp et al., 2002), or the onset of denitrification (Farias et al., 2009), however, mixing effects (Yamagishi et al., 2007) can also play a role. Due to the complex interplay of different N_2O production mechanisms, the N_2O production pathway cannot be identified from the ΔN_2O/AOU relationship alone.

3 Sea-to-air and diapycnal nitrous oxide fluxes in the eastern tropical North Atlantic Ocean

Introduction

Nitrous oxide (N_2O) is a potent greenhouse gas with a major contribution of oceanic emissions to its atmospheric budget (Denman et al., 2007). It is produced in the oxic subsurface and deep ocean during microbial nitrification, whereas in anoxic to suboxic parts of the ocean N_2O can be produced and/or consumed during canonical denitrification (see e.g. Bange et al. (2010b)).While large parts of the surface ocean are close to equilibrium with the atmosphere, enhanced emissions are observed during coastal upwelling events due to the transport of N_2O-enriched subsurface waters into the mixed layer (ML, see e.g. Nevison et al. (2004)). Pronounced coastal upwelling in the eastern tropical North Atlantic Ocean (ETNA) occurs seasonally along the coasts of Mauritania and Senegal. Consistently, N_2O emissions are found to be enhanced during winter/spring (Wittke et al., 2010).

In this study we quantify the diapycnal and sea-to-air fluxes of N_2O in the ETNA (incl. the upwelling off Mauritania) to estimate the contribution of diapycnal mixing to the N_2O ML budget: N_2O concentrations in the ML should, at steady state, represent the balance between physical processes such as vertical mixing, air-sea gas exchange with the overlying atmosphere, vertical and horizontal advection and biological processes such as nitrification. The relative importance of the different terms for the N_2O ML budget is discussed. It is found that diapycnal and sea-to-air fluxes are the leading terms in the N_2O ML budget and sea-to-air fluxes are likely overestimated when using common parameterizations for the gas transfer velocity.

Study site

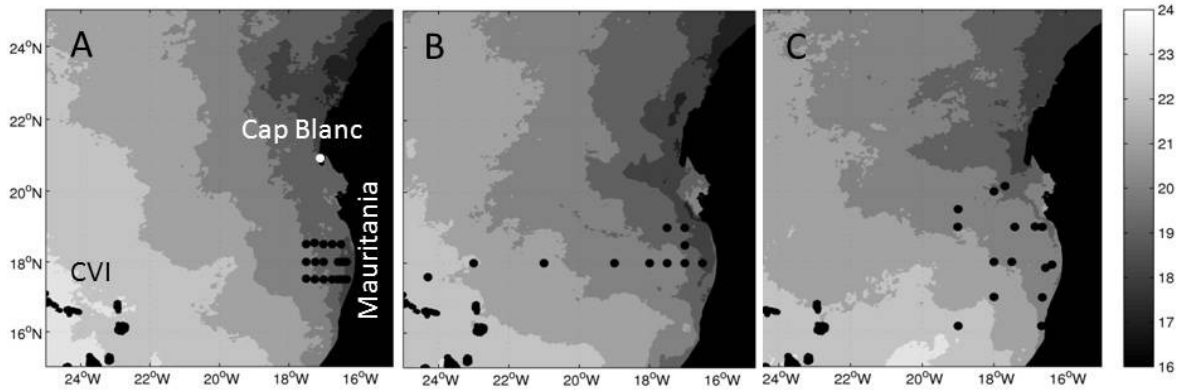

Figure 1: Map with locations of the sampled stations during P347 in January 2007 (A), P348 in February 2007 (B) and ATA3 in February 2008 (C). MODIS monthly sea surface temperatures (in °C) are also shown (http://oceandata.sci.gsfc.nasa.gov/MODISA/Mapped/). CVI stands for Cape Verde Islands.

The investigated area covers the ETNA between the Cape Verde Islands and coast of Mauritania (Fig. 1). A lack of river inputs combined with a narrow continental shelf minimizes additional contributions of N_2O originating from riverine or sedimentary sources. The Mauritanian upwelling system is the most productive southern branch of the Canary Current upwelling system (Minas et al., 1982;Signorini et al., 1999), showing a seasonality which follows the shifting of the Inter-Tropical Convergence Zone (ITCZ) throughout the year (Hagen, 2001). In the region between Cap Vert (~15°N) and Cap Blanc (~21°N) seasonal upwelling takes place during winter/spring (Schemainda et al., 1975). Compared to other eastern boundary upwelling systems, the water column in the ETNA has relatively high oxygen concentrations: minimum oxygen concentrations reach down to 40 µmol L^{-1} (Stramma et al., 2008a). We thus conclude that the main production pathway for N_2O in this region is nitrification.

Methods

N_2O concentration, microstructure and conductivity-temperature-depth (CTD) measurements were conducted during three cruises to the ETNA (Fig. 1). The cruises were part of the German BMBF joint project SOPRAN (Surface Ocean Processes in the Anthropocene, www.sopran.pangaea.de) and the DFG-funded Mauritanian upwelling and mixing process study (MUMP). They were scheduled in the upwelling season in January/February 2007 (R/V Poseidon cruises P347 and P348) and February 2008 (R/V L'Atalante cruise ATA3). Triplicate water

samples taken from the CTD/rosette casts were analyzed for dissolved N_2O on board using a GC/ECD system with a static equilibration method. For details of the method see Walter et al. (2006b). The average precision of the measurements, calculated from error propagation, was ±0.7 nmol L^{-1}.

N_2O sea-to-air fluxes F_{sta} (in nmol m^{-2} s^{-1}) were calculated from the gas exchange equation:

$$F_{sta} = k_w \Delta N_2O = k_w \cdot ([N_2O]_w - [N_2O]_a) \qquad (1),$$

where k_w is the gas transfer velocity and $(N_2O)_w$ is the measured in-situ concentration from the shallowest Niskin bottle in the surface layer (5–10 m). The N_2O equilibrium concentration $(N_2O)_a$ was calculated by using a mean dry mole fraction of 321 ppb (extracted from the monthly time series of atmospheric N_2O from the AGAGE monitoring station Ragged Point on Barbados (see http://agage.eas.gatech.edu) (Prinn et al., 1990)) and the temperature and salinity at the depth of the corresponding Niskin bottle. k_w was calculated using the k_w/wind speed relationships as defined by Nightingale et al. (2000), Liss and Merlivat (1986) and Wanninkhof (1992). Wind speeds were obtained from the ships' underway observations. Alternatively, the sea-to-air flux densities were calculated using the gas transfer velocity parameterization from Tsai and Liu (2003a) that takes into account the reduction of the air-sea gas exchange due to surfactants.

Ocean turbulence profiles were obtained by using microstructure profilers (MSS) as described in detail by Schafstall et al.(2010). Briefly, the MSS are loosely-tethered profilers that measure small-scale velocity fluctuations from which the dissipation rate of turbulent kinetic energy (ε) is determined. To estimate the diapycnal N_2O fluxes into the ML we used the station-average diapycnal diffusivities derived from microstructure measurements from 5 m below the ML depth to the depth of the next deeper N_2O water sample. The ML depth at individual stations was determined using the density criterion described by Kara et al. (2000). To avoid any influence from turbulence caused by the ship, the minimum ML depth was set to be at least 15m deep. The diapycnal diffusivity K_ρ was computed according to Osborn (1980) as

$$K_\rho = \Gamma \frac{\varepsilon}{N^2} \qquad (2),$$

and diapycnal fluxes F_{dia} of N_2O as

$$F_{dia} = K_\rho \cdot \frac{d[N_2O]}{dz} \qquad (3),$$

with the local buoyancy frequency N and the mixing efficiency Γ which was set to a constant value of 0.2 (Oakey, 1982) and the concentration gradient $d[N_2O]/dz$. Fluxes were determined

only from those microstructure profiles which were recorded concurrently with N_2O profile sampling.

Results and discussion

To illustrate the N_2O sea-to-air and diapycnal fluxes, the point estimates were projected onto the distribution of topography along 18°N (Fig. 2). This procedure implicitly assumes that the mean fluxes have larger cross-shore than along-shore gradients (Schafstall et al., 2010).

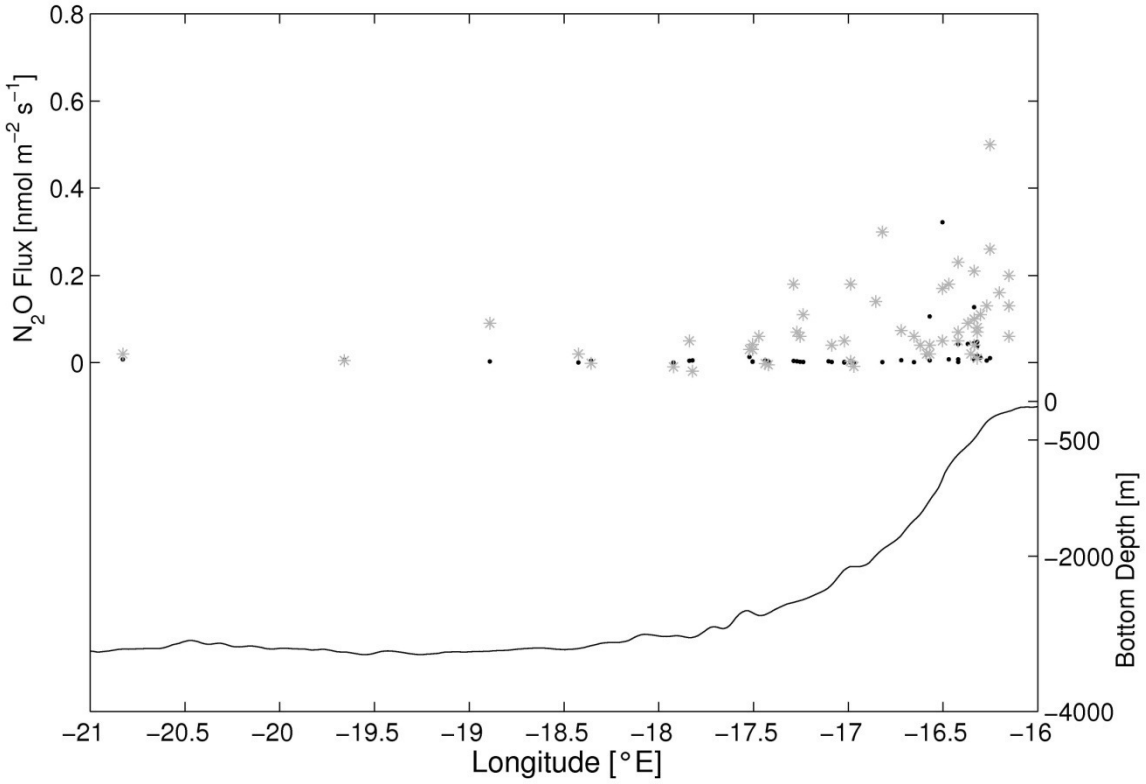

Figure 2: Diapycnal N_2O (black dots, left axis) and air-sea fluxes (grey stars, left axis) projected to 18°N and bottom depth along 18°N (solid line, right axis). Fluxes from stations to the north and south of 18°N were projected onto 18°N according to their distance from the 400 m isobath.

The N_2O sea-to-air fluxes using the Nightingale et al. (2000) parameterization ranged from -0.02 to 0.5 nmol m^{-2} s^{-1} (Fig. 2). Highest fluxes were found close to the shelf break in the zone of active upwelling indicated by low sea surface temperatures (SST). N_2O sea-to-air fluxes decreased with distance from the shelf break, which can be explained by a combination of continuous outgassing from N_2O-enriched waters and its offshore transport within cold filaments.

The open ocean sea-to-air fluxes (west of 18°W) are in agreement with the fluxes computed by Walter et al. (2006b). The coastal fluxes between 18° and 16°W are, despite resulting from a different approach, in reasonable agreement with the model-adjusted sea-to-air fluxes computed by Wittke et al. (2010). The majority of the fluxes are positive indicating a flux of N_2O from the ocean to the atmosphere. However, we also computed negative fluxes which denote a N_2O flux from the atmosphere into the ocean. These negative fluxes correspond to ΔN_2O values of max. -0.3 nmol $L^{-1}$and are therefore within the uncertainty range of the measurements.

The majority of the diapycnal N_2O fluxes were lower than the N_2O sea-to-air fluxes from the Nightingale et al. (2000) parameterization. Largest diapycnal fluxes were found in a narrow band at the shelf break. However, enhanced fluxes were also encountered at the shelf. Since the vertical N_2O gradients were rather uniform, the variability of diapycnal fluxes is predominately due to the variability of diapycnal diffusivities (K_ρ) that were greatly enhanced towards the shelf break (Schafstall et al., 2010).

To determine regional averages of the N_2O sea-to-air fluxes, the point estimates were extrapolated exploiting the dependence of surface ΔN_2O on SST anomaly (Fig. 3a). For this we used eight day mean MODIS Aqua SST data (http://oceandata.sci.gsfc.nasa.gov/MODISA/Mapped/8Day/4km/SST/) that covered the sampling periods.

The calculations were performed for an upwelling box off the Mauritanian coast. The size of the box was defined by the northernmost and southernmost sampled station, that is 20°10'N and 16°10'N respectively, the Mauritanian coastline (except the Banc D'Arguin with bottom depths < 10m) and a line parallel to the shelf break located 170 km offshore. The SST anomaly was defined as the difference between the SST at a respective position in the upwelling box and the background SST averaged along a 100 km long section to the west of the box, thereby taking into account its mean latitudinal dependence.

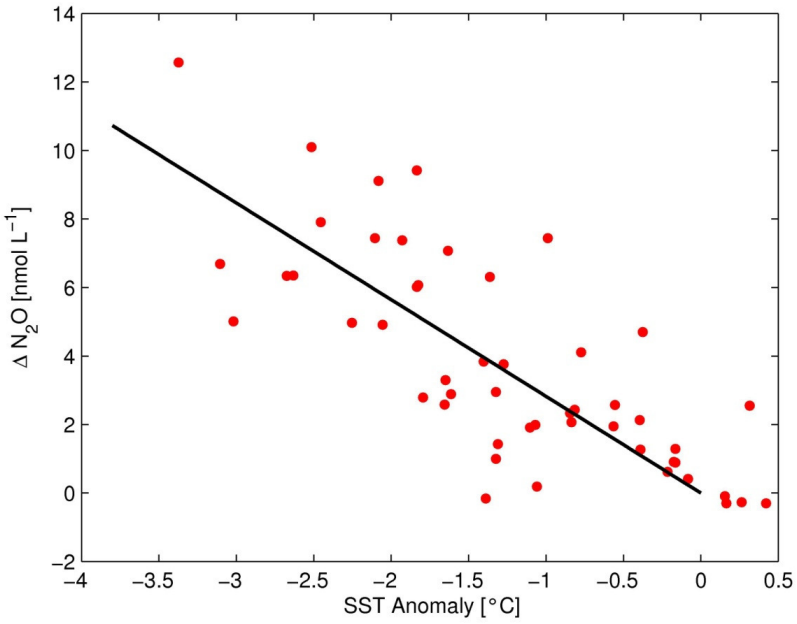

Figure 3: ΔN_2O vs. SST anomaly. The black line denotes the linear regression of ΔN_2O with respect to the SST anomaly for SST anomalies smaller than zero.

130

Negative SST anomalies (SSTA) were significantly correlated with ΔN_2O (r^2=0.54, n=45; Fig. 3). A linear regression was used to calculate the regional surface ΔN_2O distribution from the SSTA (ΔN_2O =C*SSTA, with C =-2.82 nmol L^{-1} $°C^{-1}$). ΔN_2O values from positive SST anomalies were set to zero, assuming that these values were not influenced by upwelling. The corresponding N_2O
135 sea-to-air fluxes, calculated with the Nightingale (2000) parameterizantion, were calculated from three day mean QuikScat wind speeds (ftp://ftp.ssmi.com/qscat/bmaps_v03a/) (Fig. 5a). The resulting flux, averaged over the sampling period and the upwelling box, were 0.0685 (0.0677 to 0.0693) nmol m^{-2} s^{-1}. The confidence intervals were calculated using a Monte Carlo simulation with the uncertainties of the ΔN_2O calibration and an assumed uncertainty of ±2 m s^{-1} for the wind
140 speed as input variables. To account for the large uncertainties in gas exchange velocities, we additionally calculated sea-to-air fluxes using the gas exchange parameterizations by Liss and Merlivat (1986) and Wanninkhof (1992) as lower and upper boundaries (Wanninkhof et al., 2009) (Table 1).

Table 1: Sea-to-air fluxes (F_{sta}) of N_2O calculated with different gas exchange parameterizations and corresponding N_2O production rates at a ML depth of 25 m required to compensate the discrepancy between the sea-to-air flux and the sum of diapycnal (F_{dia}) and vertical advective (F_{adv}) flux.

Parameterization	F_{sta} [nmol m^{-2} s^{-1}]	F_{sta}-(F_{dia}+F_{adv}) [nmol m^{-2} s^{-1}]	Required N_2O production rate [nmol L^{-1} yr^{-1}]
Nightingale (2000)	0.0685	0.048	61 (22 to 76)
	(0.0677 to 0.0693)	(0.018 to 0.060)	
Liss and Merlivat (1986)	0.0461	0.026	33 (-6 to 47)
	(0.0455 to 0.0467)	(-0.005 to 0.038)	
Wanninkhof (1992)	0.0836	0.064	80 (41 to 95)
	(0.0825 to 0.0846)	(0.032 to 0.076)	
Tsai and Liu (2003b)	0.0198	-0.001	-1 (-40 to 14)
	(0.0195 to 0.0201)	(-0.031 to 0.011)	

In contrast to the sea-to-air fluxes, the diapycnal fluxes were averaged in two regions according to their water depths: the shelf (water depth <400 m) and open ocean (water depth ≥400 m) region (Fig. 4). The average fluxes were 0.07 (0.025 to 0.126) nmol m^{-2} s^{-1} for the shelf and 0.004 (0.002 to 0.007) nmol m^{-2} s^{-1} for the open ocean region (Fig. 5b). This results in an overall average flux of 0.019 (0.007 to 0.048) nmol m^{-2} s^{-1}. Confidence intervals were calculated from error propagation, as detailed in Schafstall et al. (2010).

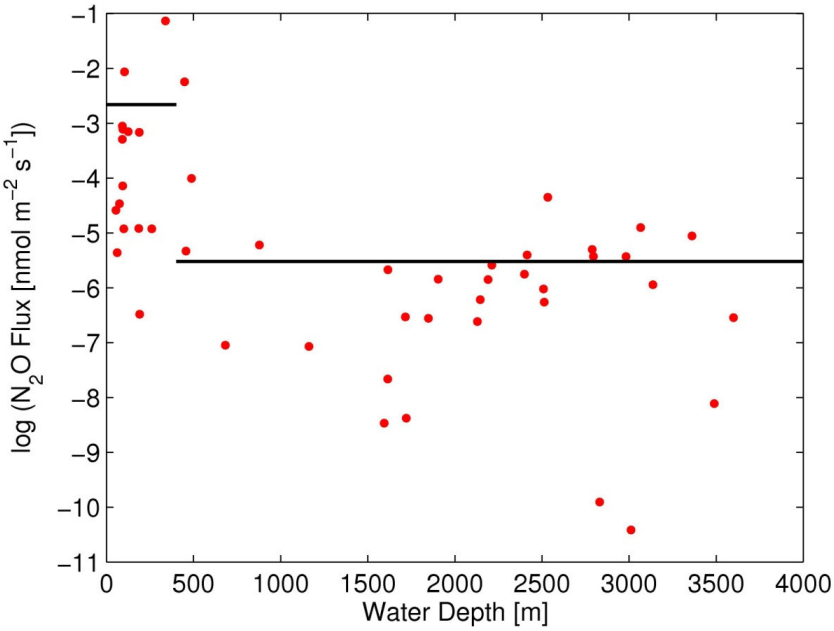

Figure 4: Diapycnal N_2O fluxes vs. water depth. The black lines denote average fluxes for the shelf and for the open ocean region.

Although the diapycnal flux estimate shows large uncertainties and the calculated sea-to-air flux strongly depends on the choice of the gas exchange parameterization, the comparison of the sea-to-air fluxes with the diapycnal flux shows a large discrepancy between the two fluxes. None of the commonly used gas exchange parameterizations is able to adequately close the discrepancy, with the average diapycnal flux only explaining about 25-30 % of the average sea-to-air flux determined from the Nightingale et al. (2000) parameterization.

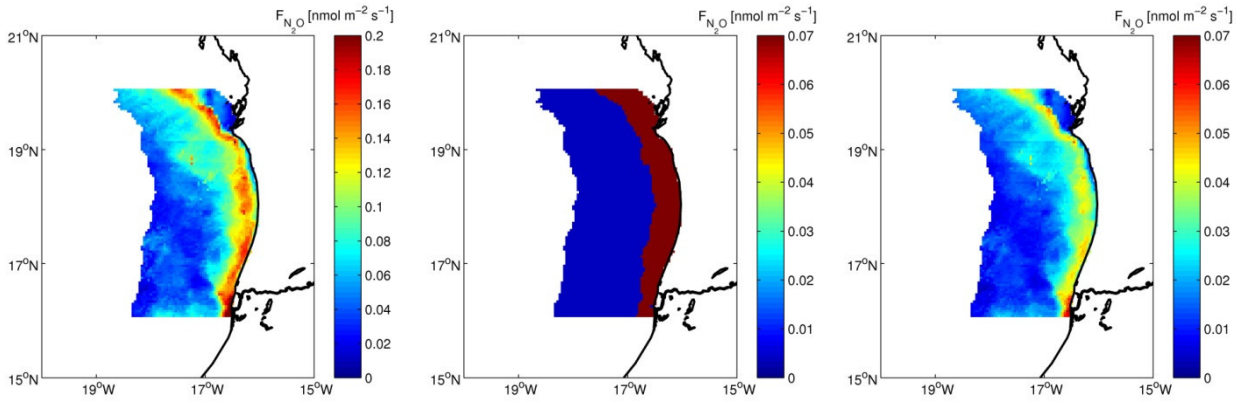

Figure 5: a) Regional distribution of the N_2O fluxes calculated from SST anomalies and averaged over the sampling time using the Nightingale (2000) parameterization. b) Regional distribution of the diapycnal N_2O flux. c) like a) but using the Tsai and Liu (2003b) parameterization. Please note the different scaling of the colorbars in a) and b), c).

The missing oceanic flux required to close the N_2O ML budget cannot be attributed to vertical advection of N_2O resulting from Ekman divergence, however. A regional average of the vertical advective flux (F_{adv}) calculated from wind stress curl using QuikSCAT winds and N_2O concentration differences between the ML and the next deeper available value, from 10 to 30 m below the ML, resulted in 0.0021 nmol m^{-2} s^{-1} (Schafstall, 2010). Vertical advection of N_2O is thus nearly an order of magnitude lower than the diapycnal flux. Similarly, the horizontal flux divergence associated with a mean N_2O gradient along the eastern boundary current is not able to close the N_2O ML budget.

N_2O production from near-surface nitrification has been previously suggested to close the discrepancy between diapycnal and sea-to-air fluxes (e.g., Dore and Karl (1996); Santoro et al. (2010)). Recent publications have shown that nitrification within the euphotic zone can play a significant role in nutrient cycling of the surface ocean (Clark et al., 2008;Santoro et al., 2010;Wankel et al., 2007;Yool et al., 2007).

Based on the estimates of diapycnal, advective and sea-to-air flux we calculated potential N_2O production rates closing the N_2O ML budget, assuming a ML depth of 25 m (Table 1). Although covering a large range, the calculated N_2O production rates are extremely high: Using the Nightingale (2000) parameterization, the average N_2O ML production rate must be as high as about 60 nmol kg^{-1} yr^{-1} (0.16 nmol L^{-1} d^{-1}). This exceeds N_2O production rates in the water column below the ML, quantified to be ≤3.2 nmol kg^{-1} yr^{1} (Freing, 2009), by far. With a molar N_2O yield during nitrification between 0.5 and 0.01 % (Bange, 2008) the corresponding nitrification rates would range from 30 to 1500 nmol L^{-1} d^{-1}. This is significantly higher than the nitrification rates of up to 5 nmol L^{-1} d^{-1} from ML samples from Mauritanian upwelling region measured by Clark et al. (2008) which, for comparison, would yield an N_2O flux of 0.001 nmol m^{-2} s^{-1} at a N_2O yield of 0.1%.

The ML budget could yet be closed using a gas exchange parameterization that takes into account the attenuating effect of surfactants on air-sea gas exchange (Tsai and Liu, 2003a). The resulting average sea-to-air flux for the upwelling box is 0.020 nmol m^{-2} s^{-1} and thus of similar magnitude as the diapycnal flux (Table 1, Fig. 5c). SeaWiFs chlorophyll images (not shown) indicate that the investigated area was highly productive during the sampling periods, which in general has been associated with the occurrence of surface slicks (Lin et al., 2002;Wurl et al., 2011). However, the Tsai and Liu (2003a) parameterization only represents a simplified approach that attributes the occurrence of surfactants with a very large reduction of air-sea gas exchange. Quantitative estimates of the surfactant effects on gas exchange reveal large uncertainties, and most field studies report smaller effects of surfactants on gas exchange (Schmidt and Schneider, 2011;Upstill-Goddard, 2006). A more quantitative understanding of the role of surfactants in

reducing the air-sea gas exchange would require dedicated studies to evaluate different physical and biogeochemical dependencies.

Summary and conclusions

For the first time, microstructure measurements were used to estimate the diapycnal flux of nitrous oxide into the ML. The comparison with sea-to-air fluxes shows a different regional distribution due to the offshore transport of the supersaturated surface waters. The regionally integrated average sea-to-air fluxes using standard parameterizations exceed the average diapycnal flux by a factor of three to four. We argue that this discrepancy is unlikely to be explained by biological N_2O production in the mixed layer or vertical advection alone. Instead, a significantly reduced gas exchange due to the occurrence of surfactants may be a plausible explanation, although there is no direct evidence for a correlation between surfactants and reduced N_2O fluxes so far. Our results indicate that neglecting the surfactant effect on air-sea gas exchange may lead to a significant overestimation of the oceanic emissions of N_2O and other trace gases in highly productive areas.

Acknowledgements

We thank the captains and crews of R/V L'Atalante and R/V Poseidon for their excellent support during the cruises. Also, we thank A. Freing for inspiring discussions about the N_2O mixed layer source and A.Körtzinger, B. Fiedler, T. Tanhua, and M. Glessmer for their support during the field work. Financial support for this study was provided by DFG grants DE 1369/1-1 and DE 1369/3-1 (JS and MD) and BMBF grant SOPRAN FKZ 03F0462A (AK). QuikScat data are produced by Remote Sensing Systems and sponsored by the NASA Ocean Vector Winds Science Team. Data are available at www.remss.com.

4 Contrasting biogeochemistry of nitrogen in the Atlantic and Pacific Oxygen Minimum Zones

Introduction

Nitrogen is a key limiting element for biological productivity and occupies a central role in ocean biogeochemistry (Gruber, 2008). Although most chemical forms of nitrogen in the ocean are bio-available (i.e. fixed nitrogen or "fixed-N") the most abundant form, N_2 is generally not. The sources of fixed-N include river inputs, atmospheric deposition and N_2 fixation (Duce et al., 2008;Gruber, 2008). Sinks of fixed-N, producing N_2, include microbial denitrification and anammox processes, both requiring very low (i.e. suboxic) [O_2] (Devol, 2008). Hence suboxic Oxygen Minimum Zones (OMZs) are the oceanic regions especially associated with denitrification (Cline and Richards, 1972;Codispoti et al., 2001;Ward et al., 2009) and anammox (Lam et al., 2009;Thamdrup et al., 2006;Hamersley et al., 2007;Galan et al., 2009) and play a particularly important role in the global nitrogen cycle as sites of N sinks from the ocean. They are located typically in areas of upwelling with high productivity which exhibit complex cycling of nutrients (Helly and Levin, 2004).

The relative importance of heterotrophic denitrification (a stepwise reduction process involving a number of intermediates, $NO_3^- \rightarrow NO_2^- \rightarrow NO \rightarrow N_2O \rightarrow N_2$), compared to autotrophic anammox (a chemosynthetic process, $NO_2^- + NH_4^+ \rightarrow N_2$) has been debated (Voss and Montoya, 2009;Koeve and Kähler, 2010).

Absence of ammonium in suboxic OMZs that should have accumulated from organic matter breakdown could be indicative of anammox, while the consumption of N_2O requires the denitrification process (Naqvi et al., 2010).

Although OMZs are found in all major ocean basins, their associated nitrogen cycle processes can vary dramatically due to contrasting minimum oxygen levels. In the Eastern Tropical South Pacific (ETSP), suboxic ([O_2] < 5 µmol/l) conditions are found, whereas in Eastern Tropical North Atlantic (ETNA), more relaxed conditions exist ([O_2] > 40 µmol/l) (Karstensen et al., 2008). In addition, fixed-N inputs associated with atmospheric deposition and, possibly, N_2-fixation, vary between the two regions (Chavez and Messie, 2009).

Cruises carried out during the collaborative research project SFB-754 (www.sfb754.de) of the German Research Foundation and the BMBF supported project SOPRAN (Surface Ocean Processes in the Anthropocene: www.sopran.pangaea.de) provided unique opportunities to sample

nitrogen species in these two contrasting regions. Here we present a comparison of N_2O concentration and stable nitrogen isotope distributions, which were measured in both OMZs to highlight the similarities and differences in nitrogen cycling between the two regions.

Sampling and analytical methods

In the Pacific OMZ, samples were collected onboard the R/V Meteor (M77 Legs 3 and 4) in December 2008 and January 2009 (Fig. 1). In the Atlantic OMZ, samples were collected on the R/V L'Atalante (cruise leg ATA03) during February 2008 from Dakar to Cape Verde Islands and on the R/V Meteor (M80) in December 2009 covering the region south to Cape Verde Islands. At each station, water samples were collected using 12 l Niskin bottles on a CTD rosette system equipped with temperature, pressure, conductivity and oxygen sensors. Nutrients and oxygen were determined onboard according to Grasshoff *et al.*(1999). Triplicate water samples were taken from the CTD/rosette casts and were analyzed for dissolved N_2O onboard using a static equilibration method. For details concerning the N_2O method, see Walter et al. (2006b).

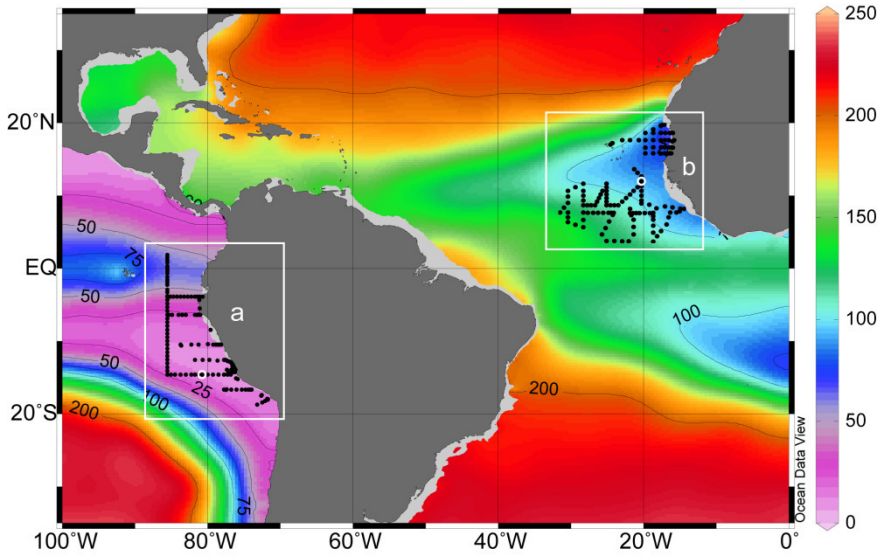

Figure 1: Oxygen distribution at 200m (Schlitzer, R., Ocean Data View, World Ocean Atlas 2005, http://odv.awi.de/en/data/ocean/world_ocean_atlas_2005/) with CTD station locations in the Pacific (a) and Atlantic (b) study regions referred to in the text. White circles indicate station 84 (a) and station 5 (b).

Water samples for $\delta^{15}N$ nitrate and nitrite analysis were collected in 125 ml HDPE bottles and kept frozen prior to analysis. For logistical reasons, samples from the M77 cruise that contained

low to negligible levels of nitrite ($[NO_2^-]$ < 0.1 µmol/l) were acidified and stored at room temperature, whereas samples with significant $[NO_2^-]$ were kept frozen prior to the $\delta^{15}N\text{-}NO_2^-$ analysis. Aliquots of these samples were treated in the laboratory with sufficient sulfanilic acid to remove $[NO_2^-]$ prior to $\delta^{15}N\text{-}NO_3^-$ analysis with any remaining sample stored at room temperature.

The isotopic composition of dissolved nitrate ($\delta^{15}N\text{-}NO_3^-$) and nitrite ($\delta^{15}N\text{-}NO_2^-$) was measured using the Cd-reduction/azide method (McIlvin and Altabet, 2005) with addition of NaCl as described by Ryabenko *et al* (2009). All the samples from the Atlantic study region and 50% of the Pacific samples were analyzed at the IFM-GEOMAR in Germany, while c. 50% of the Pacific samples were analyzed at SMAST in the USA, using the same method. The only difference was that at SMAST N_2O produced by this method was analyzed isotopically, whereas at IFM-GEOMAR N_2O was converted on-line to N_2 for isotopic analysis. The detection limit at IFM-GEOMAR was 0.2 µmol/l of nitrate or nitrite with the precision of the $\delta^{15}N$ measurements being ± 0.2‰. The detection limit at SMAST was slightly higher, 0.5 µmol/l, with the same precision of ^{15}N measurements.

The analyses of the Pacific deep water samples (> 1500 m) from both labs gave near identical values of $\delta^{15}N\text{-}([NO_2^-]+[NO_3^-])$ of 5.69 ± 0.7‰ (IFM-GEOMAR; n=31) and 5.62 ± 0.4‰ (SMAST; n=8) respectively. The Fisher test showed that we can merge the two data sets with a confidence level > 95%. The resulting mean value of 5.64 ± 0.7‰ (n=39) lies between previously published values of 6.5‰ Voss (2001) and 4.5‰ Sigman (1997) for the deep North Pacific Ocean. Deep waters of the Atlantic showed very similar values as those of the Pacific (5.3‰ ± 0.5 for > 2000 m, see auxiliary material table 1).

Hydrographic setting of the two study regions

In the North Equatorial Atlantic region, the eastward flow of the North Equatorial Counter Current (NECC) and North Equatorial Under Current (NEUC) supplies oxygen rich waters to the Atlantic OMZ (Glessmer et al., 2009). The water mass distribution in this Atlantic OMZ study region (Fig. 1b) is affected by the Cape Verde Frontal Zone, which marks the boundary between *North* and *South Atlantic Central Waters* (NACW, SACW). This separates well-ventilated waters of the subtropical gyre in the north from less-ventilated waters to the south. Our CTD data (Fig. 2) show water mass properties < 500 m intermediate between those of NACW and SACW. *Antarctic Intermediate Water* (AAIW: 3-5°C, S=34.5) is found at ~1000 m with *North Atlantic Deep Water*

(NADW) filling the depth range between ~1000 and 4000 m (Fig. 2b). A summary of the water masses properties found in both study regions is presented in Auxiliary material, Table 1.

In the South Pacific, the Equatorial Undercurrent (EUC), Southern Subsurface Counter Currents (SCCs), and the Southern Intermediate Counter Currents (SICC) supply *13°C Equatorial Water* (13CW, $25.8 < \sigma_\theta < 26.6$) to the eastern Pacific OMZ (Stramma et al., 2010a). The westward flowing South Equatorial Current (SEC) may recirculate some 13° water from the OMZ by returning eastward as the South Subsurface Counter Current at 3–5°S (Schott et al., 2004). The origin of 13CW is remote from the equator (Qu et al., 2009) mostly as *Subantarctic Mode Water* (SAMW; (Toggweiler et al., 1991)) and transports very oxygen depleted waters to the OMZ, due to its relative old age. The *South Pacific Subtropical Underwater* (STUW) is a likely O_2 source from the south which is centered on the $\sigma_\theta = 25.0$ isopycnal and is well-ventilated across nearly the full width of the subtropical gyre (O'Connor et al., 2002). The low-salinity water ($S < 34.5$) found between c. 500 and 1000 m southward of 10°S is *Antarctic Intermediate Water* (AAIW). *South Pacific Deep Water* (1.2 – 2°C) is found between c. 1500-3000 m and is underlain by *Lower Circumpolar Water* (LCPW) (Fiedler and Talley, 2006) (Fig. 2a).

Because of the differences in hydrography and significantly lower oxygen supply, the Pacific OMZ is much more intense as compared to the Atlantic (Karstensen et al., 2008). The resulting very low oxygen concentrations favor metabolic pathways that convert nitrogen from biologically reactive "fixed" forms (for example nitrate, nitrite or ammonium) to N_2 via denitrification and/or anammox.

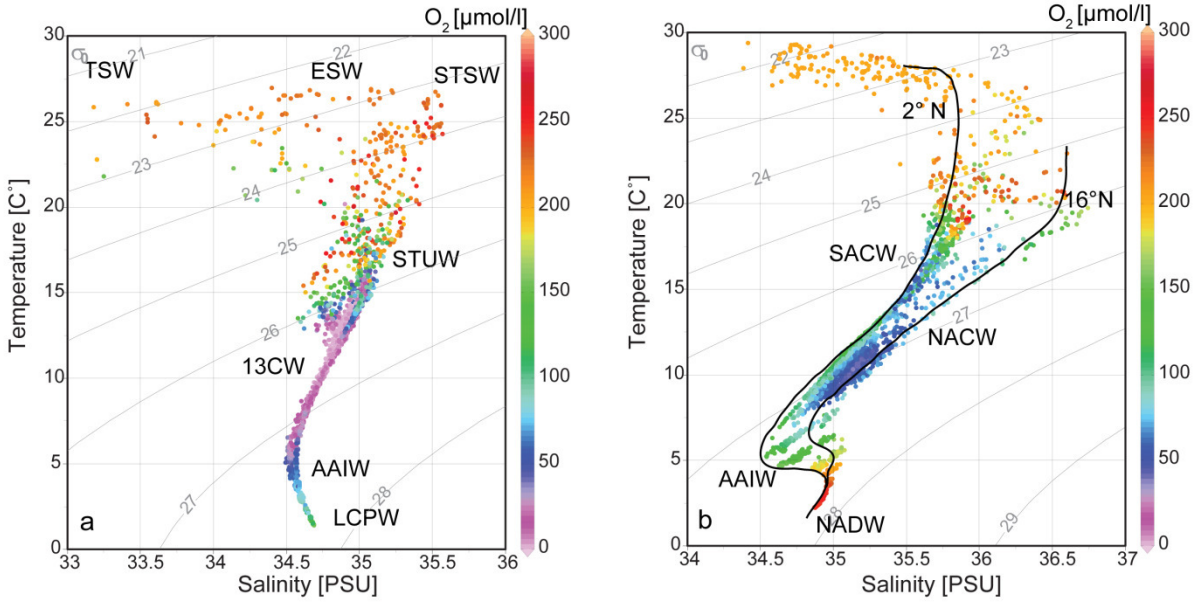

Figure 2. T-S diagrams with O_2 color coded for the Pacific (a) and the Atlantic (b) study regions from CTD data collected during the M77, M80 and L'Atalante cruises.

4. Results and discussion

4.1 Vertical distribution of nitrogen species and isotopes

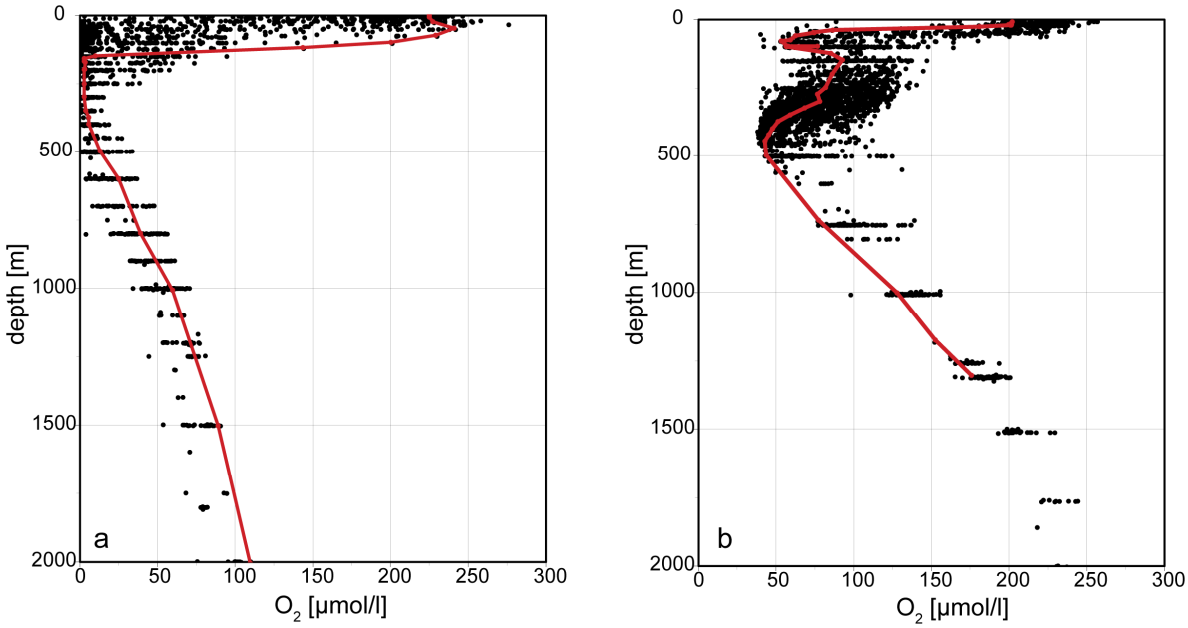

Figure 3. Oxygen distribution in the Pacific (a) and the Atlantic (b) study regions, as measured on the cruises M77, M80 and L'Atalante. The red lines show the water-column profiles for M77 station 84 in the Pacific and M80 station 5 in the Atlantic.

General: Dissolved O_2 varies considerably in its depth distribution between the Atlantic and Pacific study regions as shown in figure 3. Figure 4 presents typical water column profiles for oxygen and several nitrogen related properties from both study regions (outside of the upwelling zones). Stations 5 (Atlantic, M80) and 84 (Pacific, M77) were chosen due to synoptic availability of N_2O, $\delta^{15}N$ and $[NO_2^-]$ data. The geographic positions of the stations are indicated on figure 1 by white circles.

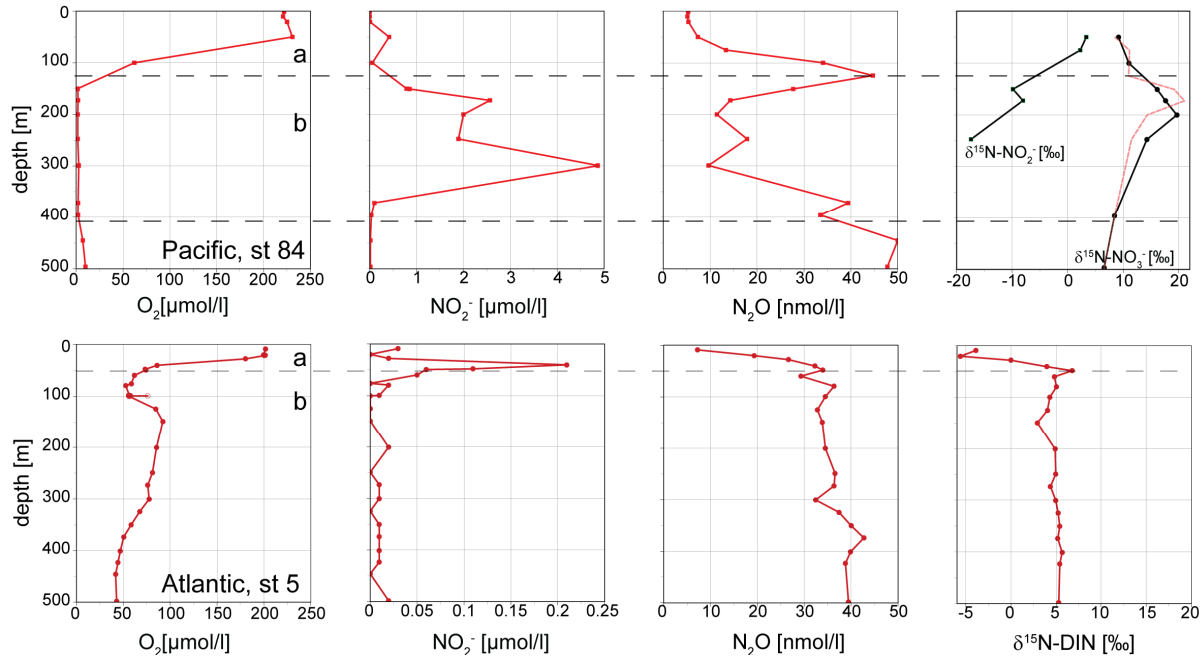

Figure 4. Typical water column profiles from the SE Pacific OMZ (st. 84, 81°W/14°S) from the M77 cruise (upper panels) and the NE Atlantic OMZ (st. 5, 20.5°W/12.3°N) from the M80 cruise (lower panels). Black lines in the Pacific indicate $\delta^{15}N\text{-}NO_3^-$ and $\delta^{15}N\text{-}NO_2^-$, and the red line indicates $\delta^{15}N\text{-}DIN$ (NO_3^- + NO_2^-). Note the different of scales for $\delta^{15}N$: -20 to +20‰ in the Pacific and -5 to +20‰ in the Atlantic.

Pacific Study Region: In the Pacific study region, the OMZ contains mostly 13CW, with oxygen concentrations < 2 µmol/l at depths as shallow as ~50 m and as deep as ~550 m. The Pacific station (Fig. 4, upper panels) is also characterized by a broad oxygen minimum with [O_2] < 2 µmol/l (170–400 m). Two [NO_2^-] maxima are located in the upper oxycline (50 m) and the core of the oxygen minimum (300 m). We divide the Pacific profile into layers (a) and (b) to focus the discussion of nitrogen transformations at the upper OMZ boundary and its core.

Layer (a) (0-120 m) includes a ~70 m deep mixed layer and the 50 m deep euphotic zone (Chavez and Messie, 2009), and contains water with the highest oxygen concentrations as well as a very sharp oxycline at 80-120 m in which [O_2] drops from ~150 to 20 µmol/l. The primary nitrite maximum lies close to the base of the euphotic zone and can be a consequence of two processes (Lomas and Lipschultz, 2006): light-limited, incomplete assimilatory reduction of nitrate by phytoplankton and microbial ammonium oxidation to nitrite (i.e. the first step of nitrification). Near-surface N_2O is close to saturation and increases within the oxycline from ~12 to ~45 nmol/l. The observed increase in nitrous oxide within the oxycline can be associated with ammonia oxidation (Codispoti, 2010), which leads to an efflux of N_2O from the mixed layer to the atmosphere via gas exchange. The concentrations of [NO_3^-] and [NO_2^-] above 80 m in layer A at this station were below our detection limit for $\delta^{15}N$ measurement (0.2 µmol/l). Higher near-

surface DIN concentrations were observed at other stations along the 86°W transect and the corresponding $\delta^{15}N\text{-}NO_3^-$ values were as high as 20‰. High surface $\delta^{15}N\text{-}NO_3^-$ is likely the result of incomplete nutrient utilization and fractionation during nitrate assimilation (Granger et al., 2004).

$\delta^{15}N\text{-}NO_2^-$ is generally much lower and its difference from $\delta^{15}N\text{-}NO_3^-$ increases from layer A to layer B, coming close to a value of ~30‰ in layer (b). Relative ^{15}N depletion in nitrite can be explained by isotopic fractionation during nitrate reduction to nitrite. A smaller difference between $\delta^{15}N\text{-}NO_3^-$ and $\delta^{15}N\text{-}NO_2^-$ observed in the oxycline is likely due to nitrification as the fractionation effect of the process is significantly smaller (~13‰) (Casciotti, 2009;Casciotti and McIlvin, 2007) than the one expected for denitrification (~25‰) (Barford et al., 1999; Granger et al., 2006). Thus there is evidence for a clear switch from nitrification to denitrification with depth.

Layer (b) (120 m to 400 m). O_2 concentrations in this layer drop below 5 µmol/l and there is a strong increase in $[NO_2^-]$ towards a "secondary" maximum at the core of OMZ. N_2O concentrations drop sharply within the OMZ core to ~10 nmol/l and increase again only towards the lower border of the layer. Denitrification is the only N-removal process which is known to consume N_2O, hence it is likely that both the increase in $[NO_2^-]$ and the increase and decrease in $[N_2O]$ within this layer can be attributed to different stages of canonical denitrification ($NO_3^- \rightarrow NO_2^- \rightarrow N_2O \rightarrow N_2$) (Bange, 2008). The vertical profiles, especially the minimum in N_2O within the OMZ's core, provide strong evidence that all stages of canonical denitrification influence nitrogen speciation in this layer. The observed increase in $\delta^{15}N\text{-}NO_3^-$ and decrease in $\delta^{15}N\text{-}NO_2^-$ at the base of the layer B are also consistent with denitrification, which leaves $[NO_2^-]$ depleted in ^{15}N. Interestingly, the difference between $\delta^{15}N\text{-}NO_3^-$ and $\delta^{15}N\text{-}NO_2^-$ values are higher (~30‰) than fractionation factor calculated for N-loss process within the OMZ (~11.4‰, see below) but close to the expected value for pure culture studies (28.6‰) (i.e. Barford et al., 1999). The reason for this could be the nitrite oxidation, which has an inverse isotopic fractionation effect, leaving $\delta^{15}N\text{-}NO_2^-$ depleted in ^{15}N (Casciotti, 2009). Nitrite oxidation can appear in nitrification-denitrification coupled systems or in anammox as a side-reaction (i.e. Straus 1998, van de Graaf 1996). The deep $[NO_2^-]$ maximum can also support anammox, which has been observed in several previous studies of this region (Galan et al., 2009;Hamersley et al., 2007;Lam et al., 2009).

Atlantic Study Region: In the Atlantic study region, the oxygen profile has two minima at ~70 m and ~400 m (Fig. 3b). The shallow minimum is strongest between Senegal and the Cape Verde Islands and is probably caused by enhanced subsurface remineralization associated with high biological productivity and a shallow mixed layer (Karstensen et al., 2008). The deeper minimum is more prominent south of Cape Verde and is associated with the water mass boundary between Central Water and AAIW (Stramma et al., 2005). The double oxygen minimum (Fig. 3) is

therefore caused by the mixing of two water masses from the North and South (NACW and SACW) of the Atlantic region.

The profiles from the Atlantic station (Fig. 4, lower panels) are considerably simpler, with fewer subsurface features. Once again, two layers have been distinguished based on oxygen concentration and its influence on dominant nitrogen cycle processes.

Layer (a) (0 – 50 m) includes the surface mixed layer which extends to ca. 30 m. This layer includes the steepest part of the oxycline, a strong increase in N_2O with depth, and a primary nitrite maximum which lies at the base of this layer. The $\delta^{15}N$ of DIN increases steadily throughout this layer and reaches a maximum at a depth close to the primary nitrite maximum. These features can be attributed to a combination of remineralization of organic matter, nitrite excretion by phytoplankton after nitrate reduction and nitrification. In contrast to the Pacific study region, the surface layer has minimum values of $\delta^{15}N$ in DIN, with some values being strongly negative (e.g. -5.6‰ at 20 m).

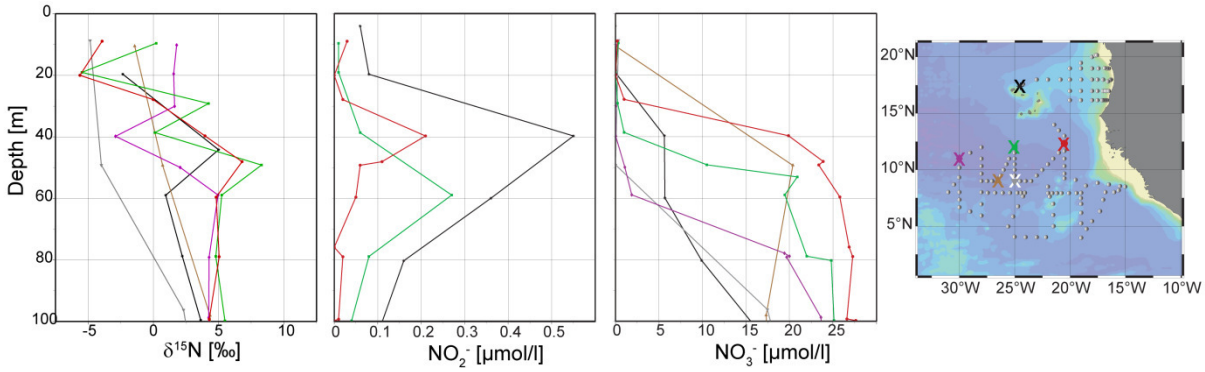

Figure 5. Shallow vertical profiles of M80 stations south to Cape Verde islands in the Atlantic. Stations: 1 (TENATSO) and 5, 67, 76, 81 and 87 located between 12°N and 9°N.

Examination of near-surface profiles from the Atlantic (Fig. 5) reveals negative values of $\delta^{15}N$ in DIN within the surface mixed layer at stations located South of Cape Verde and at the TENATSO station. There is a tendency for the values to be most negative at the shallowest depths (20 m) with extremely low $\delta^{15}N$ values almost always observed in this depth range. Generally below 20 m, both NO_3^- $\delta^{15}N$ and concentration increase with depth. We argue that the source of nitrate at the very surface of stations with low $\delta^{15}N$ NO_3^- is from atmospheric deposition (see below, section 4.2.5). Nitrite concentration was below the detection limit of 0.02µmol/l, while [NO_3^-] concentrations in the region are about 0.1 – 0.5 µmol/l. Thus contamination via nitrite cannot be the reason for low $\delta^{15}N$ values. In regions more influenced by upwelled waters, the near-surface values were higher in the range +4–+7‰ and more consistent with an isotopic signal from upwelled NO_3^-. Even though these concentration levels lie close to our detection limit for $\delta^{15}N$

measurements (0.2 µmol/l), all surface water samples were measured 5 times and gave reliable values with > 95% reliability and ± 0.3‰ standard deviation. Further, laboratory tests with dilutions of $\delta^{15}N$ standards showed no suggestion of any systematic change of measured $\delta^{15}N$ values with decreasing $[NO_3^-]$ concentrations.

Apparent exceptions are found at stations 87 at 25°W and 67 at 30°W (marked with white and purple crosses in Fig. 5) where low $\delta^{15}N$ of -4 and -3‰ are observed at 50 and 40 m respectively. Corresponding nitrate concentrations are 0.25 and 0.20 µmol/l, respectively, and nitrite concentration is below the detection limit. While these values appear to be too deep to be influenced by atmospheric input, in fact the mixed layer is indeed deeper at these stations: 40-50 m instead of 20m. Thus, we believe, that the low $\delta^{15}N$ signal at these stations could also originate from atmospheric deposition. To be conservative, we only considered the upper 20m water column for our calculations of nitrogen fluxes in the Table 1 (see section 4.2.5).

At station 1 (TENATSO, marked with black cross in Fig.5) between 40-60m isotope signature lay $0< \delta^{15}N<5$ with nitrate concentrations increasing up to 6 µmol/l and nitrite up to 0.55 µmol/l. Elevated nitrate and nitrite concentrations having a $\delta^{15}N$ signature of only few per mil is here likely due to N-fixation, which was observed in this region during other studies (i.e. Bourbonnais 2009).

Layer (b) (below 50 m) includes the core of the Atlantic OMZ. In contrast to the Pacific OMZ, the Atlantic profiles had no secondary nitrite maximum, and $\delta^{15}N$ values and N_2O concentrations remained relatively constant with depth. The N_2O profiles show no evidence for consumption as was seen in the Pacific. This is a clear indication for the absence of significant denitrification in this region. A slight increase in N_2O with depth below 50 m can be explained by nitrification (Walter et al., 2006b).

4.2 Property-Property Distributions

Nitrate to Phosphate: Figure 6 presents the NO_3^- to PO_4^{3-} relationship (with dissolved oxygen concentrations as the color code) for the Atlantic and Pacific study regions. According to Redfield stoichiometry, the average ocean ratio of N:P is 16:1. Deviations from this ratio can be an indicator for which nutrient sink/source processes are dominating in the ocean region of interest. Waters in the Pacific study region are highly N-deficient (N:P<16), with the highest deficits found in oxygen minimum waters (purple coloring, Fig 6a) and associated with the N-removal processes denitrification and/or anammox (Deutsch et al., 2001). Data from the Atlantic study region show strong positive deviations from the 16:1 Redfield stoichiometry, which can be a result of

N_2-fixation (Hansell et al., 2004;Michaels et al., 1996;Gruber and Sarmiento, 1997) and/or nutrient uptake and/or remineralization with non-Redfield stoichiometry (Monteiro and Follows, 2006). Positive deviations from Redfield stoichiometry can also, potentially, be caused by atmospheric deposition of nitrogen (Duce et al., 2008). Note that our treatment of deviations in $[NO_3^-]$:$[PO_4^{3-}]$ does not include the nitrite (NO_2^-) produced under low oxygen. Including NO_2^- in the calculation, however, does not change the ratios significantly (average DIN:$[PO_4^{3-}]$ = 15.04 in the Pacific and 16.92 in the Atlantic regions).

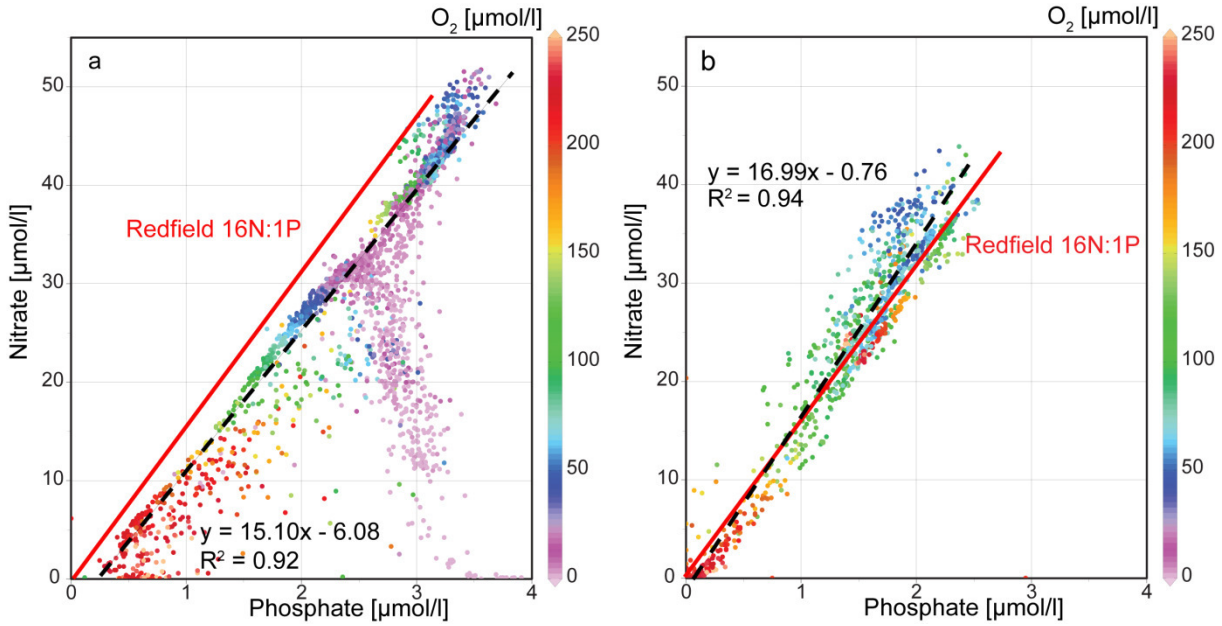

Figure 6. $[NO_3]$:$[PO_4]$ relationships in the Pacific (a) and the Atlantic (b) study regions. The data are color-coded by oxygen concentration. Note that the average $[NO_3]$:$[PO_4]$ relationship in the Pacific was calculated for $[O_2]$>50µmol/l.

N_2O vs. AOU: Property-property plots of ΔN_2O to apparent oxygen utilization (AOU) (with $[O_2]$ as the color code) are presented in figure 7, where AOU is the difference between the measured dissolved oxygen concentration and its equilibrium saturation concentration in water with the same physical and chemical properties.

ΔN_2O is the excess nitrous oxide and is defined as the difference between the measured N_2O and the equilibrium N_2O concentration at the time when a water parcel had its last contact with the atmosphere. Because the atmospheric N_2O mixing ratios have been increasing since 1800, the calculation of excess N_2O has to take into account the age of the water parcel at the time of the measurement. Freing *et al* (2009) showed that the difference in the slopes of ΔN_2O vs. AOU associated with different ways of calculating excess N_2O can be as much as 17%. The methods used include the transit time distribution (TTD) approach, where CFC-12 and SF_6 data are used to calculate a meanage of a water parcel. Alternatively, a "layer" method (Walter et al., 2004) uses

different equilibrium N_2O concentrations for mixed layer and deep waters. For the sake of simplicity we used here the "contemporary" approach, where the $[N_2O]_{eq}$ is calculated based on the contemporary atmospheric dry mole fraction of N_2O (N_2O of 322 x 10^{-9} for Pacific data and 323 x 10^{-9} for Atlantic data, http://agage.eas.gatech.edu/) (Nevison et al., 2003;Yoshinari, 1976). Although the contemporary method may lead to underestimations of ΔN_2O vs. AOU slopes of up to 17% (Freing et al., 2009), it does not affect the qualitative comparison of the Atlantic and Pacific study regions given below. An overall linear relationship of ΔN_2O to AOU for the upper oxycline (0 to 350 m in the Pacific and 0 to 500 m in the Atlantic) (Fig. 7) was observed previously in both regions (Oudot et al., 1990;Elkins et al., 1978;Nevison et al., 2003).

However, the Pacific relationship has two different slopes for oxygen concentrations below and above 50 µmol/l (which corresponds here to an AOU of c. 208 µmol/l). For $5 < [O_2] < 50$ µmol/l is 0.30 ± 0.05 the slope of the ΔN_2O to AOU relation is significantly higher than the one for $[O_2] > 50$ µmol/l (0.104 ± 0.006). This is suggestive of a higher yield of N_2O per mole NO_3^- produced by nitrification at low oxygen levels (Goreau et al., 1980;Stein and Yung, 2003). In Pacific waters with $[O_2] < 5$ µmol/l (AOU of c. 248µmol/l), ΔN_2O concentrations decrease again to near-zero values, indicative of the N_2O consumption at very low oxygen levels mentioned above. Corresponding changes in slope are not visible in the Atlantic data, likely because there are so few data with $[O_2] < 50$ µmol/l. The slopes of the ΔN_2O vs. AOU relationships for $[O_2] > 50$ µmol/l are remarkably similar in both regions: 0.104 ± 0.006 and 0.111 ± 0.003 in the Pacific and Atlantic, respectively. These values lay close to the values of 0.107 (Walter et al., 2006b) measured for tropical Atlantic but lower than those from Oudot (2002) of 0.211. The values from Oudot (2002) paper, however, should be taken with particular care as the mean atmospheric mixing ratio of N_2O presented in the paper (316 x 10^{-9}) seems to be unrealistic high in comparison to the mean atmospheric background dry mole fraction of N_2O at the time of their measurements (308 x 10^{-9}, http://agage.eas.gatech.edu/).

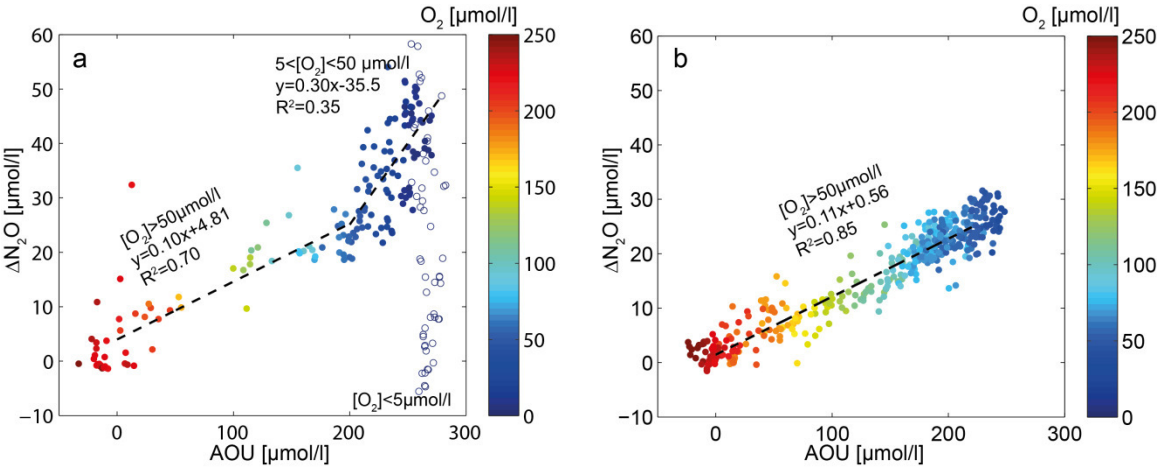

Figure 7: ΔN_2O vs. AOU in the upper 350 m (Pacific) and upper 500 m (Atlantic) with oxygen concentrations as color code in the Pacific (a) and in the Atlantic (b) study areas. Black dashed lines show the correlation between ΔN_2O and AOU, empty circles indicate the samples with $[O_2] < 5\mu mol/l$.

This higher yield of N_2O under reduced concentrations of oxygen was observed earlier (Goreau et al., 1980) and was attributed to increasing N_2O yield when ammonia oxidizing microbes become O_2 stressed. This view was challenged by Frame and Casciotti (2010), who showed that ammonia-oxidizing bacteria do not have increased N_2O yield under low O_2 conditions under environmentally relevant culture conditions. The most recent findings from both the Atlantic and Pacific oceans indicate however that archaeal ammonia-oxidizers (AOA) rather than bacteria may be key organisms for the production of oceanic nitrous oxide and can exhibit higher production rates under low oxygen conditions (Santoro et al, 2011;Löscher et al., 2011).

Regarding the Pacific observations at very low O_2, N_2O removal provides strong evidence for the occurrence of denitrification given its specificity for this process (Bange et al., 2005). However, the amount of N_2O removed (c. 50 nmol/l) is an order of magnitude lower than the observed amount of NO_3^- removal. Hence it gives no indication of the quantitative significance of this process for overall fixed nitrogen removal (e.g. compared to anammox).

Additional insight into N-loss processes is gained here from nitrogen isotope ($\delta^{15}N\text{-}NO_3^-$) and fixed nitrogen deficit (N') data.

$\delta^{15}N\text{-}NO_3$ vs.N_2O and N'. $^-$*:* Figure 8 shows ΔN_2O vs. $\delta^{15}N\text{-}NO_3^-$ (with color coding indicating oxygen concentration) in the two study regions, which helps to reveal processes responsible for the production or consumption of nitrous oxide. In the Atlantic, the profiles and property-property plots show no evidence of N_2O consumption and the nitrogen isotope values stay close to the oceanic average of 5‰, which is also consistent with a lack of denitrification. As discussed

above, the dominant process affecting N_2O in the Atlantic study region is production due to nitrification. For Pacific oxygenated waters ($[O_2] > 5$ µmol/l) the ΔN_2O vs. $\delta^{15}N\text{-}NO_3^-$ relationship is similar to that found in the Atlantic. The reason for some very low $\delta^{15}N\text{-}NO_3^-$ values in Atlantic surface water is discussed below. A trend towards high $\delta^{15}N\text{-}NO_3^-$ values in the Pacific study region (Fig. 8a) can be associated with denitrification at lower O_2 concentrations ($[O_2] < 5$ µmol/l, purple coloring) or with nitrate assimilation in near surface waters ($[O_2] > 200$ µmol/l, red coloring). These two processes cannot be distinguished in figure 8a as the ΔN_2O is close to zero both for waters with $[O_2] < 5$ µmol/l (due to denitrification), and for waters with $[O_2] > 200$ µmol/l (due to N_2O equilibration with the atmosphere). In order to differentiate between these two processes the correlation between $\delta^{15}N\text{-}NO_3^-$ and the N-deficit was calculated (Fig. 8c).

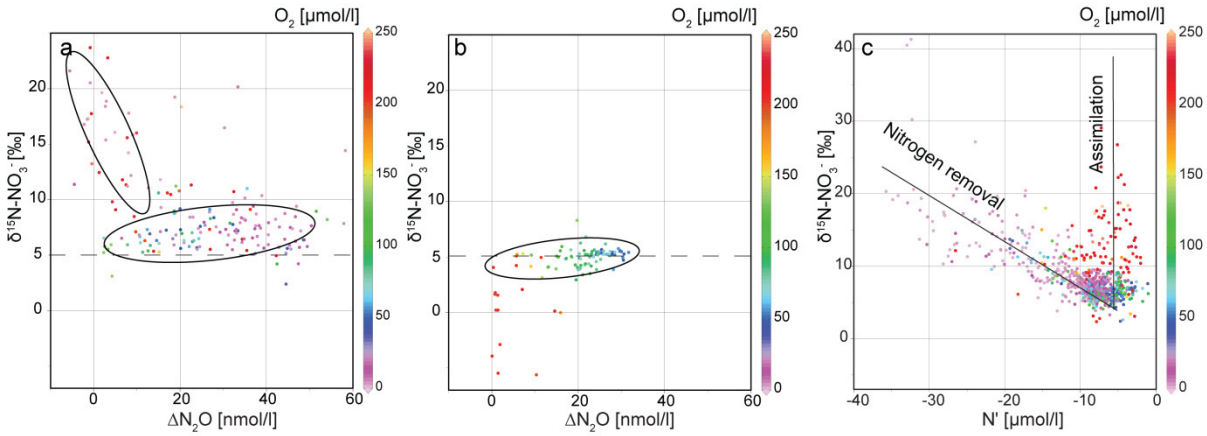

Figure 8. $\delta^{15}N\text{-}NO_3^-$ vs. ΔN_2O in the Pacific (a) and in the Atlantic (b) study areas and (c)the $\delta^{15}N$ vs. N' distribution in the Pacific. The data are color-coded by oxygen concentration. The nitrogen deficit in the figure 8c was calculated as $N' = [NO_3^-] + [NO_2^-] - 16\times[PO_4^{3-}]$). $\delta^{15}N$ vs. N' data reveal two clear trends in the Pacific study region.

In the core of the OMZ, the $\delta^{15}N$ of DIN is inversely correlated with N' (mainly negative values) and hence with N-removal, whereas in high-oxygen, near-surface waters, $\delta^{15}N\text{-}NO_3^-$ increases independent of N', reflecting fractionation during NO_3^- assimilation by phytoplankton in the euphotic zone (Granger et al., 2004).

Isotope fractionation and N-loss in the Pacific OMZ: The reduction of nitrate to nitrite is the first step of the denitrification process and is also an essential source of NO_2^- for fuelling anammox (Lam et al., 2009). We will next examine the isotope fractionation signal associated with this reduction step. The kinetic isotope fractionation factor can be represented as either $\alpha_r = {}^{15}R/{}^{14}R$ or $\varepsilon_r = (1 - \alpha) \times 1000$, where ^{15}R and ^{14}R are the rates of denitrification for $^{15}NO_3^-$ and $^{14}NO_3^-$, respectively. An effective or "apparent" value for the fractionation factor for nitrate reduction (ε_r) can be calculated through application of the Rayleigh model to the field data or the "diffusive"

model of Brandes (1998), where diffusive transport is included. The model of Brandes (1998) requires knowledge or estimations of denitrification rates and the coefficient of eddy diffusivity for fractionation factor calculation. For the Peruvian OMZ neither of those two parameters are known however, thus we calculated ε^* with the Rayleigh model. This model assumes removal from a closed pool of nitrate with constant isotopic fractionation. Hence:

$$\delta^{15}N\text{-}NO_3^-{}_{(f)} = \delta^{15}N\text{-}NO_3^-{}_{(f=1)} - \varepsilon^* \times \ln(f), \quad (2)$$

where f is the fraction of consumed NO_3^-, $f = [NO_3^-]/(16\times[PO_4^{3-}])$, the ε^* is an "apparent" fractionation factor, in this case for a nitrogen removal process.

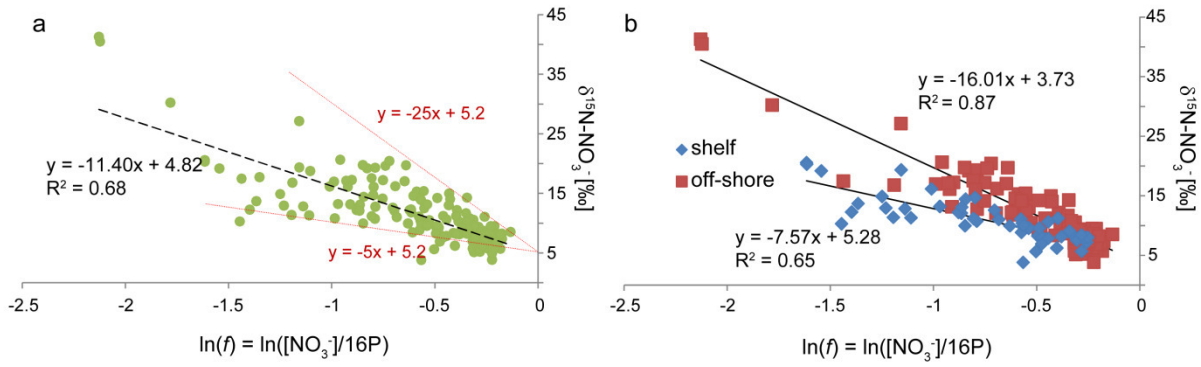

Figure 9. a) Application of Rayleigh model to assess fractionation in the Pacific OMZ for all waters with $[O_2]$ < 50 µmol/l. Dashed lines indicate relationships calculated for ε_d= 5 and 25 ‰. The average calculated or "apparent" fractionation factor for the entire region is 11.4‰. b) Apparent fractionation factors calculated separately for shelf (stations shallower then 200m) and offshore (stations deeper then 200m) stations. The shelf stations show a lower apparent fractionation factor of 7.6‰, while the value for off-shore stations is 16.0‰.

Least squares fitting of all data from the Pacific OMZ (i.e. $[O_2]$ < 50µmol/l) is shown in figure 10a, with the "apparent" isotopic enrichment factor (ε^*) estimated to be +11.4‰ (standard error of the fit is 0.7, Fig. 10). The data are scattered between relationships defined by ε^* = 5 and 25‰ (assuming a common initial value for $\delta^{15}N_{initial}$ of 5.2‰). This value of $\varepsilon^*$of +11.5‰ is significantly lower than values estimated from data from the Eastern Tropical North Pacific (22.5 – 30‰) and Arabian Sea (22 – 25‰) (Brandes et al., 1998;Sigman et al., 2003;Voss et al., 2001) and from denitrifier cultures (28.6‰) (Barford et al., 1999). However the value lies close to a values determined 30 years ago for 2 stations off southern Peru using much less sensitive analytical techniques (13.8‰) (Liu, 1979).

Separating data for shelf and offshore stations (Fig. 9b) results in fits with significantly different values of ε^* of 7.6‰ and 16.0‰, respectively. Similar observations of low ε_d have been made in Santa Barbara Basin as compared to the open ETNP (Sigman et al., 2003). This was attributed to a larger contribution from sedimentary denitrification input into the water column in the Basin, which has a significantly smaller fractionation effect of 0-5‰ due to control of overall NO_3^- removal rate by transport through the sediments (Brandes and Devol, 2002, Lehmann et al., 2007).

In marked contrast to the Pacific study region, most $\delta^{15}N\text{-}NO_3^-$ values from the Atlantic (Fig. 8b) stay close to the ocean average value of 5.2‰ (Auxiliary material Table 1, (Sigman et al., 2009)). In part this can be explained by the absence of significant fixed-N removal in this region (N' values remain positive, data not shown (Gruber and Sarmiento, 1997)). Notable also was the complete absence of any trend towards higher values associated with partial nitrate utilization in fully-oxygenated, near-surface waters on the M80 samples (stations south to Cape Verde). Significant increases of $\delta^{15}N$ (up to 12‰) in surface waters were only observed at shallow stations very close to the African coast (data from L'Atalante cruise in 2008, not shown) that are likely associated with partial phytoplankton uptake of upwelled NO_3^- (Altabet, 2001;Altabet and Francois, 1994).

Decreasing values of $\delta^{15}N$ of DIN towards the surface have been reported previously for Monterey Bay (Wankel et al., 2007), and for near-surface samples collected close to the Azores Front (30-35ºN) (Bourbonnais et al., 2009) and at Bermuda (Knapp et al., 2010). The lowest values published from this general region (Bourbonnais et al., 2009) were ~3.5‰ at a depth of 100 m. Our data indicate very similar values at this depth. The relatively low values of 3.5‰ were attributed by Bourbonnais et al (2009) to the effects of nitrogen fixation, which can result in remineralised DIN with typical values of -1‰ (-2‰ to +2‰) (Carpenter et al., 1997;Montoya et al., 2002). The strongly negative $\delta^{15}N$ values measured in surface waters south of Cape Verde (e.g. down to -5.5‰, Fig. 5) have not been observed before in oceanic surface waters and cannot be explained by ammonification and nitrification of organic nitrogen produced by nitrogen fixers. On the other hand, very low values of $\delta^{15}N$ (~ -7‰) of aerosol nitrate have been measured in samples of atmospheric dust from this region (Baker et al., 2007;Morin et al., 2009). Similarly low, negative values have been measured in samples of atmospheric dust originating in the Sahara that were collected from the eastern Mediterranean (Wankel et al., 2010). Recent work (Knapp et al., 2010) shows that the wet deposition flux of fixed-N at Bermuda can be comparable to estimates of biological N_2 fixation rates in surface waters. The $\delta^{15}N\text{-}NO_3^-$ in wet deposition at Bermuda was significantly lower (-4.5‰) then $\delta^{15}N$ added by oceanic N_2 fixation (-2 to 0‰)

(Hastings et al., 2003;Knapp et al., 2010). For our study region, dry deposition of dust from the Sahara is likely to dominate the N-flux (Duarte et al., 2006).

The N-flux due to diapycnal mixing of NO_3^- from below in the oligotrophic north Atlantic and at Cape Verde region come to values of about 7 mg N m^{-2} d^{-1} (or ~500 µmol/m^2/day) (Klein and Siedler, 1995) and at region close to Mauretania to almost double value of about 1037 µmol/m^2/day (Schafstall et al., 2010). According to Baker et al. (2007) the dry deposition N flux of soluble aerosol at 20°W in the Atlantic ocean is 80-120 µmol/m^2/day, while wet deposition is 50-70 µmol/m^2/day. In an earlier article (Baker et al., 2003), however, the dry deposition N flux was significantly lower (~20 µmol/m^2/day), which emphasizes that the flux can be highly variable. Duarte (2006), for example, estimated a dry deposition N flux of 280±70 µmol/m^2/day in tropical Atlantic region, which is significantly higher than the diapycnal flux. This deposition flux is sufficient to supply the observed DIN inventory of the top 20 m (0.2 µmol/l) within two weeks.

The most negative $\delta^{15}N$ values in surface water were observed at stations south of the Cape Verde Islands, which is also the region with the highest Saharan dust deposition (Schepanski et al., 2009;Tanaka and Chiba, 2006). A few days before our samples were collected on M80, an intensive dust event took place, and this may have influenced the $\delta^{15}N$ values observed. Satellite imagery from November and December 2009 are shown in figure 11 and indicate a significant dust event in the region over the period immediately prior to our samples being collected (between 26th November and 12th December 2009).

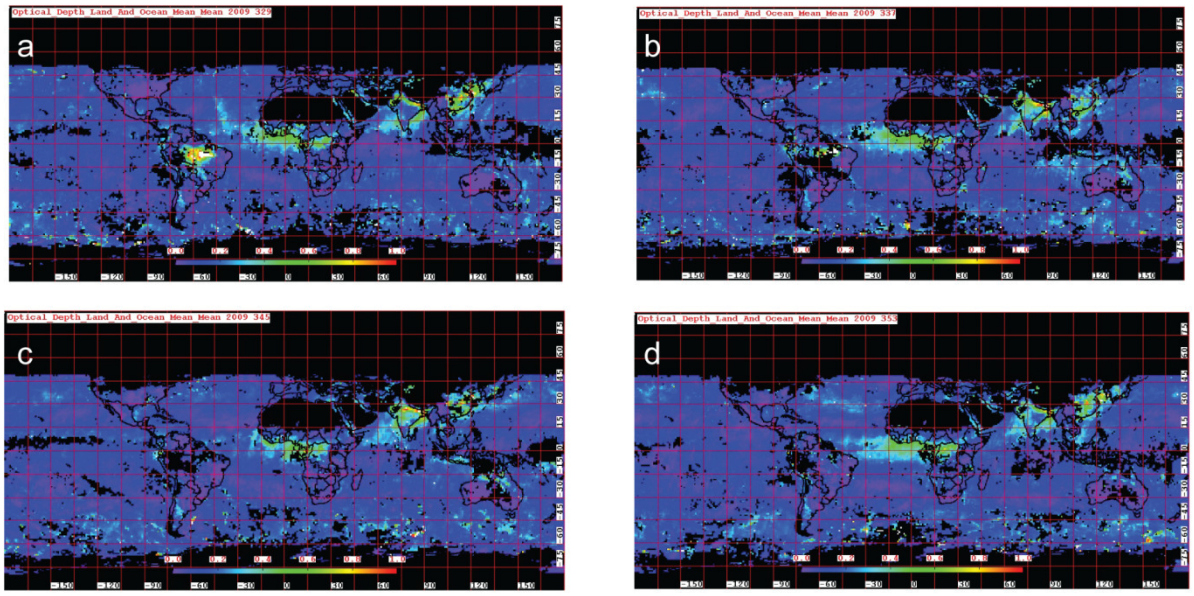

Figure 10. Satellite images of Aerosol Optical Depth at different time periods of 2009.: a)25.Oct – 2.Dec; b)3.Dec – 10.Dec; c)11.Dec – 18.Dec; d)19.Dec – 26.Dec. (http://ladsweb.nascom.nasa.gov/browse_images/l3_browser.html)

Under these conditions, the nitrogen loading to the surface layer cannot be considered to be in a steady state. We therefore examined extreme scenarios with dry deposition N flux dominating and for balance with diapycnal mixing and assimilation (Table 1). Total N flux (F_{total}) is the sum of two sources from atmospheric deposition (F_{dest}, initial value of δ^{15}N-dust = -7‰) and diapycnal mixing (F_{mix}, initial value of δ^{15}N-mixing = 5‰) and one nitrogen sink from assimilation ($F_{assimilation}$). The fractionation factor for assimilation can vary with environmental conditions and dominant phytoplankton species. In oligotrophic waters, however, observed isotope fractionation will be close to zero due to complete NO_3^- utilization. Assuming that utilized NO_3^- has an ocean-average value of δ^{15}N = 5‰ and fractionation factor close to zero, the assimilation will decrease nitrate concentration but increase δ^{15}N of it in ambient waters by 5‰, thus δ^{15}N-assimilation = -5‰.

In the first scenario, 90% of total nitrogen derives from dust deposition and only 10 % is from diapycnal mixing. This scenario results in a δ^{15}N value of -5.8‰, very close to observations. The second scenario assumes equal contribution from those two nitrogen sources resulting in a δ^{15}N of -1‰, while the third includes assimilation as a nitrogen sink and result in δ^{15}N of +1‰ (Table 1).

Table 1. Predicted surface water δ^{15}N NO_3^- under different scenarios. $F_{total} = F_{dust} + F_{mixing} + F_{assimilation}$. The end members for δ^{15}N surface water calculation were: δ^{15}N-dust = -7‰, δ^{15}N-mixing =5‰ and δ^{15}N-assimilation = 5‰.

scenario	δ^{15}N-NO_3^- surface water	F_{dust}/F_{total}, %	F_{mixing}/F_{total}, %	$F_{assimilation}/F_{total}$, %
1	-5.8	90	10	0
2	-1	50	50	0
3	1	33%	33%	33%

These scenarios do not take into consideration an isotopic signal from N_2 fixation. They do show that under non-steady state conditions, such as shortly after dust deposition events, the δ^{15}N for NO_3^- in surface waters can decrease to -5.8‰. Thus, atmospheric dust N deposition should be taken into account, together with the oceanic N_2 fixation, in explaining the low δ^{15}N NO_3^- pool

observed in subtropical thermoclines (Brandes et al., 1998;Karl et al., 2002;Knapp et al., 2005;Wannicke et al., 2010).

Summary and conclusions

In this paper we have presented an extensive amount of new data for nitrogen isotope and key nitrogen species, such as N_2O, collected from OMZ regions in the eastern tropical North Atlantic and eastern tropical South Pacific. These regions have strongly contrasting O_2 concentrations and N cycling processes. Measurements with near identical techniques in both oceans, reveal that whereas deep waters (> 2000 m) share near-identical values of δ^{15}N-DIN (5.3 ± 0.4 ‰), there are significant to major differences between the two OMZs in both surface and intermediate waters. The same AAIW water mass, for instance, has in the Pacific δ^{15}N-DIN average value of 6.7 ± 0.8 ‰ and in the Atlantic of 5.5 ± 0.6 ‰ (Auxiliary material, table 1). According to a Student t-test, the difference is highly significant ($p < 0.01$). This difference can be due to N-loss in the Pacific, increasing δ^{15}N signal of the water mass, and/or nitrogen fixation in the Atlantic, driving δ^{15}N signal in the opposite direction. Strongest differences in δ^{15}N-DIN in the two study regions are located in depth 100-500 m in the OMZs. In the Pacific δ^{15}N values tend towards strongly positive values as a result of N-loss processes within the OMZ and partial NO_3^- utilization in surface waters, while in the Atlantic the values stay close to ~5.4‰ on average.

Co-located measurements of N_2O and stable N-isotopes in waters with $[O_2] < \sim 5$ µmol/l reveal a clear signal of canonical denitrification, although its quantitative significance for overall N-loss, relative to anammox, cannot be assessed. The correlations of N_2O with δ^{15}N- NO_3^- and AOU for waters with $[O_2] > 50$ µmol/l are similar in both OMZs, reflecting similar N_2O yields during nitrification. However, waters with $5 < [O_2] < 50$ µmol/l in the Pacific exhibit correlations that are suggestive of a three times higher relative N_2O yield.

Whereas δ^{15}N-NO_3^- values in surface waters of the Pacific OMZ region are strongly positive, being controlled by partial nutrient utilization and a ^{15}N-enriched NO_3^- supply affected by subsurface denitrification, the oligotrophic surface waters south of Cape Verde in the Atlantic exhibit negative values of δ^{15}N (-5 to +2 ‰). The negative values are too low to be explained by N-fixation and we show that they are most likely the result of a transient input of NO_3^- associated with atmospheric deposition of Saharan dust. This implies that atmospheric dust input as well as nitrogen fixation should be considered in budgets and explanations of upper ocean stable N isotope data, especially in the Atlantic region.

Within the Pacific OMZ, correlation of $\delta^{15}N$ with measures of N-loss gives a calculated apparent fractionation factor for $\delta^{15}N\text{-}NO_3^-$ ($\varepsilon_r = 11.4 \pm 0.3$ ‰) which is low compared to canonical values, but close to a value estimated by the only prior study in this region (Liu, 1979). Sub-division of the data into shelf and offshore stations resulted in improved correlations and very different apparent fractionation factors for the two depth-regimes ($\varepsilon_{d\text{-}offshore} = 16 \pm 0.5$‰; $\varepsilon_{d\text{-}shelf} = 7.6 \pm 0.6$‰). Whereas the offshore value lies close to the ~20‰ fractionation factor of denitrification (Brandes et al., 1998;Granger et al., 2008), the much lower apparent fractionation factor for shelf waters likely reflects a larger contribution from sedimentary denitrification (fractionation factor of 1.5‰; (Brandes and Devol, 2002). We note that the fractionation effect from the complete set of stations ($\varepsilon_r = 11.4 \pm 0.3$ ‰) lies reasonably close to an apparent global fractionation factor for OMZ denitrification of 12‰ which was calculated for a steady state 50:50 balance between water column and sedimentary denitrification (ALTABET, 2007).

Acknowledgements

The authors thank Frank Malien, Gert Petrick and Karen Stange for technical assistance and Andreas Oschlies helpful discussion. The work was supported by the DFG-funded Sonderforschungsbereich 754 “Climate-Biogeochemistry Interactions in the Tropical Ocean” and SOPRAN (Surface Ocean Processes in the Anthropocene: www.sopran.pangaea.de; FKZ 03F0462A).

5 Production of oceanic nitrous oxide by ammonia-oxidizing archaea

Introduction

The recent finding that microbial ammonia oxidation in the ocean is performed by archaea to a greater extent than by bacteria has drastically changed the view of oceanic nitrification. The numerical dominance of archaeal ammonia-oxidizers (AOA) over their bacterial counterparts (AOB) in the ocean leads to the hypothesis that AOA rather than AOB could be the key organisms for the oceanic production of the strong greenhouse gas nitrous oxide (N_2O). Very recently, enrichment cultures of ammonia-oxidizing archaea have been described to produce N_2O (Santoro et al., 2011). Here, we demonstrate that archaeal ammonia monooxygenase genes (*amoA)* were detectable throughout the water column of the eastern tropical North Atlantic and eastern tropical South Pacific Oceans. The maxima in abundance and expression of archaeal *amoA* genes correlated with the N_2O maximum and the oxygen minimum, whereas the abundances of bacterial *amoA* genes were negligible. Moreover, selective inhibition of archaea in seawater incubations from the ETNA decreased the N_2O production significantly. Studies with the marine archaeal ammonia-oxidizer *Nitrosopumilus maritimus* SCM1 provided the first direct evidence for N_2O production in a pure culture of AOA, thus excluding the involvement of other microorganisms. *N. maritimus* showed high N_2O production rates under low oxygen concentrations comparable to concentrations existing in the oxycline of the ETNA, whereas the N_2O production from two AOB cultures was comparably low at similar conditions. Based on those findings, we hypothesize, that the observed production of N_2O in tropical ocean areas results mainly from archaeal nitrification and is largely impacted by the availability of dissolved oxygen.

Atmospheric nitrous oxide (N_2O) is a strong greenhouse gas and a major precursor of stratospheric ozone depleting radicals. The ocean is a major source of N_2O contributing approximately 30% of the N_2O in the atmosphere. Oceanic N_2O is exclusively produced during microbial processes such as nitrification (under oxic to suboxic conditions) and denitrification (under suboxic conditions). The formation of N_2O as a by-product of nitrification was reported for AOB (oxidation of ammonia (NH_4^+) via hydroxylamine (NH_2OH) to nitrite (NO_2^-) and in case of nitrifier-denitrification during reduction of NO_2^- to molecular nitrogen (N_2)). The accumulation of oceanic N_2O is favored in waters with low oxygen (O_2) concentrations, which is attributed to an enhanced N_2O yield during nitrification. The frequently observed linear correlation between

ΔN_2O (i.e., N_2O excess) and the apparent oxygen utilization (AOU) is usually taken as indirect evidence for N_2O production via nitrification (Yoshida et al., 1989).

The traditional view that oceanic NH_4^+ oxidation is only performed by ammonia-oxidizing bacteria (AOB) has been challenged by (i) the frequent presence of archaeal *amoA* genes in metagenomes of various environments (Venter et al., 2004;Treusch et al., 2005;Schleper et al., 2005;Lam et al., 2009), (ii) the successful isolation of the NH_4^+ oxidizing archaeon *N. maritimus* and (iii) the fact that archaea capable of NH_4^+ oxidation have been detected in all oceanic regions throughout the water column and in sediments . Moreover, *N. maritimus* appears to be adapted to perform NH_4^+ oxidation even under oligotrophic conditions which dominate in large parts of the open ocean. These observations point towards an important role of AOA (now constituting the novel archaeal lineage of *Thaumarchaeota* (Brochier-Armanet et al., 2008;Spang et al., 2010)) for the oceanic nitrogen cycle which has been overlooked until recently . Archaeal N_2O production has been proposed to contribute significantly to the upper ocean N_2O production in the central California Current and has moreover very recently been demonstrated to occur in two AOA enrichment cultures (Santoro et al., 2011). However, the capacity of AOA to produce N_2O in the ocean has yet not been demonstrated directly.

The eastern tropical North Atlantic (ETNA) and the eastern tropical South Pacific (ETSP) Oceans represent two contrasting oceanic O_2 regimes: While O_2 concentrations in the ETNA are always above 40 µmol L^{-1}, the ETSP regime is characterized by a pronounced depletion of O_2 in intermediate waters between ~75 and 600 m resulting in a oxygen minimum zone (OMZ) with O_2 concentrations close or even below the detection limit (~2 µmol L^{-1}) of conventional analytical methods.

The *amoA* gene coding for the alpha subunit of the ammonia monooxygenase is present in archaea as well as in β- and γ-proteobacterial ammonia-oxidizers and is commonly used as a functional biomarker for this physiological group (Hallam et al., 2006;Schleper et al., 2005;Treusch et al., 2005;Venter et al., 2004). Thus, in order to identify whether archaeal or bacterial *amoA* was associated with the maximum in N_2O concentration in the ocean, we determined the archaeal and bacterial *amoA* gene abundances and expression in relation to N_2O concentrations along vertical profiles during three cruises (in February 2007, February 2008, and June 2010) to the ETNA and one cruise (in January 2009) to the ETSP. We further demonstrate the N_2O production in a pure culture of *N. maritimus* SCM1, establish the O_2 sensitivity of archaeal N_2O production which is of highest impact at times of ocean deoxygenation (Stramma et al., 2010b). N_2O production from pure cultures of the two marine nitrifying bacteria *Nitrosococcus oceani* NC10 and *Nitrosomonas marina* NM22 is low compared to the rates achieved by the archaeal isolate.

Vertical distribution of AOA and AOB along N_2O depth profiles

70

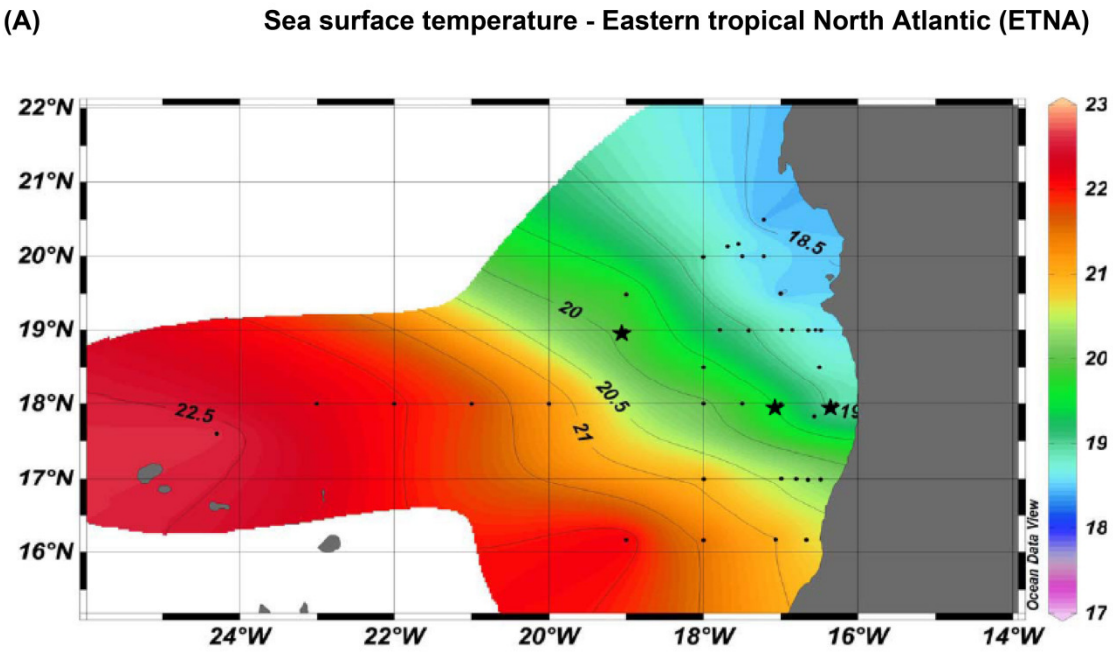

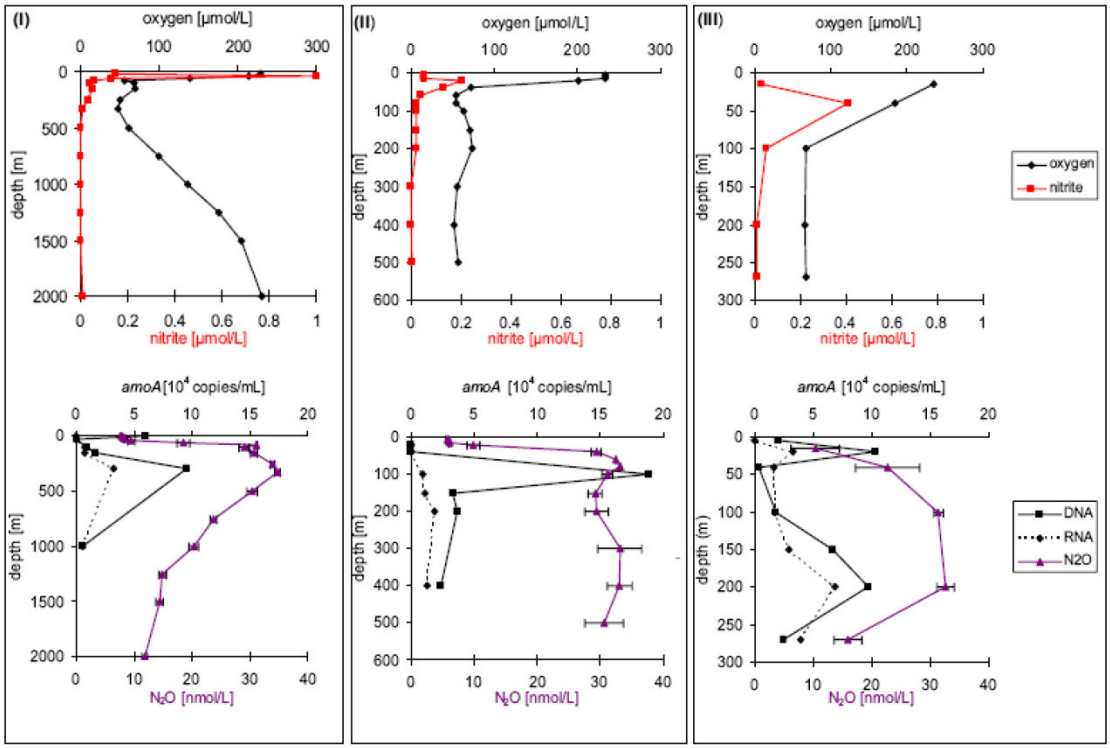

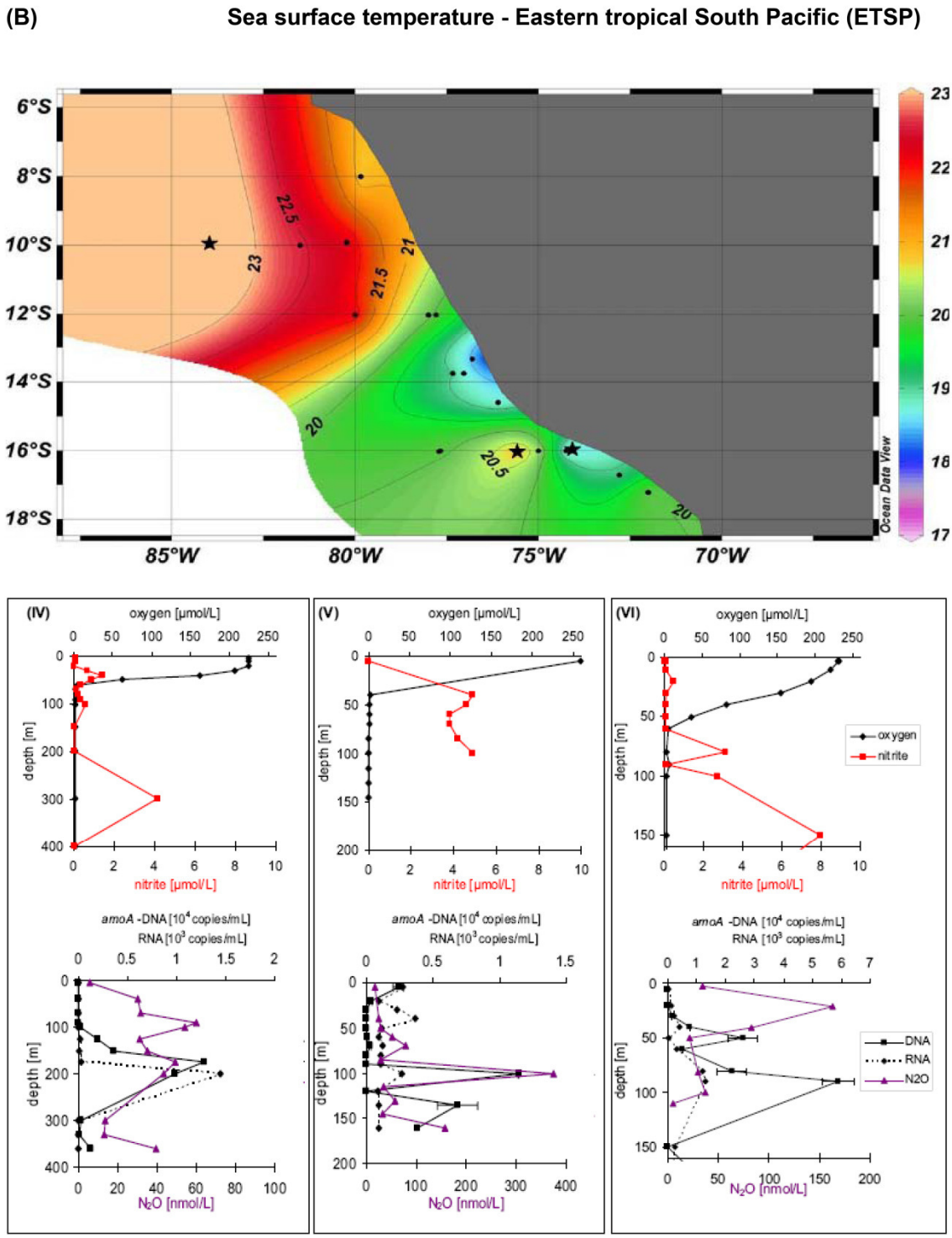

Figure 1: Maps of sea surface temperatures (A) from the eastern tropical North Atlantic Ocean and (B) from the eastern tropical South Pacific Ocean. The locations of sampling stations are indicated with dots in the maps. Selected vertical profiles (I-VI) of O_2, NO_2^-, N_2O (measured in triplicates) and archaeal *amoA* (measured in duplicates by qPCR) are shown; (I) and (IV) are located offshore, (II) and (V) are located on the continental slope, and (III) and (VI) are onshore/coastal stations.

Vertical profiles of N_2O showed a distribution with concentrations between 10 and 35 nmol L^{-1} in the ETNA whereas the N_2O concentrations in the ETSP were in the range from 10 to 374 nmol L^{-1} (Fig. 1). In the majority of the sampled stations in the ETNA and ETSP, the accumulation of dissolved N_2O was associated with minimum O_2 concentrations as expected (Codispoti, 2010). Maximum N_2O concentrations in the ETNA were generally lower compared to the ETSP because O_2 concentrations in the ETSP were extremely depleted below 75 m resulting in enhanced N_2O accumulation (Suntharalingam et al., 2000;Codispoti, 2010).

The well-established linear correlation between ΔN_2O and AOU as well as NO_3^- was found for the ETNA (Fig. 2) indicating that nitrification was the likely pathway for N_2O production. High copy numbers of archaeal *amoA* genes and high N_2O concentrations co-occurred in the ETNA suggesting a tight coherence between AOA abundance and N_2O accumulation in the layers with low O_2 (Fig. 3). A coherence of N_2O and archaeal *amoA* was detected at some stations in the ETSP, but was not a general feature (Fig. 1) possibly resulting from N_2O production via other processes such as denitrification, nitrifier-denitrification or anammox (Kartal et al., 2007) at present suboxic conditions. Gene abundances of archaeal *amoA* in the ETNA and ETSP were detectable throughout the water column and reached values of up to 1.9×10^5 and 6×10^4 copies mL^{-1}, respectively (Fig. 1). Gene abundances of β- and γ-proteobacterial *amoA* were much lower (up to 950 and 735 copies mL^{-1} in the ETNA and ETSP, respectively) and in comparison seem to be negligible. This is in line with previous studies reporting 1-4 orders of magnitude higher abundances of AOA than AOB in various oceanic regions (Wuchter et al., 2006;Santoro et al., 2010;Lam et al., 2009;Francis et al., 2005;Church et al., 2009). Thus, we propose that N_2O production occurs via archaeal nitrification in the ETNA and might also be present in the ETSP despite the fact that we did not find the ΔN_2O/AOU correlation in the ETSP.

A difference of one order of magnitude between *amoA* copies in RNA and in DNA is present in vertical profiles of the ETSP, with copy numbers up to 7×10^4 copies mL^{-1} present in the DNA and up to 1.5×10^3 copies mL^{-1} in the RNA. A similar tendency is detectable in the ETNA, however, the difference is less pronounced compared to the ETSP. This discrepancy, already reported by Lam *et al*. 2009 (Lam et al., 2009), is hypothesized to be due to a diurnal cycle of ammonia-oxidation and therefore variable *amoA* expression. Moreover, a sampling bias due to comparably long filtration times (up to 30 min) might have led to RNA degradation; as previous studies reported transcript half-lives of down to 0.5 min (Steglich et al., 2010).

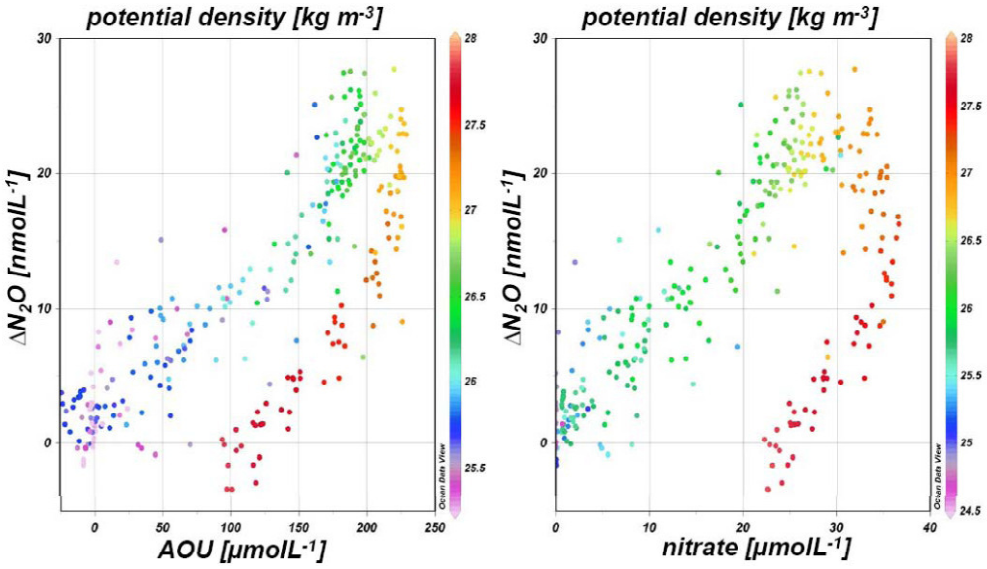

Figure 2: ΔN_2O versus the apparent oxygen utilization (AOU) and nitrate in the ETNA (data from cruises ATA03 and P348), the potential density is colour–coded.

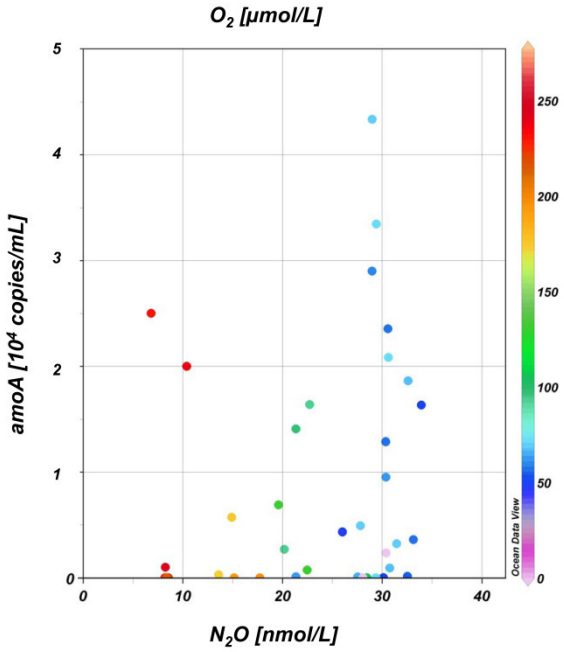

Figure 3: Archaeal *amoA* versus N_2O and O_2 in the ETNA (data from the cruises ATA03, P348 and P399/2). The O_2 concentration is colour-coded.

Phylogenetic diversity of archaeal *amoA*

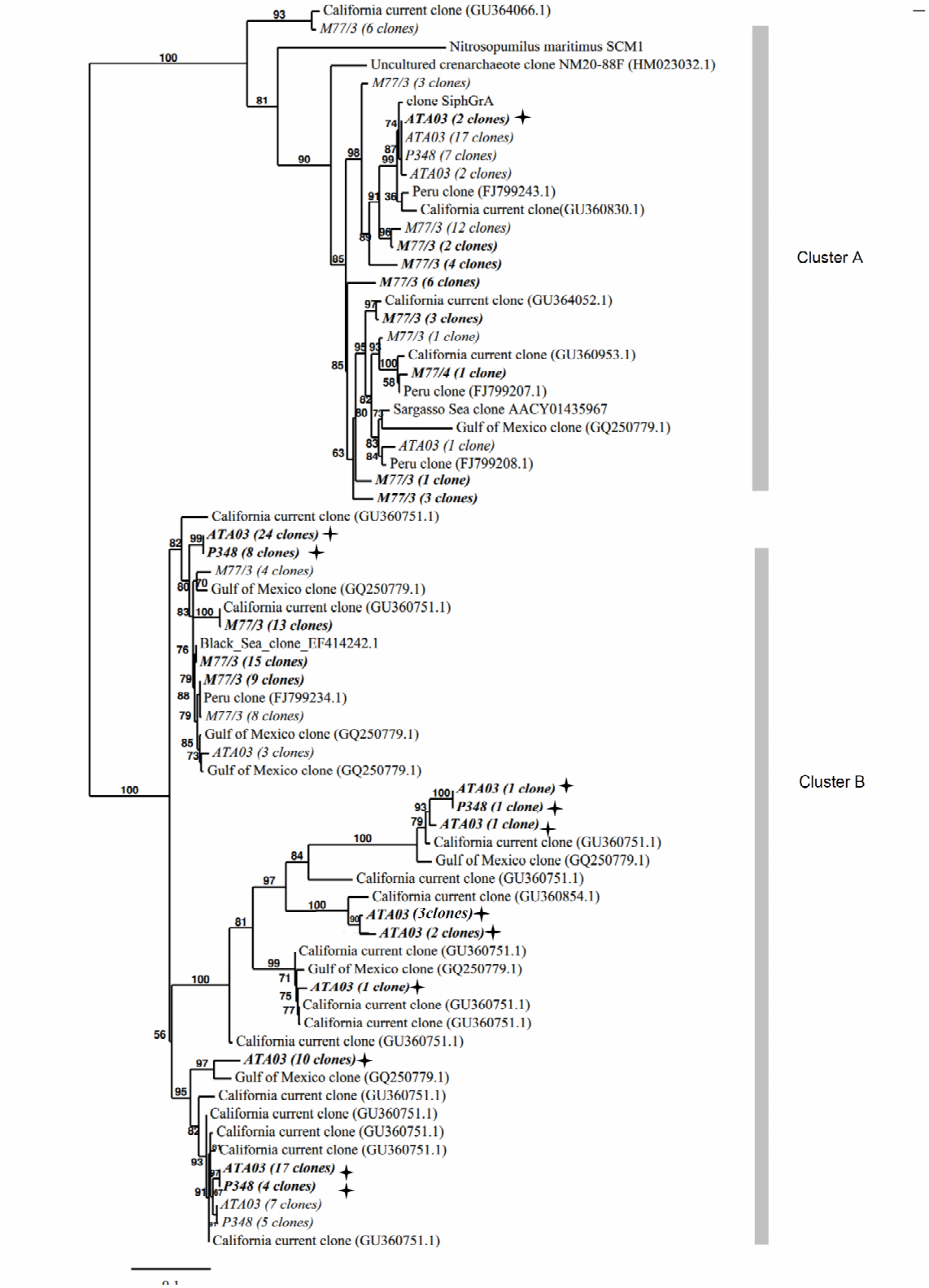

Figure 4: Distance-based neighbour-joining phylogenetic tree of archaeal *amoA* sequences from the ETNA (cruises ATA03 and P348) and ETSP (cruise M77/3). Sequences derived from the oxygen minimum zone (OMZ) of the ETNA are in italics, bold and marked with solid stars, sequences from above the OMZ are in italics. Sequences from the OMZ of the ETSP are in italics and bold; sequences from above the OMZ are in italics.

The diversity of AOA present in the ETNA was determined based on the analysis of 106 *amoA* sequences from 7 stations of 2 cruises (P348, ATA03). Sequences were derived from 10 depths between the ocean surface and 1000 m. The sequences split into two main clusters, with sequences from the O_2 minimum clustering mainly in cluster B (Fig. 4). Only 2.7% of sequences derived from samples from the O_2 minimum fall into cluster A. Sequences derived from depths between the surface and the upper oxycline distribute over both clusters (Fig.4). In the ETSP, sequences from the OMZ as well as from depths above separated into both clusters, with the majority of absolute sequence numbers from the OMZ affiliating with cluster B (Fig. 4), as already observed for the sequences from the O_2 minimum in the Atlantic Ocean.

Potential importance of cluster B affiliated Thaumarchaeota for N_2O production

The distribution of archaeal *amoA* genotypes along vertical profiles in the ETNA suggest a production of N_2O by *Thaumarchaeota* affiliated with cluster B, which was previously reported to be a deep marine cluster (Hallam et al., 2006) associated mainly with O_2 and NH_4^+ poor waters (Molina et al., 2010). These findings suggest a niche separation based on O_2 concentrations of cluster B affiliated AOA, which is consistent with our data from the ETSP. Regarding the potential decrease in dissolved O_2 concentrations in tropical ocean areas (Stramma et al., 2010b), we hypothesize that cluster B affiliated AOA might dominate the production of N_2O and the balance between reduced and oxidized nitrogen species in the ocean, gradually.

N_2O production in the ETNA

In two out of three 24h seawater incubations performed at three different stations in the ETNA at the depth of the OMZ, N_2O production was significantly lower in samples treated with N^1-guanyl-1,7-diaminoheptane (GC_7), a hypusination inhibitor shown to selectively inhibit the cell cycle of archaea (Jansson et al., 2000) (Fig. 5). In the third experiment a similar trend was observed, however it was lacking the statistical significance. These findings strongly support the hypothesis that N_2O production in large parts of the ETNA occurs within the OMZ and is mainly carried out by archaea.

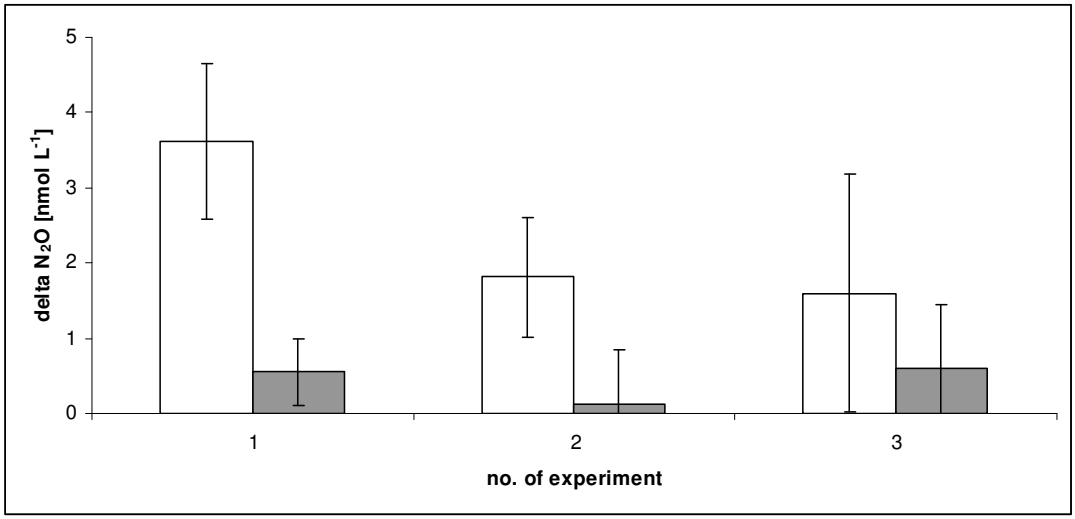

Figure 5: N_2O production determined from seawater incubations at three different stations (1-3) from the ETNA (P399). DeltaN_2O was calculated as the difference of N_2O concentrations over the incubation time (i.e. 24h). Open columns represent samples with no inhibitor, filled columns represent samples with the archaeal inhibitor GC_7. Error bars indicate the standard deviation of three technical replicates.

N_2O production in *N. maritimus* pure culture experiments

A direct evidence for N_2O production in archaea was detected in *N. maritimus* pure culture experiments. Production of N_2O in *N. maritimus* cultures was inversely correlated to O_2 concentrations (Fig. 6) which were chosen according to the O_2 concentrations present in the ETNA (112, 223 and 287 µmol L^{-1}, Fig. 1). *N. maritimus* cultures grew at comparable rates under the varying O_2 conditions and showed similar nitrification rates. Thus, the observed variation of the measured N_2O production can be assumed to exclusively depend on the prevailing initial O_2 conditions. N_2O production rates from the two AOB cultures (*Nitrosomonas marina* NM22 and *Nitrosococcus oceani* NC10) were considerably lower compared to the N_2O produced by *N. maritimus* (Fig. 6, Tab S1). The N_2O yields from NH_4^+ oxidation ranged from 0.002%-0.03% in the culture of *N. maritimus* to 0.001%-0.006% in the AOB cultures. The N_2O production rates derived from our AOB experiments are in accordance to those reported by Goreau *et al.* (Goreau et al., 1980), even though a different experimental setup was used. Culture experiments such as those presented here, are performed with AOB cell densities (~10^5 cells mL^{-1}) which are much higher than usually found in the ocean (10^2-10^3 cells mL^{-1}) (Wuchter et al., 2006;Lam et al., 2009). Thus, the N_2O production rates from the AOB cultures are probably overestimated and not representative as N_2O production per cell by AOB is also depending on the present cell densities (Frame, 2010). In contrast, the AOA cell densities in our culture experiment (~10^5 -10^7 cells mL^{-1}) were comparable to those present in the oceanic environment (~10^5 cells mL^{-1}) and thus seem to be reasonably representative.

Using the results from culture experiments as an approximation, the observed archaeal N_2O production rate for low O_2 conditions (140 nmol L^{-1} d^{-1}; normalized to 10^6 cells mL^{-1} yielding ~24 nmol L^{-1} d^{-1}, see Tab. S1) translates roughly estimated into a maximal potential oceanic production rate of about 14 nmol m^{-2} s^{-1} under the assumption of a low O_2 layer thickness of about 50 m as typically found in the ETNA. Compared to estimates of N_2O emissions from the ETNA to the atmosphere of up to 2 nmol m^{-2} s^{-1} (Wittke et al., 2010), potential oceanic archaeal N_2O production might be indeed significant.

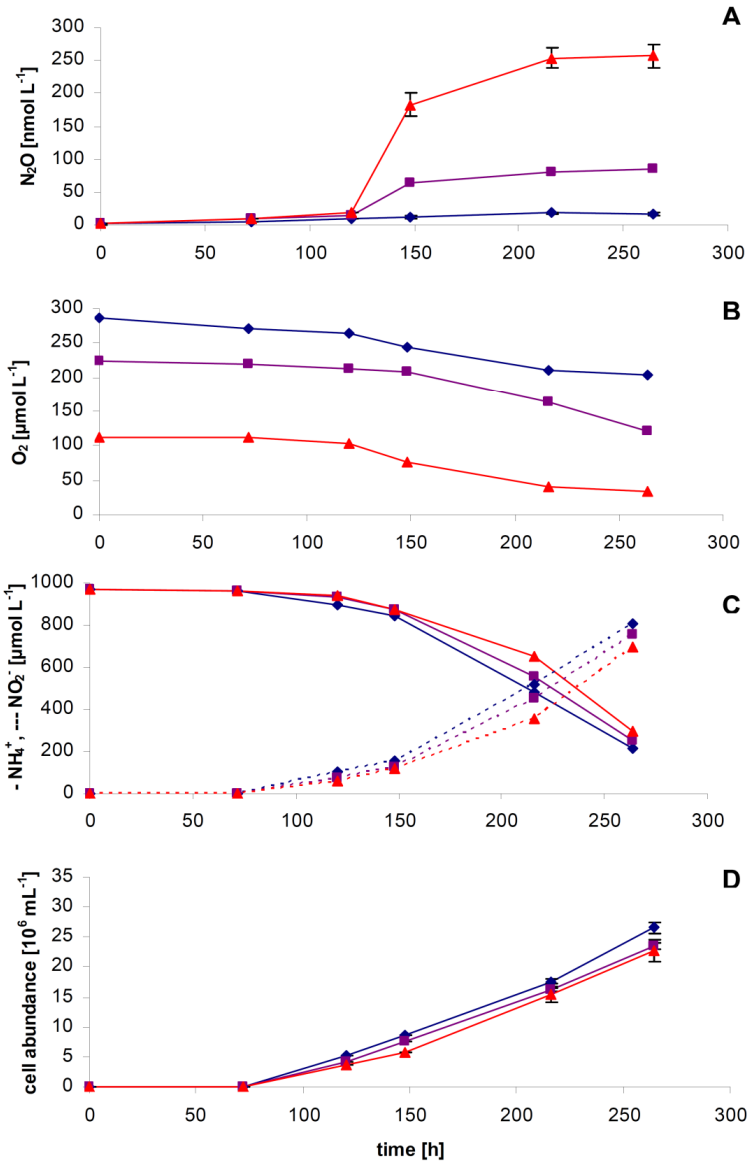

Figure 6: N_2O (A), O_2 (B), NH_4^+ and NO_2^- (C) as well as cell abundances (D) determined from incubation experiments with pure cultures of *N. maritimus*. Experiments are colour-coded according to their initial O_2 concentrations: red (112 µmol L^{-1}); violet (223 µmol L^{-1}); and blue (287 µmol L^{-1}). N_2O and cell abundances were measured in triplicates and the associated error ranges are indicated (please note that in the most cases the error bars are too small to be visible in the figure).

Potential pathways for archaeal N_2O production

AOB can produce N_2O from NH_2OH during nitrification or from NO_2^- during nitrifier-denitrification (Kool et al., 2010;Shaw et al., 2006). In AOA however, no equivalent to the hydroxylamine-oxidoreductase, which catalyzes the oxidation of NH_2OH to NO_2^- during nitrification, has been identified (Könneke et al., 2005;Martens-Habbena et al., 2009). Contrastingly, the detection of the nitrite reductase gene *nirK* in the sequenced genomes of cultured *Thaumarchaeota* (Könneke et al., 2005;Martens-Habbena et al., 2009) led to the theory that AOA might produce N_2O by nitrifier- denitrification. To identify the origin of N_2O formation isotopomeric studies were performed with *N. maritimus* pure cultures. A ^{15}N site preference (SP_{N2O}) in N_2O of 33-37‰ was detected in a total of 12 experiments, consistent with results from AOA enrichments (Santoro et al., 2011), which is in agreement with the SP_{N2O} of ~33‰ typically found in AOB cultures performing NH_4^+ oxidation (Sutka et al., 2006) (for comparison: nitrifier-denitrification of AOB results in a SP_{N2O} of about 0‰). Thus, a production via the oxidation of NH_4^+ to NO_2^-, potentially via an unknown intermediate, is suggested, whereas N_2O production via nitrifier-denitrification is unlikely.

Summary

The dominating abundance of archaeal *amoA*, the coherence of N_2O accumulation and *amoA,* inhibited N_2O production in seawater experiments in the presence of the archaeal inhibitor GC_7 as well as the N_2O production by *N. maritimus* point to the fact that in large parts of the ocean N_2O is produced by archaeal and not by bacterial nitrification. Further, the archaeal N_2O production appears highly sensitive to the dissolved O_2 concentration, with highest N_2O production rates at low O_2 concentrations such as present in the OMZ of the ETNA. The expansion of OMZs in the future in many parts of the ocean (Stramma et al., 2008b) may lead to an enhanced N_2O production in the ocean and therefore may have severe consequences for the budget of N_2O in the atmosphere as well.

Acknowledgements

We thank the authorities of Cape Verde, Mauritania and Peru for the permission to work in their territorial waters. We acknowledge the support of the captains and crews of R/V Poseidon, R/V L'Atalante, and R/V Meteor as well as the chief scientists of ATA03, A. Körtzinger, and M77/3,

Martin Frank. Moreover, we thank T. Kalvelage for sampling during P348, and T. Großkopf and H. Schunck for sampling during M77/3; we further thank K. Stange, F. Malien, M. Lohmann, V. Leon and P. Fritsche for oxygen and nutrient measurements. We thank A. Pommerening-Röser for providing cultures of *N. oceani* NC10 and *N. marina* NM22 and C. Fehling for performing the isotopomeric studies. Financial support for this study was provided by the DFG Sonderforschungsbereich 754 (www.sfb754.de) and the BMBF Verbundprojekt SOPRAN (www.sopran.pangaea.de; SOPRAN grants 03F0462A and 03F0611A). MK was financially supported by the DFG.

6 An improved method for measurements of dissolved hydroxylamine in seawater

1. Introduction

Hydroxylamine (NH_2OH) is a short-lived compound of the marine N cycle (Arp and Stein, 2003;Ward, 2008). It is formed as an intermediate during the first step of nitrification by ammonia-oxidizing bacteria (AOB) (Rajendran and Venugopalan, 1976;Yoshida and Alexander, 1964):

$$NH_4^+ \xrightarrow{AMO} NH_2OH \xrightarrow{HAO} NO_2^- \qquad (1)$$

It has been shown that nitrous oxide N_2O can be produced from hydroxylamine in a side reaction during ammonium oxidation (Arp and Stein, 2003;Otte et al., 1999). However, there is increasing evidence that ammonium oxidation in the ocean is dominated by archaea and not bacteria (Wuchter et al., 2006), and potential formation of NH_2OH during archaeal nitrification remains to be proven.

NH_2OH has also been proposed as an intermediate during microbial dissimilatory reduction of nitrate to ammonia (DNRA) (Yordy and Ruoff, 1981), but only under anoxic conditions. A recent study revealed that it is only released from the enzyme under strongly acidic conditions and thus its occurrence as a free intermediate of DNRA in the ocean is unlikely (Einsle et al., 2002), however, it may be released after acidification of samples from anoxic environments.

The detection of dissolved hydroxylamine in oceanic waters may lead to additional insights in the mechanisms of the marine N cycle and especially the production mechanisms of N_2O since it could serve as a tracer for the occurrence of bacterial nitrification in the water column.

A various number of methods for hydroxylamine detection in aqueous solutions are known, including a number of volumetric, electrochemical and spectrophotometric methods (Kolasa and Wardenck, 1974). All of these methods report detection limits in micromolar or larger range, and in most methods nitrite has to be removed from the samples to get reliable results.

Butler and Gordon (1986a) developed a method (the so-called FAS conversion method, FAS stands for ferric ammonium sulfate) for the detection of nanomolar concentrations of NH_2OH in seawater. Their method is based on the oxidation of NH_2OH to N_2O using iron (III) as oxidation

agent and subsequent quantitative analysis of the resulting N_2O which was first introduced by von Breymann et al. (1982). The reaction pathway involves a series of reaction steps that leave the possibility of numerous side reactions to take place (Butler and Gordon, 1986c) and leads to reduced conversion rates of about 50% (Von Breymann et al., 1982). Butler and Gordon (1986a) modified the original method by lowering the pH to 3 during the reaction, which yielded more stable and reproducible recovery rates. Hydroxylamine concentrations from marine environments determined with this method range from 0 to >300 nmol L^{-1}, showing a large variability not only between the measurements but also within single depth profiles (Schweiger et al., 2007) (Table 1).

Table 1: Summary of hydroxylamine measurements in marine environments using the FAS conversion method.

Reference	Region	Range [nmol L^{-1}]	Mean [nmol L^{-1}]	Median [nmol L^{-1}]	Number of Samples
Von Breymann et al. (1982)	Coast off Oregon	0 to 7.8	2.86	1.5	5
Butler and Gordon (1986b)	Cariaco Basin	0 to 5.5	1.13	0.1	10
Butler and Gordon (1987)	Yaquina Bay, Oregon	0 to 362	59.6	26	69
Butler and Gordon (1988)	Big Lagoon, Califonia	0 to 175	13.83	3	32
Gebhardt et al. (2004)	Baltic Proper	2.1 to 179	37.2	27.2	83
Schweiger et al. (2007)	Boknis Eck (SW Baltic Sea)	0 to 18.5	4.3	2.8	46
Kock (2009), unpublished	Eastern Tropical South Pacific	0 to 123	23.2	15.0	36

A significant correlation of hydroxylamine and nitrite was found in the Baltic Sea (Gebhardt et al., 2004) and in the eastern tropical South Pacific Ocean off Peru (Fig. 1, unpublished), which was attributed to enhanced nitrification and, in suboxic to anoxic zones, DNRA that lead to the accumulation of hydroxylamine as well as nitrite.

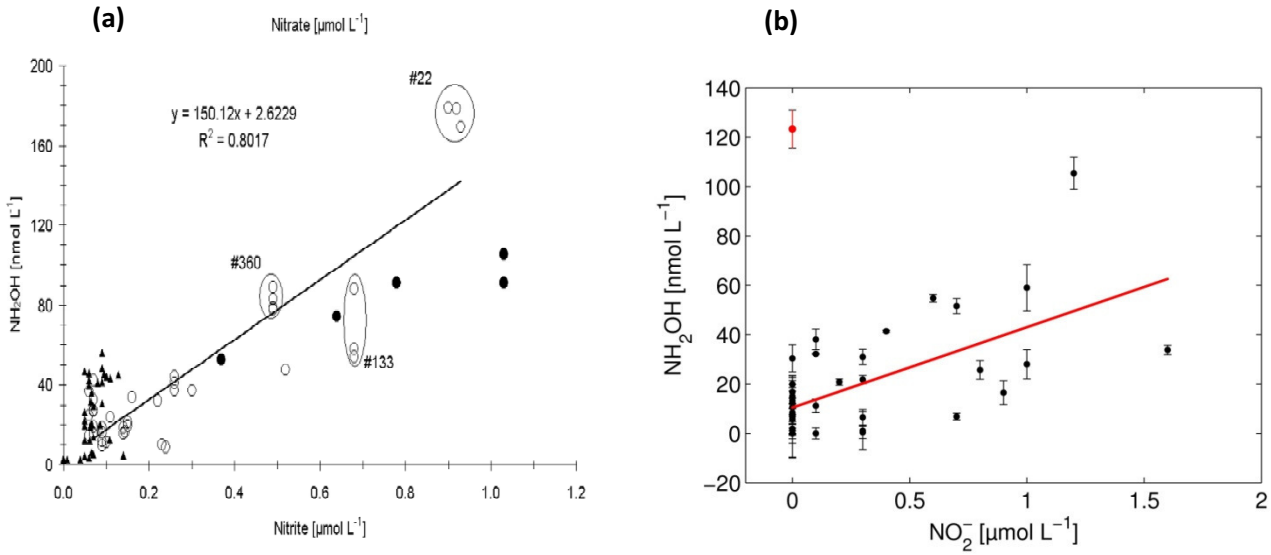

Figure 1: Hydroxylamine vs. nitrite from (a) Gebhardt et al. (2004) and (b) the Meteor Cruise 77-4 (unpublished data) to the eastern tropical South Pacific Ocean in February 2009. The regression line in (b) was calculated excluding the outlier at $[NO_2^-]$=0 µmol L^{-1}, $[NH_2OH]$=123 nmol L^{-1} (red dot). Regression parameters are: y=32.6x+10.5; r^2=0.38.

Butler and Gordon (1986a) reported that, in contrast to previous hydroxylamine analyses, nitrite would not interfere with the FAS conversion method. This is true for the reaction of hydroxylamine with FAS, however, nitrite has to be considered as a potential source of uncertainty as it can interfere through some side reactions: under acidic conditions NO_2^- is prevalent mainly in its protonized form, nitrous acid (HNO_2, pK_a=3.398). This can bias the hydroxylamine determination via conversion to N_2O in two ways:

1) Nitrous acid is not stable in aqueous solution with one of the decomposition pathways leading to N_2O production (van Cleemput, 1998):

$$4HNO_2 \rightarrow 2HNO_3 + N_2O + H_2O \qquad (1)$$

Although this pathway is not the main decomposition pathway for nitrous acid the amount of N_2O produced from ambient nitrite concentrations, which can reach up to 13 µmol L^{-1} (Kamykowski and Zentara, 1991), may reach nanomolar levels and thus lead to significantly biased hydroxylamine measurements. This effect may especially be important when the samples are stored under acidic conditions for days or weeks.

2) Hydroxylamine reacts with nitrous acid to hyponitrous acid ($H_2N_2O_2$) which rapidly decomposes to nitrous oxide and water (Spott et al., 2011):

$$NH_2OH + HNO_2 \rightarrow H_2N_2O_2 + H_2O \qquad (2)$$

$$H_2N_2O_2 \rightarrow N_2O + H_2O \qquad (3)$$

This reaction has a different stoichiometry than the conversion of hydroxylamine by iron (III) which requires two molecules of hydroxylamine to form one molecule of nitrous oxide. In the reaction of nitrous acid with hydroxylamine, the stoichiometry is 1:1, instead. Moreover, different conversion rates of the concurring reactions may lead to further bias in the data.

It is also known that similar to NH_2OH, hydrazine (N_2H_2) can react with nitrous acid with N_2O being one of the reaction products (Perrott et al., 1976;Stanbury, 1998). However, there are no measurements for dissolved hydrazine in seawater yet, but its role as an important intermediate during the anammox process and its possible role as an intermediate in nitrogen fixation (Dilworth and Eady, 1991;Jetten, 2009) suggest that it, indeed, may occur in some oceanic environments. A potential N_2O production from the reaction of hydrazine with nitrite may thus be another source for the bias of hydroxylamine measurements, whereas the reaction of hydrazine with FAS was found not to produce N_2O (Meyer, 2009).

The aim of this study was to evaluate the potential of side reactions of nitrite to bias the hydroxylamine analysis and to find an appropriate sample treatment for the analysis of hydroxylamine in nitrite-containing seawater samples. The specific questions addressed in different sets of experiments were:

1) Is there a potential nitrous oxide production from ambient nitrite in the water column?

2) Can the reaction of hydroxylamine with nitrous acid from ambient nitrite bias the conversion rates of the hydroxylamine conversion via FAS?

3) Is there a selective mechanism to eliminate the side reactions of nitrite?

4) Test the new method with samples from the Boknis Eck Time Series Station and the equatorial Atlantic Ocean.

2. Materials and Methods

2.0.1 Principle of Hydroxylamine Measurements

The determination of hydroxylamine using the FAS conversion method relies on the differential determination of nitrous oxide in samples with and without the addition of acetic acid and FAS which converts hydroxylamine to N_2O (Fig. 2).

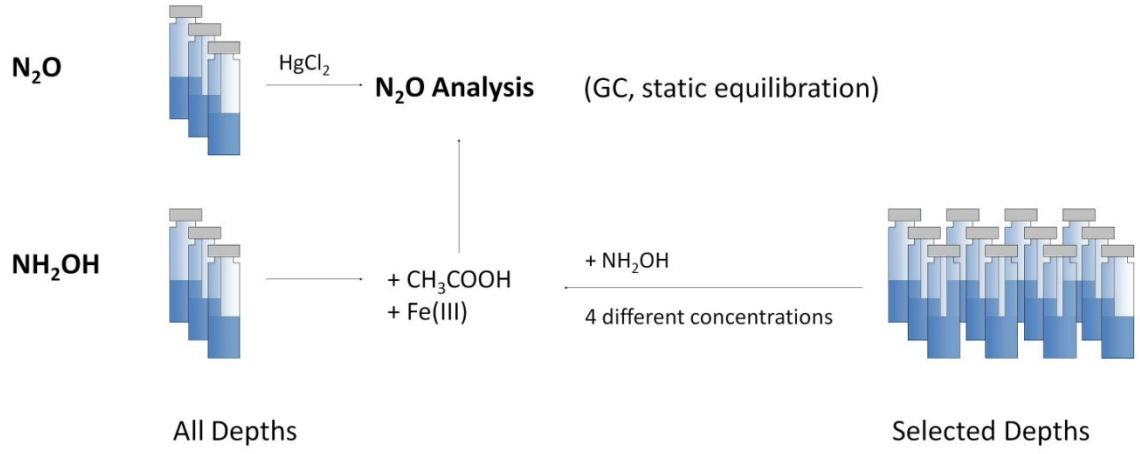

Figure 2: Measurement principle for hydroxylamine analysis with the FAS conversion method. Hydroxylamine concentrations are calculated from the difference in N_2O concentrations of samples with and without addition of acetic acid/FAS. The FAS conversion efficiency is determined from standard addition at selected depths.

The conversion efficiency of the method, expressed as "recovery factor (*RC*)", is determined from selected depths for each station using standard addition of four different hydroxylamine concentrations in the range between 0 and 100 nmol L^{-1}. The hydroxylamine concentration is calculated as follows:

$$[NH_2OH] = \frac{([N_2O]_{FAS} - [N_2O]_{BG})}{RC} \qquad (4),$$

$$RC = 2 * m_{stadd} \qquad (5),$$

m_{stadd} is the regression slope of the standard addition and $[N_2O]_{FAS}$ and $[N_2O]_{BG}$ are the N_2O concentrations of samples with and without the addition of acetic acid/FAS. The factor of two in the calculation of the recovery factor results from the stoichiometry of the reaction between hydroxylamine and FAS. The analytical uncertainty of the hydroxylamine analysis was calculated according to Schweiger et al. (2007).

All samples were analyzed for their N_2O concentrations using a static equilibration method: 9 to 9.5 mL of the headspace volume was extracted from the vials using a gas-tight syringe (VICI Precision Sampling, Baton Rouge, Louisiana). The extracted volume was replaced with seawater or MilliQ water with approximately the same salinity as the samples. The headspace subsamples were analyzed with a GC-ECD system that was calibrated using at least four different standard gas mixtures or dilutions of the highest standard gas mixtures. For details of the analytical method see Walter et al. (2006b).

Due to the different stoichiometry of the reaction of hydroxylamine with FAS and nitrite and the potential of other side reactions producing N_2O, hydroxylamine concentrations were not calculated according to equation (4) from the experiments in section 2.1 to 2.3. Instead, the background corrected N_2O concentrations and, for standard addition experiments, the conversion factor (= m_{stadd}) were compared.

2.0.2 Sample Preparation

If not stated differently, all experiments were carried out in 20 to 25 mL opaque glass vials that were sealed with butyl rubber stoppers and crimped with aluminum caps. The average volume of the vials was determined gravimetrically from ten to twelve randomly chosen sample vials. Two sets of vials were used for analysis, with volumes (+/- standard deviation) of 23.94 ± 0.11 mL and 20.03 ± 0.14 mL.

Stock solutions of sodium nitrite (~20 mg/100 mL, the exact concentration was calculated from the mass weight) were prepared in MilliQ maximal three days before analysis and stored at 4° C prior to analysis. If necessary, the stock solution was diluted further to obtain different nitrite concentrations.

Ferric ammonium sulfate (FAS) solutions (1.206 g/100 mL) were prepared in MilliQ minimum three days before the experiments to ensure the complete dissolution of the FAS. The FAS solutions were used for multiple experiments but were renewed at least on a monthly basis to prevent contaminations.

Stock solutions of hydroxylammonium chloride (~20 mg/100 mL, the exact concentration was calculated from the mass weight) were prepared in an aquaeous solution of acetic acid (3 mL acetic acid (glacial)/1L MilliQ, pH 3) to stabilize the hydroxylamine solutions. The stock solutions were diluted further to obtain four different standard concentrations leading to final concentrations in the vials between 0 and 100 nmol L^{-1} at an addition of 100 µmol/vial. All standard solutions were prepared maximum seven days before analysis and stored in the dark at 4 °C.

In contrast to Butler and Gordon (1986c), hydroxylamine samples were not treated with mercuric chloride, as most samples were analyzed within a few days after sampling and acidification of the samples was tested to be efficient to prevent further N_2O production in another experiment (data not shown).

2.1.1 Nitrous Oxide Production from Nitrous Acid

Background production of N_2O from acidification of nitrite-containing samples was tested in MilliQ as well as in water from the Boknis Eck Time Series Station, located in the Eckernförde Bay in the southwestern Baltic Sea (hereafter referred to as BE water). BE water has a lower salinity (12.5-24.5; 95 % percentile) than open ocean seawater (~35) but a high load of organic matter even under non-bloom conditions (Bange et al., 2010a). The latter point is especially important, because Butler and Gordon (1986a) speculated that organic compounds may play a role in the reduction of the conversion rates of hydroxylamine. While processes in MilliQ water were designed to study experiments without matrix (i.e. organic matter) effects, the experiments with BE water were conducted to determine if similar results were found in a seawater matrix with a high load of possibly interfering substances.

Two sets of experiments were carried out: background production in MilliQ and BE water were measured from unpurged samples (Exp. 2.1.1), leading to some uncertainties due to the variability in the background N_2O concentrations. To verify the results from BE water samples, this experiment was repeated with BE water samples that were purged with N_2 to remove the background N_2O (Exp. 2.1.2). Furthermore, one experiment was carried out to test the potential of a pH change to alkaline conditions to inhibit N_2O production from nitrous acid (Exp. 2.1.3).

Exp. 2.1.1:10 mL of MilliQ or unfiltered BE water was placed into the vials which were sealed and crimped. Samples were acidified with 100µL of acetic acid, and 100µL nitrite solution was subsequently added in two different concentrations to half of the samples each. The resulting nitrite concentrations in the vials were 0.504 and 9.54 µmol L^{-1}.The N_2O concentration was determined from triplicate samples between 0 and 336 h after nitrite addition. All samples were corrected for background N_2O by subtracting the measured N_2O concentration at T0.

Exp. 2.1.2: 10 mL of unfiltered BE water was placed into the vials before sealing and crimping. Each vial was purged with molecular nitrogen for at least 20 min to remove the background N_2O from the samples. After 100 µL of glacial acetic acid was added, 100 µL of a NO_2^- stock solution with two different concentrations was added to one third of the samples each. The remaining samples were measured as control samples without addition of nitrite. The N_2O concentration was measured after 0, 12, 24, 48 and 168 hours from three samples of each concentration.

Exp. 2.1.3: 10 mL of MilliQ were placed into the vials before sealing. Samples were acidified with hydrochloric acid to pH 1 before the addition of 1, 10 and 100 µmol L^{-1}sodium nitrite. One half of the samples with a nitrite concentration of 10 µmol L^{-1} was analyzed for N_2O after 24, 48, 72 and 246 hours, while the other half of the samples was treated with 220 µL NaOH solution

(2M) to adjust the pH to ten. The alkaline samples were analyzed for N_2O one week after NaOH addition.

2.2 Reaction of Hydroxylamine with Nitrite to N_2O with and without FAS Addition

The conversion of hydroxylamine by different concentrations of nitrite was first tested in MilliQ, as background N_2O production from nitrous acid became significant in BE water within the time of the conversion reaction (see section 3.1). The potential of different nitrite concentrations for conversion of hydroxylamine to N_2O was tested in Exp. 2.2.1. Additionally, conversion in BE water was tested in a separate experiment (Exp. 2.2.2). To evaluate the dominance of the concurring reactions between nitrite or FAS and hydroxylamine, FAS conversion in presence of different nitrite concentrations was tested in Exp. 2.2.3.

Exp. 2.2.1: 10 mL of MilliQ were placed into the vials which were sealed with butyl rubber stoppers and crimped. All samples were acidified with 100 µL of acetic acid, and different aliquots of a nitrite stock solution were added to six samples each. The final nitrite concentrations in the vials were 0.23 µmol L^{-1}, 0.54 µmol L^{-1}, 1.07 µmol L^{-1}, 2.14 µmol L^{-1}, 3.54 µmol L^{-1}. Half of the samples were additionally treated with 100 µL of a hydroxylamine stock solution (final concentration in the vials: 49.4 nmol L^{-1}). Samples were analyzed for N_2O after 24 h.

Exp. 2.2.2: 10 mL of BE water was placed into the vials which were sealed and crimped. After acidification, 100 µL of two different nitrite stock solutions were added to one third of the samples each, with the remaining samples being left without nitrite addition. The final nitrite concentrations were: 0 µmol L^{-1}, 0.151 µmol L^{-1} and 0.739 µmol L^{-1}. To all subsets hydroxylamine standards were added in three different concentrations. Samples were analyzed for N_2O after 72 h.

Exp. 2.2.3: 10 mL of MilliQ were placed into the vials that were sealed and crimped. The samples were divided into three experiments with different nitrite concentrations: 100 µL of a nitrite stock solution were added to the subsets. The resulting nitrite concentrations in the three subsets were 0.162 µmol L^{-1}, 0.539 µmol L^{-1} and 2.63 µmol L^{-1}. All subsets were then treated the same way: After 100 µL of glacial acetic acid were added, 100µL of a hydroxylamine stock solution with two different concentrations were added to three quarters of the samples. The remaining samples were left without hydroxylamine addition. All samples were subsequently treated with 100µL ferric ammonium sulfate and were left at room temperature for 23 h. After 23h, 100 µL of NaOH (8M) were added, adjusting the pH to 10 to stop the background nitrite conversion. The pH was measured in 5 random samples for control using pH control strips (pH 0-

14, Macherey-Nagel), all of them showing a pH close to ten. All samples were analyzed for N_2O within three days after conversion.

2.3 Removal of Nitrite

The removal of nitrite before hydroxylamine analysis is the easiest way to eliminate the undesired side reactions of nitrite. However, this process needs to leave the conversion reaction between hydroxylamine and FAS unaffected. Two substances were tested for their potential of selective removal of nitrite from our samples: Granger et al. (2006) used ascorbic acid to mask nitrite during the determination of the isotopic composition of nitrate in culture experiments. Ascorbic acid acts as a relatively mild reducing agent. During the reaction with nitrite, nitric oxide (NO) is formed which can be removed from the samples by continuous purging with nitrogen gas or synthetic air.

The second tested nitrite scavenger was an acidic solution of sulfanilamide. Sulfanilamide or sulfanilic acid are widely used as a reagent in the detection of nitrite and nitrate. It reacts selectively with nitrite under formation of a diazonium salt. In the nutrient analysis, this diazonium salt is coupled to 1-naphthylamine and forms a spectrometrically detectable dye (Grasshoff et al., 1999).Without addition of 1-naphthylamine, the diazonium salt reacts with a number of nucleophiles under formation of nitrogen gas.

2.3.1 Ascorbic acid addition

According to Granger et al. (2006), samples should be purged permanently with N_2 gas during reaction to remove the reaction product NO which may react back to NO_2^-. This, however, is not applicable for samples used for headspace analysis, as in the case of the hydroxylamine analysis. Two experiments were therefore carried out to determine the potential of this method: Nitrite removal was tested according to Granger et al. (2006) (Exp. 2.4.1), while samples were tested separately for hydroxylamine conversion without purging (Exp. 2.4.2).

Exp. 2.3.1: Nitrite removal: 50 mL MilliQ were placed into 100 mL vials which were sealed and crimped. Samples were purged for 30 min with N_2 before further treatment. After addition of 100 µL of nitrite (22.2 mg/100 mL, final concentration: 6.42 µmol L^{-1}), 100 µL of an ascorbic acid solution (17.9 g/100 mL, final concentration: 10.1 mmol L^{-1}) were added. Further acidification of the samples was not necessary as the pH was close to 3 due to the addition of ascorbic acid. Samples were purged continuously after addition and were analyzed for nitrite and hydroxylamine after 0, 4, 8, 12 h.

Exp. 2.3.2, Hydroxylamine conversion: 10 mL of MilliQ were placed into 20 mL vials which were sealed and crimped with butyl rubber stoppers and aluminum caps. Three subsets of samples were built, with two third of the samples being acidified with ascorbic acid (final concentration: 10 mmol L^{-1}) and one third of the samples being acidified with acetic acid to pH 3. 100µL of four different hydroxylamine stock solutions were added to each subset. Hydroxylamine conversion with FAS was started by addition of 100 µL FAS directly after hydroxylamine addition in half of the samples with ascorbic acid, while in the other half and in the samples without ascorbic acid the conversion reaction was started four hours after hydroxylamine addition. Samples were analyzed for N_2O 12-18 h after FAS addition.

2.3.2 Sulfanilamide addition

The conversion of hydroxylamine with FAS in presence of two different nitrite concentrations (0.87 µmol L^{-1}; 4.5 µmol L^{-1}) was tested for seawater and MilliQ samples with and without the addition of sulfanilamide (Exp. 2.4.3). The seawater used in the experiments was filtered seawater from the tropical North Atlantic Ocean (R/V Meteor cruise 80-2, surface, ~10 °N, 30 °W, aged 13 months). Additionally, this method was field tested at the BE Time Series Station (see Section 4.1).

Exp. 2.3.3: 10 mL of MilliQ or filtered seawater were placed into the vials which were sealed and crimped. All vials were purged with nitrogen gas for 20 min (flow rate: 80-100 mL min^{-1}) to remove excess N_2O. All samples were acidified with 100 µL of acetic acid and spiked with 100µL of three different hydroxylamine standards and one quarter of the samples left without addition. Afterwards, 100µL of two different nitrite stock solutions were added to half of the vials each. The final nitrite concentrations in the samples were 0.873 and 4.37 µmol L^{-1}. 100µL of an acidic solution of sulfanilamide (1mL HCl (25%)/100mL; final sulfanilamide concentration/vial = 100 µmol L^{-1}) were added to half of each subset directly after nitrite addition, the other half was left untreated. 100 µL of a FAS solution were added within 10 min after sulfanilamide addition. Samples were left to react for 20-25 hours and directly measured afterwards.

2.4 Field measurements of hydroxylamine

The application of the modified method was tested in the field during the monthly sampling from February to April 2011 and June to September 2011 at the Boknis Eck Time Series Station. During the September sampling, two subsets of samples were taken that were treated with and without the addition of 100 µmol L^{-1} sulfanilamide for comparison between the original method and the modified method with sulfanilamide addition.

Triplicates of bubble free water samples were taken from the rosette water sampler for hydroxylamine and N_2O measurements and sealed with butyl rubber stoppers and aluminum caps. Samples were stored at ambient temperature until treatment in the laboratory at IFM-GEOMAR, where 10 mL of a helium headspace were added to the hydroxylamine samples before the addition of 100 µL of glacial acetic acid, 100 µL of a sulfanilamide solution and 100 µL of FAS to each vial. Standard additions of hydroxylamine were carried out each month from an additional set of 12 samples from 15 m depth by addition of 100 µL of four different hydroxylamine standards. N_2O samples were treated with 50 µL of a saturated mercuric chloride solution. All samples were conserved within six hours after sampling, and stored at room temperature until N_2O analysis. The measured N_2O concentrations from hydroxylamine samples were corrected for the change in the water phase volume due to the addition of the chemicals.

The modified method was furthermore applied during the Maria S. Merian cruise MSM 18-2 to the equatorial Atlantic Ocean in May/June 2011. In contrast to the measurements at the Boknis Eck Time Series Station, hydroxylamine was sampled in clear glass vials with a volume of 56.6 ± 0.72 mL. Samples were stored at 4 °C in the dark before the addition of a 10 mL headspace of synthetic air and 400 µL of a mixture of acetic acid/sulfanilamide (172 mg sulfanilamide/100 mL acetic acid (glacial)) and 200 µL aqueous FAS solution (1.206 g FAS/50 mL MilliQ). Standard additions of hydroxylamine were carried out in an additional subset of samples from 200 m at each station by addition of 100 µL of four different standard concentrations. Samples were stored at room temperature for at least 24 h before analysis. N_2O concentrations of the hydroxylamine measurements were corrected for the change in the volume of the water phase due to the addition of the reagents and due to the heating of the samples from 4 °C to room temperature.

3. Results and discussion

3.1 Background production of nitrous oxide from nitrous acid.

Figure 3 shows the N_2O concentration over time from unpurged (Fig.1a) and purged (Fig.1b) samples with nitrite additions of different concentrations.

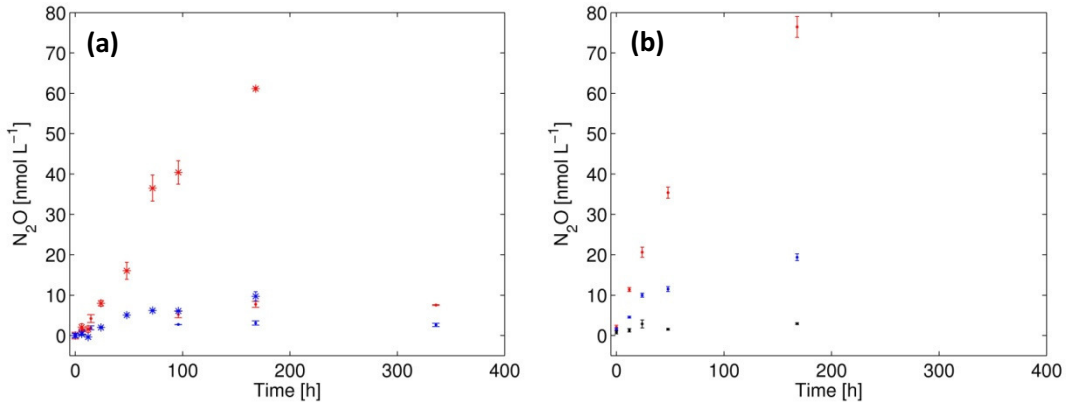

Figure 3: Nitrous oxide production from nitrous acid. Different colors represent different nitrite additions: red: 9.54 µmol L^{-1}; blue: 0.504 µmol L^{-1}; black: 0 µmol L^{-1}. a) unpurged samples, MilliQ (•) and BE water (✳); the N_2O concentration at T0 was subtracted to correct for background N_2O. b) purged samples, BE water only.

In all experiments with nitrite addition, N_2O concentrations significantly increased over time (Fig. 3a and 3b). Comparing the experiments with MilliQ and BE water (Fig. 3a), it is obvious that the N_2O production in BE water is significantly higher than in MilliQ: In MilliQ samples, the N_2O produced from nitrous acid did not exceed 10 nmol L^{-1} even from samples with high nitrite additions. The increase in N_2O leveled off rapidly and stayed constant after 96 h, suggesting the complete degradation of nitrite by this time. N_2O production in BE water even from low nitrite additions exceeded the maximum production in MilliQ, both for purged and unpurged samples. This can be explained by an increased number of side reactions that favor N_2O production in the BE water matrix (van Cleemput, 1998). High background nitrite concentrations in the BE water can be excluded as the background production was measured during the second experiment and showed no significant increase in N_2O.

N_2O production from purged samples was slightly higher than from unpurged samples. The experiment with purged samples was conducted one week later, which may have an influence through the aging of organic matter contained in the water. Another possible explanation is a change in the redox state of the medium due to the purging with nitrogen gas.

It can be concluded that while N_2O production in MilliQ stayed relatively moderate even for high nitrite concentrations the N_2O production in BE water samples exceeds the statistical uncertainty of the N_2O measurements at concentrations as low as 0.5 µmol L^{-1} in less than 24 h. This has broad implications for the hydroxylamine analysis: the complete conversion reaction between hydroxylamine and FAS takes at least 3h (Butler and Gordon, 1986c). Without any additional treatments for sample conservation, this leaves only a very limited time window for the analysis.

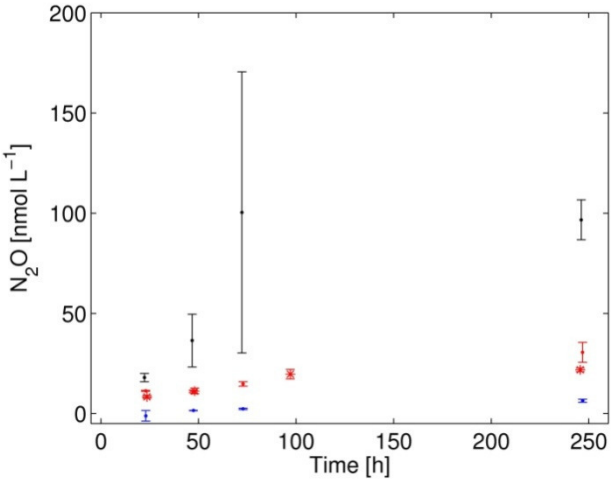

345 **Figure 4: Inhibition of N_2O production from nitrous acid. Samples without NaOH addition were directly measured for N_2O (blue, red, black dots; 1µmol L^{-1} (blue), 10 µmol L^{-1} (red), 100 µmol L^{-1} (black)). Samples with NaOH addition (red stars, 10 µmol L^{-1}) were measured one week after pH change to alkaline conditions. All samples were corrected for background N_2O concentrations.**

350

N_2O production from nitrous acid can effectively be inhibited by pH conversion to alkaline conditions, however (Fig. 4). While background production in MilliQ at pH 1 showed similar results to the previous experiments (Fig. 3), samples showed no further N_2O production after addition of sodium hydroxide additions. This provides a possibility to reduce the side effect of
355 background N_2O production in further experiments.

3.2 Reaction of hydroxylamine with nitrite

As mentioned above, nitrous acid can convert hydroxylamine to N_2O, leading to biased recovery factors (Bothner-By and Friedman, 1952). The potential of this reaction for further bias was
360 analyzed in experiments with and without FAS addition.

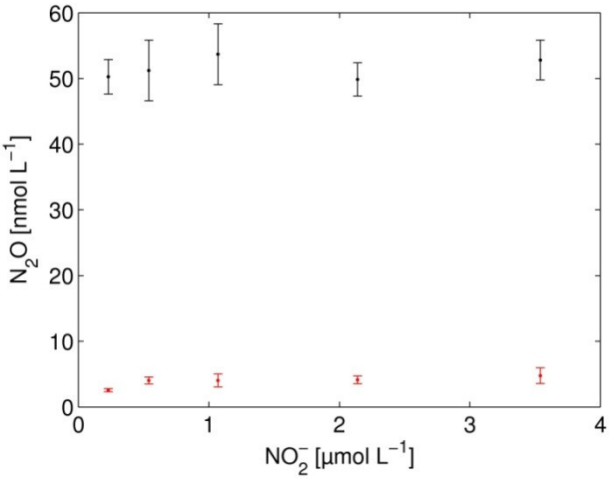

Figure 5: Nitrous oxide production in MilliQ from acidified samples with different nitrite additions without hydroxylamine (red) and with hydroxylamine (black). The concentration of hydroxylamine in the samples was 49.4 nmol L^{-1}.

Figure 5 shows the N_2O production in MilliQ from different nitrite concentrations with and without the addition of hydroxylamine. Samples without hydroxylamine addition showed little N_2O production with only a slight increase in production with increasing nitrite concentrations which is in reasonable agreement with the results from Exp. 2.1.1. In contrast, samples with hydroxylamine addition showed highly elevated concentrations around 50 nmol L^{-1} for all nitrite concentrations. No significant difference between the samples with different nitrite concentrations was found, and the conversion factors, calculated as the ratio between ΔN_2O (= N_2O_{HA}-N_2O_{NO2-}) and hydroxylamine concentrations were close to one, indicating that N_2O is produced almost quantitatively from the comproportionation of nitrite and hydroxylamine.

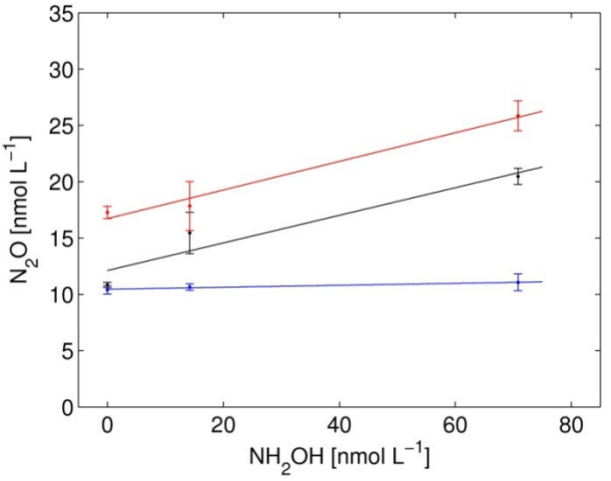

Figure 6: Nitrous oxide production in BE water from conversion of hydroxylamine at different nitrite additions: blue: 0 µmol L^{-1}; black: 0.151 µmol L^{-1}; red: 0.739 µmol L^{-1}. Reaction time: 72h. Regression statistics are: blue: 0.009(±0.002)x+10.45(±0.07), r^2=0.96; black: 0.12(±0.04)x+12.11(±1.63), r^2=0.91; red: 0.13(±0.02)x+16.72(±0.70);

The reaction of nitrite and hydroxylamine in BE water yielded conversion factors of less than 20 % for nitrite concentrations below 1 µmol L^{-1} (Fig. 6), indicating that the seawater matrix may enhance the potential of side reactions that lead to other products than N_2O. Although associated with relatively large uncertainties, the consistency of the regression slopes for samples with different nitrite additions indicates that the reduced conversion factors are unlikely to be explained by a different threshold for the reaction between nitrite and hydroxylamine. However, all measurements with nitrite addition are attributed with relatively large uncertainties which can be partly explained by the dominance of background nitrite production that leads to large offsets in the measurements.

Both experiments show that even ambient concentrations of nitrite have the potential to convert hydroxylamine to N_2O, with highly variable conversion factors. In combination with the results from section 2.1 this implicates that samples with even small amounts of nitrite must not be left acidified unless any precautions against the side reactions of nitrite are taken. However, in all conversion experiments, samples were left to react for minimum 24 h, while the conversion with FAS should be completed after 3 h (Butler and Gordon, 1986c). Therefore, the conversion of hydroxylamine with FAS in presence of nitrite was additionally tested (Fig. 7).

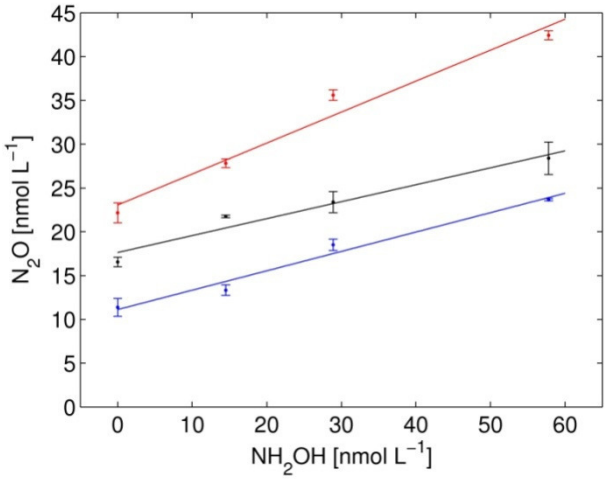

Figure 7: Conversion of hydroxylamine in MilliQ with FAS in presence of nitrite. Nitrite additions were 0.162 µmol L^{-1} (blue), 0.539 µmol L^{-1} (black), 2.695 nmol L^{-1} (red). The regression parameters are: blue: y=0.22(±0.02)x+11.18(±0.80), r^2=0.98;black: y=0.19(±0.03)x+17.63(±0.97), r^2=0.96; red: 0.35(±0.05)x+23.06(±1.50), r^2=0.97.

All samples showed conversion factors which were in the range of previous observations (Gebhardt et al., 2004;Schweiger et al., 2007). They were significantly lower than the "nitrite-only" conversion factor obtained in Exp. 2.2.1. A significant change in slope occurred between samples with low (<0.54 µmol L^{-1}) and high (2.695 µmol L^{-1}) nitrite additions. This suggests that the conversion of hydroxylamine is likely dominated by the reaction with FAS, but high

background concentrations of nitrite have the potential to bias the conversion rates towards higher values.

3.3 Reduction of side effects

As a potential scavenger for nitrite in hydroxylamine analysis, the effect of ascorbic acid on the FAS conversion of hydroxylamine was tested. While nitrite could not be detected in all samples treated with ascorbic acid and was thus rapidly removed, no conversion of hydroxylamine was observed in samples with addition of ascorbic acid (Fig. 8). This can have two reasons: hydroxylamine is either reduced by ascorbic acid more rapidly than it can be converted by FAS, or the ascorbic acid reduces the iron (III) which cannot react with hydroxylamine in its reduced form. From our measurements the underlying processes cannot be identified, but the results clearly show that the application of ascorbic acid as nitrite scavenger does not work for hydroxylamine analysis.

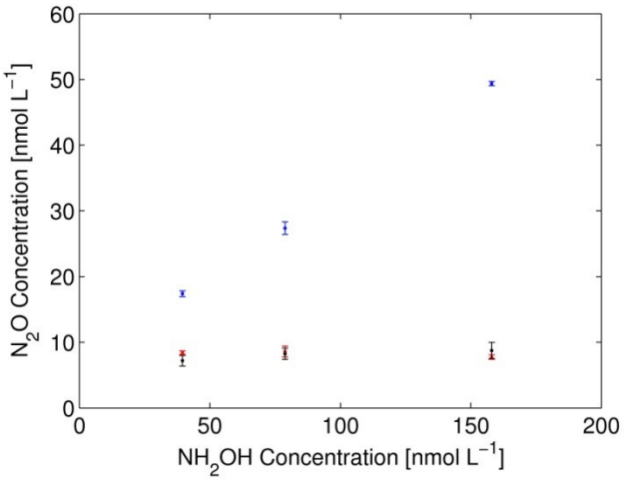

Figure 8: Conversion of hydroxylamine by FAS without addition of ascorbic acid (blue) and with addition of ascorbic acid (black, red). Conversion with FAS was started directly after hydroxylamine addition (black or red) and after 4 h (black or red).

Figure 9 shows the FAS conversion with and without sulfanilamide addition in MilliQ. While no difference could be found between samples with and without sulfanilamide addition at low nitrite concentrations, an offset of 2.4 (±1.9) nmol L^{-1} was observed at high nitrite concentrations. This offset can be explained by the increase in N_2O from background production in samples without sulfanilamide addition. While no difference was observed between the slopes of the regression lines in samples with and without sulfanilamide addition at both nitrite concentrations, a decrease

in the regression slope is observed with increasing nitrite concentrations, however, the uncertainties in the regression slopes were relatively large in this experiment.

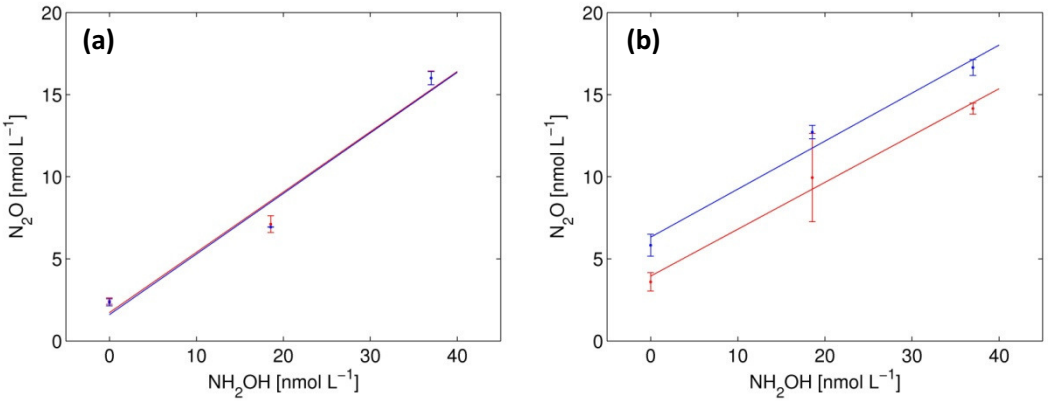

Figure 9: FAS conversion of hydroxylamine in MilliQ in presence of nitrite with (red) and without (blue) sulfanilamide addition. Nitrite additions were: a) 0.87 µmol L^{-1}; b) 4.5 µmol L^{-1}. The regression parameters are
a) with sulfanilamide addition (red line):y=0.37(±0.07)x+1.72(±1.59), r^2=0.97; without addition (blue line): y=0.37(±0.07)x+1.60(±1.69), r^2=0.96;
b) with sulfanilamide addition (red line): y=0.29(±0.03)x+3.95(±0.79), r^2=0.99; without addition (blue line): y=0.29(±0.05)x+6.32(±1.09), r^2=0.98.

The same experiment in seawater showed a significant increase in the conversion slopes with increasing nitrite concentrations, but only for samples without sulfanilamide addition (Fig. 10). Also, a significant offset could be observed between samples with and without sulfanilamide additions for both nitrite additions, which is increasing with the increase of the nitrite concentration. This can be explained by the larger background N_2O production in seawater than in MilliQ (see Exp. 2.1.1). N_2O production from samples with sulfanilamide addition did not change with increasing nitrite concentration, which leads to the conclusion that nitrite was successfully removed from the samples. The conversion rates obtained from samples with sulfanilamide addition were in reasonable agreement with conversion rates obtained in experiments without sulfanilamide addition (Exp. 2.2.3), it can thus be concluded that potential effects of sulfanilamide on the conversion reaction can be neglected.

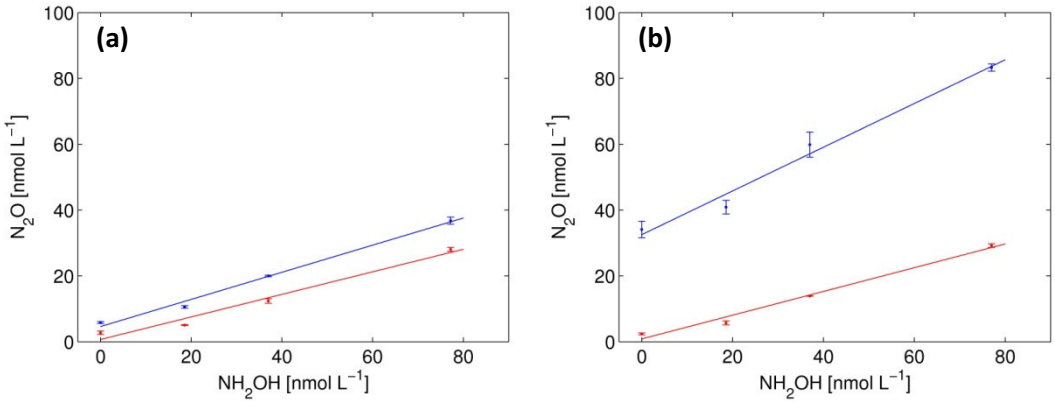

Figure 10: FAS conversion of hydroxylamine in seawater in presence of nitrite with (red) and without (blue) sulfanilamide addition. Nitrite additions were 0.87 µmol L^{-1} (left panel) and 4.5 µmol L^{-1} (right panel). The regression slopes are
a) with sulfanilamide addition (red line): y=0.34(±0.04)x+0.70(±1.70), r^2=0.97; without addition (blue line): y=0.41(±0.03)x+4.63(±1.14), r^2=0.99;
b) with sulfanilamide addition (red line): y=0.36(±0.03)x+0.87(±1.4), r^2=0.99; without addition (blue line):y=0.66(±0.06)x+32.5(±2.76) , r^2=0.98.

4. Field measurements

4.1 Measurements at the Boknis Eck Time Series Station

Hydroxylamine measurements have been continuously conducted at the Boknis Eck Time Series station since 2005 (Gebhardt et al., 2004;Schweiger et al., 2007) using the FAS conversion method according to Butler and Gordon (1986a). The modified FAS conversion method with sulfanilamide addition has been used for samplings from February to April and in June, August and September 2011. The results from seven months of sampling are shown in Figure 13.

Additionally, a comparison of the modified and the original method was performed during the monthly sampling in September 2011. Two subsets of samples were taken that were treated with and without the addition of 100 µmol L^{-1} sulfanilamide. Samples were analyzed for N_2O one week after conversion.

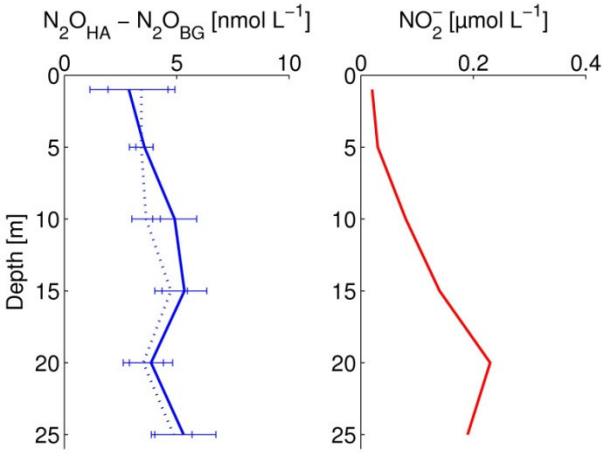

Figure 11: $N_2O_{Hydroxylamine}$ – $N_2O_{Background}$ for samples with (solid line) and without (dotted line) sulfanilamide addition (left) and nitrite concentrations (right) at Boknis Eck in September 2011.

At all depths, no significant difference between samples with and without sulfanilamide addition was observed. Nitrite concentrations were relatively throughout the water column, with a maximum nitrite concentration of 0.23 µmol L^{-1} at 25 m (Fig. 11).

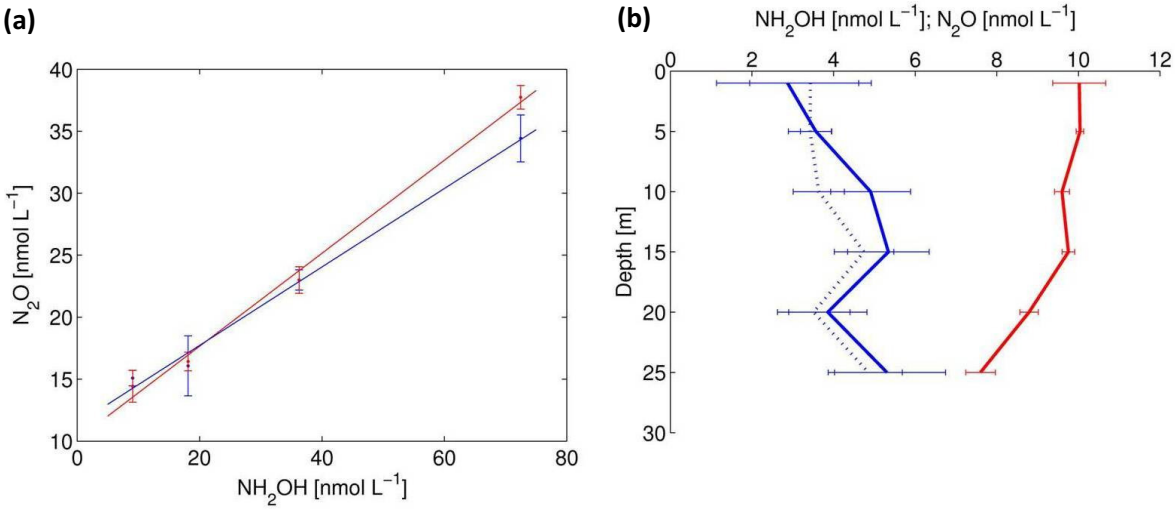

Figure 12: Hydroxylamine conversion for samples without (red) and with (blue) sulfanilamide addition. Regression parameters are: red: y=0.38 (±0.014)x+10.15(±0.58), r^2=0.99; blue: y=0.33(±0.014)x+11.39(±0.60) (left panel) and depth profiles for N_2O (red) and NH_2OH (blue), calculated from measurements with (solid line) and without (dotted line) sulfanilamide addition (right panel).

Hydroxylamine conversion in samples without sulfanilamide addition showed slightly higher regression slopes (Fig. 12a). Both regression slopes are in reasonable agreement with the recovery factors obtained by Schweiger et al. (2007) at the same sampling site. The differences between the

hydroxylamine concentrations of samples with and without sulfanilamide addition were too small to reveal a significant difference between the hydroxylamine profiles obtained with the two methods (Fig. 12b). It can be thus concluded that no significant N_2O production from nitrite was observed in the samples treated without sulfanilamide addition even at a storage time of the samples of one week which is considerably longer than the storage times during the laboratory experiments. Nitrite concentrations in the Boknis Eck samples were also lower than in the laboratory experiments, however, and side production of N_2O from higher nitrite concentrations cannot be excluded yet.

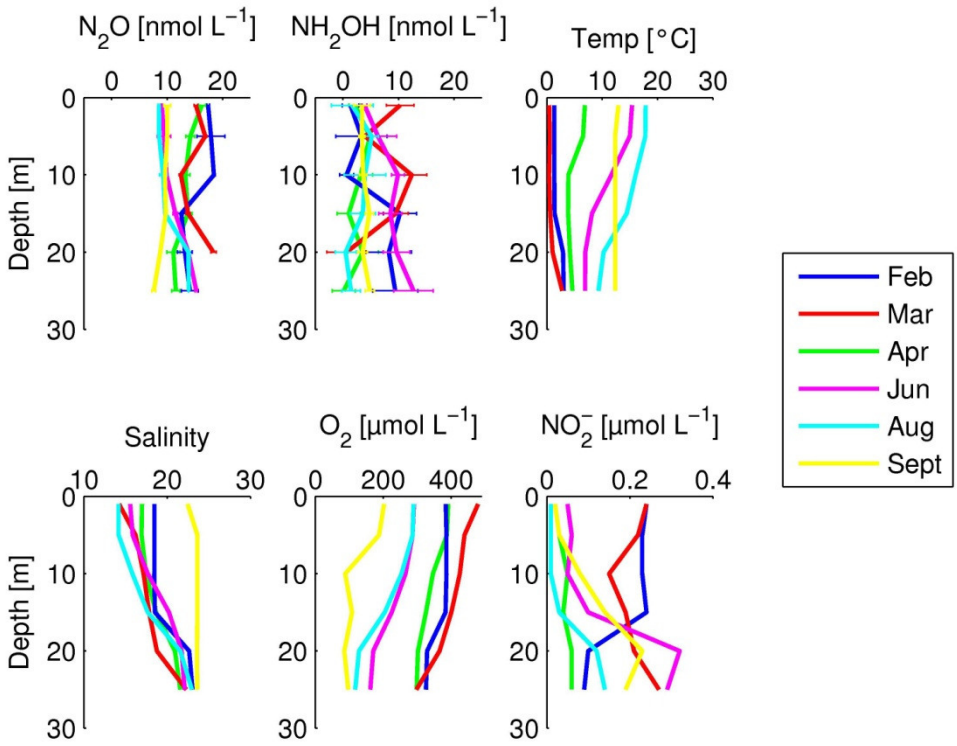

Figure 13: Time series measurements of nitrous oxide, hydroxylamine and other parameters at the Boknis Eck Time Series Station from February to September 2011.

Hydroxylamine concentrations from the time series measurements were relatively low compared to previously reported concentrations (Fig. 13, Table 1) and are in the same order of magnitude as the measurements by Schweiger et al. (2007). Hydroxylamine was highest during the months with highest nitrite concentrations (February to March and June), however, a simple correlation between nitrite and hydroxylamine could not be identified.

4.2 Hydroxylamine Measurements in the Eqatorial Atlantic Ocean

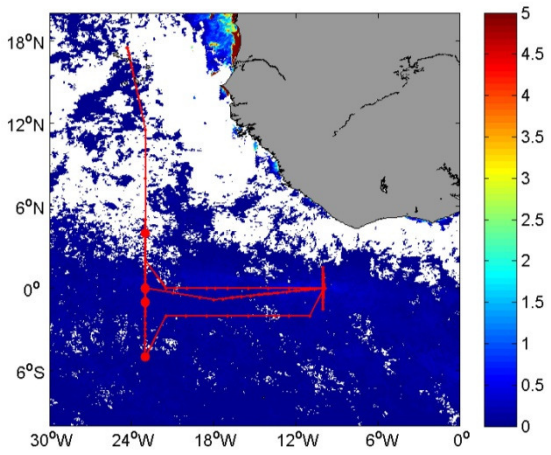

Figure 14: Surface chlorophyll a (in mg m^{-3}) distribution during the Maria S. Merian Cruise MSM 18-2 in May/June 2011. The cruise track is shown in red, with stations sampled for hydroxylamine highlighted. Chlorophyll data were obtained from MODIS aqua eight day chlorophyll images (http://oceandata.sci.gsfc.nasa.gov/MODISA/Mapped/8Day/4km/chlor/).

In oceanic environments, measurements of hydroxylamine have been conducted in coastal zones and estuaries (Butler et al., 1987;Butler et al., 1988;Gebhardt et al., 2004;Schweiger et al., 2007). No measurements of hydroxylamine in open ocean environments have been published so far. During the Maria S. Merian cruise MSM 18-2 in May/June 2011 to the equatorial Atlantic hydroxylamine profiles were measured at five stations using the modified method with sulfanilamide addition (Fig 14). The surface chlorophyll a distribution, obtained from MODIS aqua chlorophyll a satellite images for the sampling period, showed a very weak signal of a phytoplankton bloom due to equatorial upwelling.

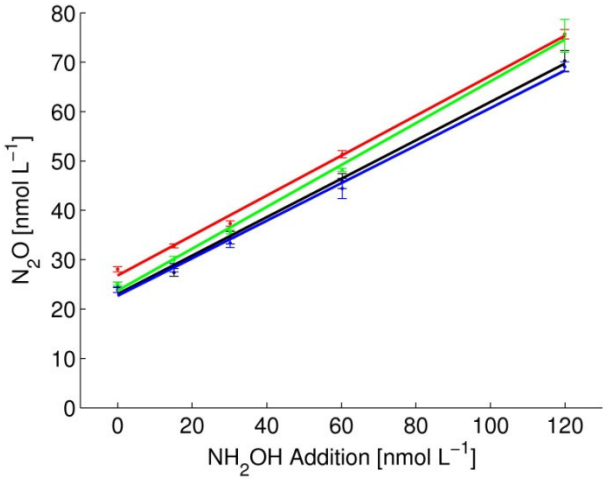

Figure 15: Hydroxylamine conversion during MSM 18-2. Standard additions were conducted at four stations with samples from 200 m water depth. All regression slopes were between 0.38 and 0.43.

The standard addition of hydroxylamine at four stations revealed very similar conversion rates for all experiments (Fig. 15). Recovery factors ranged from 0.76 to 0.86, which is close to the recovery factors obtained by Butler and Gordon (1986a) and in reasonable agreement with the recovery factors obtained in seawater in experiment 2.3.2, but significantly larger than the recovery factors obtained at the Boknis Eck Time Series Station (see section 4.1). This may be explained by lower concentrations of trace metals and organic matter in the open ocean waters compared to the coastal waters at Boknis Eck.

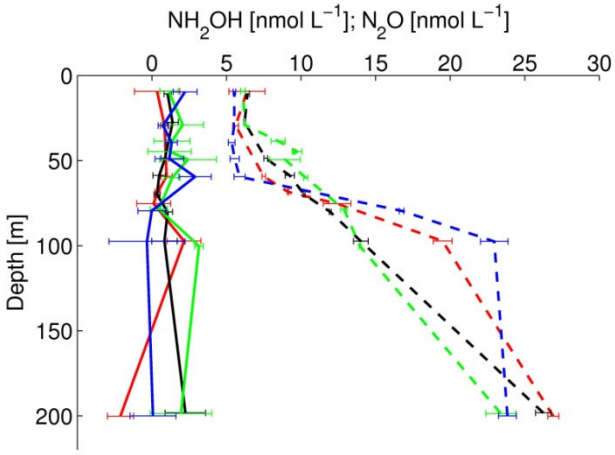

Figure 16: Hydroxylamine (solid lines) and N_2O (dotted lines) depth profiles during MSM 18-2. Hydroxylamine concentrations were calculated using a mean recovery factor of 0.906 for all stations. The locations of the stations were: 23 °W, 4 °N (black); 23 °W, 0° N (red); 23° W, 1 °S (blue); 23 °W, 5 °S (green).

While N_2O profiles showed a sharp increase in N_2O concentrations from ~5 to ~25 nmol L^{-1}, all depth profiles obtained during MSM18-2 showed hydroxylamine concentrations close to or below the detection limit of the method (Fig. 16). Negative hydroxylamine concentrations were calculated at several depths, but these values were close to the detection limit of the analysis, too. Nitrite concentrations were zero except for a subsurface maximum at the base of the mixed layer with maximum concentrations of 0.3 µmol L^{-1} (data not shown). These concentrations are relatively low compared to nitrite concentrations in the primary nitrite maximum of productive areas (Kamykowski and Zentara, 1991).

The absence of hydroxylamine in the equatorial upwelling could be explained by:

1) Low nitrification rates that do not accumulate significant amounts of hydroxylamine. This is supported by the low primary productivity at the time of the measurements (Fig. 14) and the low concentrations of nitrite in the primary nitrite maximum. However, hydroxylamine measurements in open ocean areas with high primary productivity are required to verify this hypothesis.

2) Low accumulation of hydroxylamine due to its efficient consumption which is independent from nitrification activity. An effective consumption of the hydroxylamine produced in the first step of ammonium oxidation would keep the steady-state concentration of hydroxylamine low. Hydroxylamine accumulation would thus be an indication for a delay in the hydroxylamine oxidation which could be the case directly after the onset of nitrification (Schweiger et al., 2007).

3) Archaeal ammonium oxidation, not producing hydroxylamine, dominating over bacterial nitrification. Archaeal nitrifiers have been shown to be more abundant than bacterial nitrifiers throughout the world's oceans (e.g. Beman et al. (2008), Molina et al. (2010), Wuchter et al. (2006)) and have been suggested to dominate global nitrification. Although there are indications for a different pathway of ammonium oxidation in archaea and bacteria (Wankel et al., 2007), hydroxylamine production during archaeal ammonium oxidation cannot be ruled out yet, however.

The current measurements of hydroxylamine do not provide enough information to exclude one of the explanations above. Additional measurements of hydroxylamine in the water column as well as from incubation and culture experiments are required to explain the occurrence of hydroxylamine in the ocean.

5. Summary

The conversion factors of all experiments with hydroxylamine conversion are given in Table 2.

Table 2: Conversion factors of hydroxylamine standard addition experiments and field measurements.

Exp.	Medium	FAS addition [µmol L^{-1}]	Nitrite scavenger addition	Nitrite addition [µmol L^{-1}]	Conversion factor	Correlation coefficient
2.2.1	MilliQ	-	-	0.23 to 3.54	~0.9	-
2.2.2	BE water	-	-	-	0.009	0.96
2.2.2	BE water	-	-	0.15	0.12	0.91
2.2.2	BE water	-	-	0.74	0.13	
2.2.3	BE water	220	-	0.16	0.22	0.98
2.2.3	BE water	220	-	0.54	0.19	0.97
2.2.3	BE water	220	-	2.7	0.35	0.97
2.3.1	MilliQ	220	-	-	0.27	0.99
2.3.1	MilliQ	220	Ascorbic acid, 10 mmol L^{-1}, T0	-	0.01	0.29
2.3.1	MilliQ	220	Ascorbic acid, 10 mmol L^{-1}, T1	-	-0.01	0.04
2.3.2	MilliQ	220	-	0.87	0.37	0.97
2.3.2	MilliQ	220	Sulfanilamide, 100µmol L^{-1}	0.87	0.37	0.96
2.3.2	MilliQ	220	-	4.5	0.29	0.99
2.3.2	MilliQ	220	Sulfanilamide, 100µmol L^{-1}	4.5	0.29	0.98
2.3.2	Filtered seawater	220	-	0.87	0.34	0.97
2.3.2	Filtered seawater	220	Sulfanilamide, 100µmol L^{-1}	0.87	0.36	0.99
2.3.2	Filtered seawater	220	-	4.5	0.36	0.98
2.3.2	Filtered seawater	220	Sulfanilamide, 100µmol L^{-1}	4.5	0.66	0.98
3.4	BE water, monthly sampling	220	Sulfanilamide, 100µmol L^{-1}	-	0.21 to 0.37	0.98 (average)
3.4	Seawater,Equatorial Atlantic	220	Sulfanilamide, 100µmol L^{-1}	-	0.38 to 0.43	0.99 (average)

Our results show that in contrast to the findings by Butler and Gordon (1986a) the detection of hydroxylamine via FAS conversion is largely affected by the presence of nitrite. The large

number of side reactions and their different behavior in different reaction media (Table 2) demand the removal of nitrite from seawater samples before hydroxylamine detection. While ascorbic acid was found not suitable as nitrite scavenger in hydroxylamine analysis, sulfanilamide successfully removed nitrite from the samples without affecting the FAS conversion. Based on these results, we suggest a modification of the original method by the addition of 100 µmol L^{-1} acidic sulfanilamide solution to the reaction medium before or directly after acidification of the samples to inhibit potential N_2O production from side reactions with nitrite.

Field measurements of hydroxylamine using the modified method from the Boknis Eck Time Series Station showed low concentrations of hydroxylamine throughout the water column. No significant difference between measurements with and without sulfanilamide addition were found at nitrite concentrations below 0.25 µmol L^{-1} and a storage time of one week, but the effect of longer storage times and higher nitrite concentrations has to be further investigated. Monthly measurements of N_2O at the Boknis Eck Time Series Station showed hydroxylamine concentrations in the same order of magnitude as measured by Schweiger et al. (2007). No clear correlation between hydroxylamine and other parameters could be found for the period of the samplings; however, a detailed analysis of the dataset including at least one full annual cycle of measurements has to be done yet. Hydroxylamine concentrations from measurements in the equatorial Atlantic Ocean were below the detection limit of the method. This can have a number of reasons, and the current amount of data is not sufficient to explain the dynamics of hydroxylamine cycling in the water column.

7 Conclusions and outlook

The results presented in this thesis give some new insights into the understanding of oceanic N_2O and hydroxylamine production. Our results can be summarized as follows:

Archaeal N_2O production has recently been detected by Santoro et al. (2011) from Pacific Ocean enrichment cultures. Our results complement these findings by the evidence for archaeal N_2O production from a pure culture of an ammonium oxidizing archaeon. Together with field data and onboard experiments, archaea could be identified as the main producers of oceanic N_2O.

Moreover, an increase of N_2O yields with decreasing oxygen concentrations was detected. This is especially important as most current studies imply higher yields of N_2O from nitrification with decreasing oxygen (Codispoti, 2010), this assumption for example was made in a number of modeling studies (Nevison et al., 2003;Suntharalingam and Sarmiento, 2000). However, the exponential increase of the N_2O yield with decreasing oxygen concentrations applied in the model simulations was derived from a similar culture experiment with a bacterial ammonium oxidizer (Goreau et al., 1980). The strong evidence for archaeal nitrification as the main driver for N_2O production thus requires the additional investigation of the oxygen dependence of archael nitrification.

Additionally, the metabolic pathway of archaeal ammonium oxidation has to be investigated, too. The interpretation of the isotopic composition of N_2O in oceanic waters relies on laboratory experiments with bacterial nitrifiers (Sutka et al., 2006;Sutka et al., 2003;Stein and Yung, 2003), and the isotopic composition of N_2O from archaeal nitrification is not well investigated yet (Santoro et al., 2011). The here introduced method of hydroxylamine measurements can be used as another possibility to shed light on the pathway of archaeal ammonium oxidation. Hydroxylamine measurements can also give insights in the dynamics of nitrogen cycling in the ocean: First measurements from a coastal time series station and four open ocean stations are presented here. Hydroxylamine was not detected in the water column at four open ocean stations which can be explained 1) by different pathways of ammonium oxidation in archaea and bacteria, 2) by an effective recycling of hydroxylamine in the water column that prevents its accumulation or 3) by low nitrification activity in the investigated area. At the coastal time series station, hydroxylamine concentrations showed a large variability, and the dynamics of hydroxylamine accumulation could not be explained by simple correlations yet. However, if we understand the pathways of hydroxylamine production and consumption in the nitrogen transformations, hydroxylamine measurements can provide new information about the short-term dynamics of the marine nitrogen cycle. Additional water column measurements, but also hydroxylamine measurements in incubation and culture experiments with ammonium oxidizing archaea and bacteria will help to identify the underlying processes.

Although nitrogen cycling has been shown to be very different in the ETNA and in the ETSP, our measurements do not indicate that these differences are controlled by other factors than the oxygen concentrations. A similar regression slope for ΔN_2O/AOU in the ETNA and ETSP indicates a similar yield of N_2O during oxygen consumption in both areas. An increase in ΔN_2O/AOU was observed for oxygen concentrations between 5 and 50 µmol L^{-1} in the ETSP, which may be due to a shift in the N_2O production pathway from hydroxylamine oxidation to nitrifier-denitrification (Popp et al., 2002;Ostrom et al., 2000) or the onset of N_2O production by denitrification (Farias et al., 2009;Bange et al., 2005). However, N_2O production from archaeal nitrification was not taken into account in these studies, and production pathways are still unclear. If archaeal ammonium oxidation accounts for the majority of the aerobic N_2O production, its production pathways are the main control on the isotopic composition of N_2O. A mixture of hydroxylamine oxidation and nitrifier-denitrification was identified as N_2O production pathway from isotopic studies with enrichment cultures (Santoro et al., 2011), while nitrifier-denitrification was excluded as N_2O production pathway from *N. maritimus* cultures in our study. A different production pathway from cluster B affiliated *Thaumachaeota* which are prevalent in oxygen-deficient waters (Molina et al., 2010) cannot be excluded yet. In the ETNA, a slope change was not observable as minimum oxygen concentrations were close to 50 µmol L^{-1}. If in the ETNA a similar slope change to the ETSP is established, a decrease in oxygen concentrations as a result of climate change (Stramma et al., 2008b) would lead to a disproportional increase in N_2O concentrations which, in turn, could also lead to enhanced N_2O emissions from the Mauritanian upwelling by an increase in the N_2O transport from subsurface waters.

For the Mauritanian upwelling N_2O production in the mixed layer was found not sufficient to close the large discrepancy between upward N_2O flux into the mixed layer and sea-to-air flux. A large discrepancy between diapycnal and sea-to-air fluxes has been explained by N_2O production from mixed layer nitrification in earlier studies (Morell et al., 2001;Santoro et al., 2010;Dore and Karl, 1996;Cline et al., 1987). However, most of the studies did not calculate N_2O production rates for the mixed layer, and these studies were carried out in regions where surface N_2O concentrations were close to equilibrium and therefore, the absolute discrepancy of the fluxes was smaller than in an upwelling area. Charpentier et al. (2010) calculated a mixed layer budget for N_2O in the upwelling area off Chile and introduced an unidentified production pathway of N_2O in the mixed layer to close the budget. In contrast, in our study we argue that the discrepancy is rather explained by a reduced gas exchange due to the occurrence of surfactants. Although there are some indications for a reducing effect of surfactants on gas exchange (Upstill-Goddard, 2006;Schmidt and Schneider, 2011), direct evidence that this effect is responsible for the unbalance of the budget is still missing, and further investigation on this effect is required to verify our hypothesis. A reduced gas exchange would have large implications on the oceanic N_2O emissions to the atmosphere, yet. Depending on the extension of surfactants in the oceans and on the magnitude of the reduction of gas exchange in different oceanic regions, a reduced gas exchange may lead to significantly reduced oceanic N_2O emissions. Moreover,

a reduction of the gas exchange would not only affect N_2O emissions but also the flux balance of other trace gases.

References

Altabet, M. A., and Francois, R.: Sedimentary Nitrogen Isotopic Ratio as a Recorder for Surface Ocean Nitrate Utilization, Global Biogeochemical Cycles, 8, 103-116, 1994.

Altabet, M. A.: Nitrogen isotopic evidence for micronutrient control of fractional NO_3^- utilization in the equatorial Pacific, Limnology and Oceanography, 46, 368-380, 2001.

Altabet, M. A.: Constraints on oceanic N balance/imbalance from sedimentary ^{15}N records, Biogeosciences, 4, 75-86, 10.5194/bg-4-75-2007, 2007.

Arp, D. J., and Stein, L. Y.: Metabolism of inorganic N compounds by ammonia-oxidizing bacteria, Critical Reviews in Biochemistry and Molecular Biology, 38, 471-495, 10.1080/10409230390267446, 2003.

Baker, A. R., Kelly, S. D., Biswas, K. F., Witt, M., and Jickells, T. D.: Atmospheric deposition of nutrients to the Atlantic Ocean, Geophysical Research Letters, 30, 2296-2300, 10.1029/2003gl018518, 2003.

Baker, A. R., Weston, K., Kelly, S. D., Voss, M., Streu, P., and Cape, J. N.: Dry and wet deposition of nutrients from the tropical Atlantic atmosphere: Links to primary productivity and nitrogen fixation, Deep Sea Research Part I: Oceanographic Research Papers, 54, 1704-1720, 10.1016/j.dsr.2007.07.001, 2007.

Bange, H. W., Rapsomanikis, S., and Andreae, M. O.: Nitrous oxide in coastal waters, Global Biogeochem. Cycles, 10, 197-207, 1996.

Bange, H. W., Andreae, M. O., Lal, S., Law, C. S., Naqvi, S. W. A., Patra, P. K., Rixen, T., and Upstill-Goddard, R. C.: Nitrous oxide emissions from the Arabian Sea: A synthesis, Atmospheric Chemistry and Physics, 1, 61-71, 2001.

Bange, H. W., Naqvi, S. W. A., and Codispoti, L. A.: The nitrogen cycle in the Arabian Sea, Progress in Oceanography, 65, 145-158, 10.1016/j.pocean.2005.03.002, 2005.

Bange, H. W.: Gaseous nitrogen compounds (NO,N2O,N2,NH3) in the ocean, in: Nitrogen in the Marine Environment, 2 ed., edited by: Capone, D. G., Bronk, D. A., Mulholland, M. R., and Carpenter, E. J., Academic Press/Elsevier 51-94, 2008.

Bange, H. W., Bell, T. G., Cornejo, M., Freing, A., Uher, G., Upstill-Goddard, R. C., and Zhang, G. L.: MEMENTO: a proposal to develop a database of marine nitrous oxide and methane measurements, Environmental Chemistry, 6, 195-197, 10.1071/en09033, 2009.

Bange, H. W., Bergmann, K., Hansen, H. P., Kock, A., Koppe, R., Malien, F., and Ostrau, C.: Dissolved methane during hypoxic events at the Boknis Eck time series station (Eckernforde Bay, SW Baltic Sea), Biogeosciences, 7, 1279-1284, 2010a.

Bange, H. W., Freing, A., Kock, A., and Löscher, C. R.: Marine pathways to nitrous oxide, in: Nitrous Oxide and Climate Change, edited by: Smith, K., Earthscan, London, 36-62, 2010b.

Barford, C. C., Montoya, J. P., Altabet, M. A., and Mitchell, R.: Steady-state nitrogen isotope effects of N_2 and N_2O production in *Paracoccus denitrificans*, Applied and Environmental Microbiology, 65, 989-994, 1999.

Behar, D., Shapira, D., and Treinin, A.: Photolysis of hydroxylamine in aqueous solution, Journal of Physical Chemistry, 76, 180-&, 10.1021/j100646a006, 1972.

Beman, J. M., Popp, B. N., and Francis, C. A.: Molecular and biogeochemical evidence for ammonia oxidation by marine Crenarchaeota in the Gulf of California, Isme Journal, 2, 429-441, 10.1038/ismej.2007.118, 2008.

Bothner-By, A., and Friedman, L.: The Reaction of Nitrous Acid with Hydroxylamine, 3, AIP, 459-462 pp., 1952.

Bourbonnais, A., Lehmann, M. F., Waniek, J. J., and Schulz-Bull, D. E.: Nitrate isotope anomalies reflect N_2 fixation in the Azores Front region (subtropical NE Atlantic), Journal of Geophysical Research-Oceans, 114, C03003, 10.1029/2007JC004617, 2009.

Bouwman, A. F.: Direct emission of nitrous oxide from agricultural soils, Nutrient Cycling in Agroecosystems, 46, 53-70, 10.1007/bf00210224, 1996.

Brandes, J. A., Devol, A. H., Yoshinari, T., Jayakumar, D. A., and Naqvi, S. W. A.: Isotopic composition of nitrate in the central Arabian Sea and eastern tropical North Pacific: A tracer for mixing and nitrogen cycles, Limnology and Oceanography, 43, 1680-1689, 10.4319/lo.1998.43.7.1680, 1998.

Brandes, J. A., and Devol, A. H.: A global marine-fixed nitrogen isotopic budget: Implications for Holocene nitrogen cycling, Global Biogeochemical Cycles, 16, 1120-1134, 10.1029/2001GB001856, 2002.

Brochier-Armanet, C., Boussau, B., Gribaldo, S., and Forterre, P.: Mesophilic crenarchaeota: proposal for a third archaeal phylum, the Thaumarchaeota, Nat Rev Micro, 6, 245-252, 2008.

Butler, J. H., and Gordon, L. I.: An improved gas-chromatographic method for the measurement of hydroxylamine in marine and fresh waters, Marine Chemistry, 19, 229-243, 1986a.

Butler, J. H., and Gordon, L. I.: Hydroxylamine and nitrous oxide over the Cariaco Trench, West Basin, 14-17 March 1986, Cooperative Institute for Research in Environmental Sciences, University of Colorado/NOAA, Boulder, CO, USAReport for R/V Columbus Iselin Cruise CI 8601, Leg 2, 1986b.

Butler, J. H., and Gordon, L. I.: Rates of nitrous oxide production in the oxidation of hydroxylamine by iron(III), Inorganic Chemistry, 25, 4573-4577, 1986c.

Butler, J. H., Jones, R. D., Garber, J. H., and Gordon, L. I.: Seasonal distribution and turnover of reduced trace gases and hydroxylamine in Yaquina Bay, Oregon, Geochimica et Cosmochimica Acta, 51, 697-706, 1987.

Butler, J. H., Pequegnat, J. E., Gordon, L. I., and Jones, R. D.: Cycling of methane, carbon monoxide, nitrous oxide and hydroxylamine in a meromictic, coastal lagoon, Estuarine Coastal and Shelf Science, 27, 181-203, 1988.

Canfield, D. E., Glazer, A. N., and Falkowski, P. G.: The Evolution and Future of Earth's Nitrogen Cycle, Science, 330, 192-196, 10.1126/science.1186120, 2010.

Carpenter, E. J., Harvey, H. R., Fry, B., and Capone, D. G.: Biogeochemical tracers of the marine cyanobacterium *Trichodesmium*, Deep-Sea Research Part I-Oceanographic Research Papers, 44, 27-38, 10.1016/S0967-0637(96)00091-X, 1997.

Casciotti, K. L., and McIlvin, M. R.: Isotopic analyses of nitrate and nitrite from reference mixtures and application to Eastern Tropical North Pacific waters, Marine Chemistry, 107, 184-201, 10.1016/j.marchem.2007.06.021, 2007.

Casciotti, K. L.: Inverse kinetic isotope fractionation during bacterial nitrite oxidation, Geochimica et Cosmochimica Acta, 73, 2061-2076, 0.1016/j.gca.2008.12.022, 2009.

Charpentier, J., Farias, L., and Pizarro, O.: Nitrous oxide fluxes in the central and eastern South Pacific, Global Biogeochemical Cycles, 24, -, Artn Gb3011 Doi 10.1029/2008gb003388, 2010.

Chavez, F. P., and Messié, M.: A comparison of Eastern Boundary Upwelling Ecosystems, Prog. Oceanogr., 83, 80-96, 2009.

Church, M. J., Wai, B., Karl, D. M., and DeLong, E. F.: Abundances of crenarchaeal amoA genes and transcripts in the Pacific Ocean, Environmental Microbiology, 12, 679-688, 10.1111/j.1462-2920.2009.02108.x, 2009.

Clark, D. R., Rees, A. P., and Joint, I.: Ammonium regeneration and nitrification rates in the oligotrophic Atlantic Ocean: Implications for new production estimates, Limnol. Oceanogr., 53, 52-62, 2008.

Cline, J. D., and Richards, F. A.: Oxygen deficient conditions and nitrate reduction in Eastern Tropical North-Pacific Ocean, Limnology and Oceanography, 17, 885-900, 1972.

Cline, J. D., Wisegarver, D. P., and Kelly-Hansen, K.: Nitrous oxide and vertical mixing in the equatorial Pacific during the 1982-1983 El Niño, Deep Sea Research Part A. Oceanographic Research Papers, 34, 857-873, 1987.

Codispoti, L. A.: An oceanic fixed nitrogen sink exceeding 400 Tg Na(-1) vs the concept of homeostasis in the fixed-nitrogen inventory, Biogeosciences, 4, 233-253, 2007.

Codispoti, L. A.: Interesting Times for Marine N_2O, Science, 327, 1339-1340, 10.1126/science.1184945, 2010.

Codispoti, L. A., Friederich, G. E., Packard, T. T., Glover, H. E., Kelly, P. J., Spinrad, R. W., Barber, R. T., Elkins, J. W., Ward, B. B., Lipschultz, F., and Lostaunau, N.: High nitrite levels off northern Peru: A signal of instability in the marine denitrification rate, Science, 233, 1200-1202, 1986.

Codispoti, L. A., J.W. Elkins, T. Yoshinari, G.E. Friederich, C.M. Sakamoto, and T.T. Packard: On the nitrous oxide flux from productive regions that contain low oxygen waters, in Oceanography of the Indian Ocean, A.A. Balkema, Rotterdam, 271-284 pp., 1992.

Codispoti, L. A., Brandes, J. A., Christensen, J. P., Devol, A. H., Naqvi, S. W. A., Paerl, H. W., and Yoshinari, T.: The oceanic fixed nitrogen and nitrous oxide budgets: Moving targets as we enter the anthropocene?, Sci. Mar., 65, 85-105, 10.3989/scimar.2001.65s285, 2001.

Cohen, Y., and Gordon, L. I.: Nitrous oxide in oxygen minimum of eastern tropical North Pacific - evidence for its consumption during denitrification and possible mechanisms for its production, Deep-Sea Research, 25, 509-524, 10.1016/0146-6291(78)90640-9, 1978.

Cohen, Y., and Gordon, L. I.: Nitrous oxide production in the ocean, Journal of Geophysical Research, 84, 347-353, 1979.

Czeschel, R., Stramma, L., Schwarzkopf, F. U., Giese, B. S., Funk, A., and Karstensen, J.: Middepth circulation of the eastern tropical South Pacific and its link to the oxygen minimum zone, Journal of Geophysical Research-Oceans, 116, C0101510.1029/2010jc006565, 2011.

David, H. A.: Further applications of range to analysis of variance, Biometrika, 38, 393-409, 1951.

Denman, K. L., Brasseur, G., Chidthaisong, A., Ciais, P., Cox, P. M.,Dickinson, R. E., Hauglustaine, D., Heinze, C., Holland, E., Jacob, D., Lohmann, U., Ramachandran, S., Leite da Silva Dias, P., Wofsy, S. C., and Zhang, X.: Couplings between changes in the climate system and biogeochemistry, in: Climate Change 2007: The Physical Science Basis. Contribution of Working Group I to the Fourth Assessment Report of the Intergovernmental Panel on Climate Change, edited by: Solomon, S., Cambridge University Press, Cambridge, UK and New York, NY, USA, 499-588, 2007.

Deutsch, C., Gruber, N., Key, R. M., Sarmiento, J. L., and Ganachaud, A.: Denitrification and N_2 fixation in the Pacific Ocean, Global Biogeochemical Cycles, 15, 483-506, 10.1029/2000GB001291, 2001.

Deutsch, C., Sarmiento, J. L., Sigman, D. M., Gruber, N., and Dunne, J. P.: Spatial coupling of nitrogen inputs and losses in the ocean, Nature, 445, 163-167, 10.1038/nature05392, 2007.

Devol, A. H.: Denitritfication including anammox, in: Nitrogen in the marine environment, 2 ed., edited by: Capone, D. G., Bronk, D. A., Mulholland, M. R., and Carpenter, E. J., Academic Press/Elsevier, 263-302, 2008.

Diaz, F., and Raimbault, P.: Nitrogen regeneration and dissolved organic nitrogen release during spring in a NW Mediterranean coastal zone (Gulf of Lions): implications for the estimation of new production, Marine Ecology-Progress Series, 197, 51-65, 10.3354/meps197051, 2000.

Dilworth, M. J., and Eady, R. R.: Hydrazine is a product of dinitrogen reduction by the vanadium-nitrogenase from Azotobacter chroococcum, Biochem. J., 277, 465-468, 1991.

Dore, J. E., and Karl, D. M.: Nitrification in the euphotic zone as a source for nitrite, nitrate, and nitrous oxide at Station ALOHA, Limnol. Oceanogr., 41, 1619-1628, 1996.

Duarte, C. M., Dachs, J., Llabres, M., Alonso-Laita, P., Gasol, J. M., Tovar-Sanchez, A., Sanudo-Wilhemy, S., and Agusti, S.: Aerosol inputs enhance new production in the subtropical northeast Atlantic, Journal of Geophysical Research-Biogeosciences, 111, G04006, 10.1029/2005jg000140, 2006.

Duce, R. A., LaRoche, J., Altieri, K., Arrigo, K. R., Baker, A. R., Capone, D. G., Cornell, S., Dentener, F., Galloway, J., Ganeshram, R. S., Geider, R. J., Jickells, T., Kuypers, M. M., Langlois, R., Liss, P. S., Liu, S. M., Middelburg, J. J., Moore, C. M., Nickovic, S., Oschlies, A., Pedersen, T., Prospero, J., Schlitzer, R., Seitzinger, S., Sorensen, L. L., Uematsu, M., Ulloa, O., Voss, M., Ward, B., and Zamora, L.: Impacts of Atmospheric Anthropogenic Nitrogen on the Open Ocean, Science, 320, 893-897, 10.1126/science.1150369, 2008.

Einsle, O., Messerschmidt, A., Huber, R., Kroneck, P. M. H., and Neese, F.: Mechanism of the six-electron reduction of nitrite to ammonia by cytochrome c nitrite reductase, Journal of the American Chemical Society, 124, 11737-11745, 10.1021/ja0206487, 2002.

Elkins, J. W., Wofsy, S. C., McElroy, M. B., Kolb, C. E., and Kaplan, W. A.: AQUATIC SOURCES AND SINKS FOR NITROUS-OXIDE, Nature, 275, 602-606, 10.1038/275602a0, 1978.

Farias, L., Castro-Gonzalez, M., Cornejo, M., Charpentier, J., Faundez, J., Boontanon, N., and Yoshida, N.: Denitrification and nitrous oxide cycling within the upper oxycline of the eastern tropical South Pacific oxygen minimum zone, Limnology and Oceanography, 54, 132-144, 2009.

Fehling, C., and Friedrichs, G.: A precise high-resolution near infrared continuous wave cavity ringdown spectrometer using a Fourier transform based wavelength calibration, Rev. Sci. Instrum., 81, 8, 053109, DOI: 10.1063/1.3422254, 2010.

Ferguson, S. J.: Denitrification and its control, Antonie Van Leeuwenhoek International Journal of General and Molecular Microbiology, 66, 89-110, 1994.

Fischer, G., Reuter, C., Karakas, G., Nowald, N., and Wefer, G.: Offshore advection of particles within the Cape Blanc filament, Mauritania: Results from observational and modelling studies, Prog. Oceanogr., 83, 322-330, 10.1016/j.pocean.2009.07.023, 2009.

Fiedler, P. C., and Talley, L. D.: Hydrography of the eastern tropical Pacific: A review, Progress In Oceanography, 69, 143-180, 10.1016/j.pocean.2006.03.008, 2006.

Forster, G., Upstill-Goddard, R. C., Gist, N., Robinson, C., Uher, G., and Woodward, E. M. S.: Nitrous oxide and methane in the Atlantic Ocean between 50 degrees N and 52 degrees S: Latitudinal distribution and sea-to-air flux, Deep-Sea Res Pt Ii, 56, 964-976, 10.1016/j.dsr2.2008.12.002, 2009.

Forster, P., V., R., P., A., T., B., Betts, R., Fahey, D. W., J., H., J., L., Lowe, D. C., Myhre, G., Nganga, J., Prinn, R., Raga, G., Schulz, M., and Van Dorland, R.: Changes in Atmospheric Constituents and in Radiative Forcing, in: Climate Change 2007: The Physical Science Basis. Contribution of Working Group I to the Fourth Assessment Report of the Intergovernmental Panel on Climate Change, edited by: Solomon, S., Qin, D., Manning, M., Chen, Z., Marquis, M., Averyt, K. B., Tignor, M., and Miller, H. L., Cambridge University Press, Cambridge, UK and New York, NY, USA, 129-234, 2007.

Frame, C. H., and Casciotti, K. L.: Biogeochemical controls and isotopic signatures of nitrous oxide production by a marine ammonia-oxidizing bacterium, Biogeosciences 7, 3019-3059, 10.5194/bgd-7-3019-2010, 2010.

Francis, C. A., Roberts, K. J., Beman, J. M., Santoro, A. E., and Oakley, B. B.: Ubiquity and diversity of ammonia-oxidizing archaea in water columns and sediments of the ocean, Proceedings of the National Academy of Sciences of the United States of America, 102, 14683-14688, 10.1073/pnas.0506625102, 2005.

Francis, C. A., Beman, J. M., and Kuypers, M. M. M.: New processes and players in the nitrogen cycle: the microbial ecology of anaerobic and archaeal ammonia oxidation, Isme Journal, 1, 19-27, 10.1038/ismej.2007.8, 2007.

Freing, A.: Production and emissions of oceanic nitrous oxide, PhD, RD-2 Chemical Oceanography, Christian-Albrechts-Universität, Kiel, 128 pp., 2009.

Freing, A., Wallace, D. W. R., Tanhua, T., Walter, S., and Bange, H. W.: North Atlantic production of nitrous oxide in the context of changing atmospheric levels, Global Biogeochem. Cycles, 23, 10.1029/2009gb003472, 2009.

Fuenzalida, R., Schneider, W., Garcés-Vargas, J., Bravo, L., and Lange, C.: Vertical and horizontal extension of the oxygen minimum zone in the eastern South Pacific Ocean, Deep Sea Research Part II: Topical Studies in Oceanography, 56, 992-1003, 2009.

Galan, A., Molina, V., Thamdrup, B., Woebken, D., Lavik, G., Kuypers, M. M. M., and Ulloa, O.: Anammox bacteria and the anaerobic oxidation of ammonium in the oxygen minimum zone off northern Chile, Deep-Sea Research Part II-Topical Studies in Oceanography, 56, 1125-1135, 10.1016/j.dsr2.2008.09.016, 2009.

Gebhardt, S., Walter, S., Nausch, G., and Bange, H. W.: Hydroxylamine (NH_2OH) in the Baltic Sea, Biogeosciences Discussions, 1, 709-724, 2004.

Glessmer, M. S., Eden, C., and Oschlies, A.: Contribution of oxygen minimum zone waters to the coastal upwelling off Mauritania, Progress In Oceanography, 83, 143-150, 10.1016/j.pocean.2009.07.015, 2009.

Goreau, T. J., Kaplan, W. A., Wofsy, S. C., McElroy, M. B., Valois, F. W., and Watson, S. W.: Production of NO_2^- and N_2O by nitrifying bacteria at reduced concentrations of oxygen, Appl. Environ. Microbiol., 40, 526-532, 1980.

Granger, J., Sigman, D. M., Needoba, J. A., and Harrison, P. J.: Coupled nitrogen and oxygen isotope fractionation of nitrate during assimilation by cultures of marine phytoplankton, Limnology and Oceanography, 49, 1763-1773, 10.4319/lo.2004.49.5.1763, 2004.

Granger, J., Sigman, D. M., Prokopenko, M. G., Lehmann, M. F., and Tortell, P. D.: A method for nitrite removal in nitrate N and O isotope analyses, Limnology and Oceanography-Methods, 4, 205-212, 2006.

Granger, J., Sigman, D. M., Lehmann, M. F., and Tortell, P. D.: Nitrogen and oxygen isotope fractionation during dissimilatory nitrate reduction by denitrifying bacteria, Limnology and Oceanography, 53, 2533-2545, 10.4319/lo.2008.53.6.2533, 2008.

Grasshoff, K., Kremling, K., and Ehrhardt, M.: Methods of seawater analysis – third, completely revised and extended version, Seawater Analysis Wiley-VCH, 1999.

Gruber, N., and Sarmiento, J. L.: Global patterns of marine nitrogen fixation and denitrification, Global Biogeochemical Cycles, 11, 235-266, 1997.

Gruber, N.: The marine nitrogen cycle: overview and challenges, in: Nitrogen in the marine environment, 2 ed., edited by: Capone, D. G., Bronk, D. A., Mulholland, M. R., and Carpenter, E. J., Academic Press/Elsevier, 30-79, 2008.

Gruber, N., and Galloway, J. N.: An Earth-system perspective of the global nitrogen cycle, Nature, 451, 293-296, 10.1038/nature06592, 2008.

Guerrero, M. A., and Jones, R. D.: Photoinhibition of marine nitrifying bacteria .1. Wavelength-dependent response, Marine Ecology-Progress Series, 141, 183-192, 1996.

Hagen, E.: Northwest African upwelling scenario, Oceanologica Acta, 24, S113-S127, 2001.

Hallam, S., Mincer, T., Schleper, C., Preston, C., Roberts, K., Richardson, P., and DeLong, E.: Pathways of carbon assimilation and ammonia oxidation suggested by environmental genomic analyses of marine crenarchaeota (vol 4, art. no. e95, 2006), Plos Biology, 4, 2412-2412, e437, DOI: 10.1371/journal.pbio.0040437, 2006.

Hamersley, M. R., Lavik, G., Woebken, D., Rattray, J. E., Lam, P., Hopmans, E. C., Damste, J. S. S., Kruger, S., Graco, M., Gutierrez, D., and Kuypers, M. M. M.: Anaerobic ammonium oxidation in the Peruvian oxygen minimum zone, Limnology and Oceanography, 52, 923-933, 10.4319/lo.2007.52.3.0923, 2007.

Hansell, D. A., Bates, N. R., and Olson, D. B.: Excess nitrate and nitrogen fixation in the North Atlantic Ocean, Marine Chemistry, 84, 243-265, 10.1016/j.marchem.2003.08.004, 2004.

Hastings, M. G., Sigman, D. M., and Lipschultz, F.: Isotopic evidence for source changes of nitrate in rain at Bermuda, Journal of Geophysical Research-Atmospheres, 108, art.# 4790, 4790, DOI: 10.1029/2003jd003789, 2003.

Helly, J. J., and Levin, L. A.: Global distribution of naturally occurring marine hypoxia on continental margins, Deep-Sea Research Part I-Oceanographic Research Papers, 51, 1159-1168, 10.1016/j.dsr.2004.03.009, 2004.

Horrigan, S. G., Carlucci, A. F., and Williams, P. M.: Light inhibition of nitrification in sea-surface films, Journal of Marine Research, 39, 557-565, 1981.

Hughes, M. N., and Nicklin, H. G.: Oxidation of hydroxylamine by molecular oxygen in alkaline solutions, Chemistry & Industry, 2176-&, 1967.

Hughes, M. N., and Nicklin, H. G.: Autoxidation of hydroxylamine in alkaline solutions, Journal of the Chemical Society a -Inorganic Physical Theoretical, 164-&, 10.1039/j19710000164, 1971.

Isaksen, I. S. A., and Stordal, F.: Ozone perturbations by enhanced levels of CFCs, N2O and CH4 - a two-dimensional diabatic circulation study including uncertainty estimates., J. Geophys. Res.-Atmos., 91, 5249-5263, 1986.

Jetten, M. S. M., van Niftik, L., Strous, M., Kartal, B., Keltjens, J. T., Op den Camp, H. J. M. : Biochemistry and molecular biology of anammox bacteria, Critical Reviews in Biochemistry and Molecular Biology, 44, 65-84, 2009.

Kamykowski, D., and Zentara, S. J.: Spatiotemporal and process-oriented views of nitrite in the world oceans as recorded in the historical data set, Deep-Sea Research Part a-Oceanographic Research Papers, 38, 445-464, 10.1016/0198-0149(91)90046-i, 1991.

Kara, A. B., Rochford, P. A., and Hurlburt, H. E.: An optimal definition for ocean mixed layer depth, Journal of Geophysical Research, 105, 16803-16821, 2000.

Karl, D., Michaels, A., Bergman, B., Capone, D., Carpenter, E., Letelier, R., Lipschultz, F., Paerl, H., Sigman, D., and Stal, L.: Dinitrogen fixation in the world's oceans, Biogeochemistry, 57, 47-98, 10.1023/A:1015798105851 2002.

Karstensen, J., Stramma, L., and Visbeck, M.: Oxygen minimum zones in the eastern tropical Atlantic and Pacific oceans, Prog. Oceanogr., 77, 331-350, 10.1016/j.pocean.2007.05.009, 2008.

Kartal, B., Kuypers, M. M. M., Lavik, G., Schalk, J., den Camp, H., Jetten, M. S. M., and Strous, M.: Anammox bacteria disguised as denitrifiers: nitrate reduction to dinitrogen gas via nitrite and ammonium, Environmental Microbiology, 9, 635-642, 10.1111/j.1462-2920.2006.01183.x, 2007.

Kartal, B., Maalcke, W. J., de Almeida, N. M., Cirpus, I., Gloerich, J., Geerts, W., den Camp, H., Harhangi, H. R., Janssen-Megens, E. M., Francoijs, K. J., Stunnenberg, H. G., Keltjens, J. T., Jetten, M. S. M., and Strous, M.: Molecular mechanism of anaerobic ammonium oxidation, Nature, 479, 127-U159, 10.1038/nature10453, 2011.

Khalil, M. A. K., Rasmussen, R. A., and Shearer, M. J.: Atmospheric nitrous oxide: patterns of global change during recent decades and centuries, Chemosphere, 47, 807-821, 2002.

Klein, B., and Tomczak, M.: Identification of diapycnal mixing through optimum multiparameter analysis. 2. Evidence for unidirectional diapycnal mixing in the front between North-Atlantic and South-Atlantic central water., Journal of Geophysical Research-Oceans, 99, 25275-25280, 10.1029/94jc01948, 1994.

Klein, B., and Siedler, G.: Isopycnal and Diapycnal Mixing at the Cape-Verde Frontal Zone, Journal of Physical Oceanography, 25, 1771-1787, 1995.

Knapp, A. N., Sigman, D. M., and Lipschultz, F.: N isotopic composition of dissolved organic nitrogen and nitrate at the Bermuda Atlantic time-series study site, Global Biogeochemical Cycles, 19, GB1018, 10.1029/2004GB002320, 2005.

Knapp, A. N., Hastings, M. G., Sigman, D. M., Lipschultz, F., and Galloway, J. N.: The flux and isotopic composition of reduced and total nitrogen in Bermuda rain, Marine Chemistry, 120, 83-89, 10.1016/j.marchem.2008.08.007, 2010.

Koeve, W., and Kähler, P.: Heterotrophic denitrification vs. autotrophic anammox - quantifying collateral effects on the oceanic carbon cycle, Biogeosciences, 7, 2327-2337, 10.5194/bg-7-2327-2010, 2010.

Kolasa, T., and Wardenck, W.: Quantitative determination of hydroxylamine, Talanta, 21, 845-857, 10.1016/0039-9140(74)80222-5, 1974.

Könneke, M., Bernhard, A. E., de la Torre, J. R., Walker, C. B., Waterbury, J. B., and Stahl, D. A.: Isolation of an autotrophic ammonia-oxidizing marine archaeon, Nature, 437, 543-546, 10.1038/nature03911, 2005.

Kool, D. M., Wrage, N., Zechmeister-Boltenstern, S., Pfeffer, M., Brus, D., Oenema, O., and Van Groenigen, J.-W.: Nitrifier denitrification can be a source of N2O from soil: a revised approach to the dual-isotope labelling method., European Journal of Soil Science, 61, 759–772, 2010.

Korner, H., and Zumft, W. G.: Expression of denitrification enzymes in response to the dissolved oxygen level and respiratory substrate in continuous culture of pseudomonas stutzeri, Appl. Environ. Microbiol., 55, 1670-1676, 1989.

Kroeze, C.: Nitrous oxide and global warming, The Science of The Total Environment, 143, 193-209, 1994.

Kuypers, M. M. M., Lavik, G., Woebken, D., Schmid, M., Fuchs, B. M., Amann, R., Jørgensen, B. B., and Jetten, M. S. M.: Massive nitrogen loss from Benguela upwelling system through anaerobic ammonium oxidation, Proceedings of the National Academy of Sciences, 102, 6478-6483, 2005.

Lam, P., Jensen, M. M., Lavik, G., McGinnis, D. F., Muller, B., Schubert, C. J., Amann, R., Thamdrup, B., and Kuypers, M. M. M.: Linking crenarchaeal and bacterial nitrification to anammox in the Black Sea, Proceedings of the National Academy of Sciences of the United States of America, 104, 7104-7109, 10.1073/pnas.0611081104, 2007.

Lam, P., Lavik, G., Jensen, M. M., van de Vossenberg, J., Schmid, M., Woebken, D., Dimitri, G., Amann, R., Jetten, M. S. M., and Kuypers, M. M. M.: Revising the nitrogen cycle in the Peruvian oxygen minimum zone, Proceedings of the National Academy of Sciences of the United States of America, 106, 4752-4757, 10.1073/pnas.0812444106, 2009.

Law, C. S., and Owens, N. J. P.: Significant flux of atmospheric nitrous oxide from the Northwest Indian Ocean, Nature, 346, 826-828, 10.1038/346826a0, 1990.

Lehmann, M. F., Sigman, D. M., McCorkle, D. C., Granger, J., Hoffmann, S., Cane, G., and Brunelle, B. G.: The distribution of nitrate $^{15}N/^{14}N$ in marine sediments and the impact of benthic nitrogen loss on the isotopic composition of oceanic nitrate, Geochimica et Cosmochimica Acta, 71, 5384-5404, 10.1016/j.gca.2007.07.025, 2007.

Lin, I. I., Wen, L. S., Liu, K. K., Tsai, W. T., and Liu, A. K.: Evidence and quantification of the correlation between radar backscatter and ocean colour supported by simultaneously acquired in situ sea truth, Geophys. Res. Lett., 29, 1464, DOI: 10.1029/2001gl014039, 2002.

Liu, K.-K.: Geochemistry of Inorganic Nitrogen Compounds in Two Marine Environments: The Santa Barbara Basin and the Ocean off Peru, PhD in Geochemistry, University of California, Los Angeles, 1979.

Liss, P. S., and Merlivat, L.: Air-sea exchange rates: introduction and synthesis, in: The role of air-sea exchange in geochemical cycling, edited by: Buat-Ménard, P., Series C: Mathem. & Phys. Sciences, D. Reidel Publishing Company, Dordrecht, 113-127, 1986.

Lomas, M. W., and Lipschultz, F.: Forming the primary nitrite maximum: Nitrifiers or phytoplankton?, Limnology and Oceanography, 51, 2453-2467, 10.4319/lo.2006.51.5.2453, 2006.

Longhurst, A., Sathyendranath, S., Platt, T., and Caverhill, C.: AN ESTIMATE OF GLOBAL PRIMARY PRODUCTION IN THE OCEAN FROM SATELLITE RADIOMETER DATA, Journal of Plankton Research, 17, 1245-1271, 10.1093/plankt/17.6.1245, 1995.

Löscher, C. R., Kock, A., Könneke, M., LaRoche, J., Bange, H. W., and Schmitz, R. A.: Production of oceanic nitrous oxide by ammonia-oxidizing archaea, ms submitted to Biogeosciences, 2011.

Martens-Habbena, W., Berube, P. M., Urakawa, H., de la Torre, J. R., and Stahl, D. A.: Ammonia oxidation kinetics determine niche separation of nitrifying Archaea and Bacteria, Nature, 461, 976-U234, 10.1038/nature08465, 2009.

McIlvin, M. R., and Altabet, M. A.: Chemical Conversion of Nitrate and Nitrite to Nitrous Oxide for Nitrogen and Oxygen Isotopic Analysis in Freshwater and Seawater, Analytical Chemistry, 77, 5589-5595, 10.1021/ac050528s, 2005.

Messie, M., Ledesma, J., Kolber, D. D., Michisaki, R. P., Foley, D. G., and Chavez, F. P.: Potential new production estimates in four eastern boundary upwelling ecosystems, Prog. Oceanogr., 83, 151-158, 10.1016/j.pocean.2009.07.018, 2009.

Meyer, S.: Entwicklung einer Methode zur Messung von Hydrazin in Seewasser, IFM-GEOMAR, Universität Kiel, Kiel, 64 pp., 2009.

Michaels, A. F., Olson, D., Sarmiento, J. L., Ammerman, J. W., Fanning, K., Jahnke, R., Knap, A. H., Lipschultz, F., and Prospero, J. M.: Inputs, losses and transformations of nitrogen and phosphorus in the pelagic North Atlantic Ocean, Biogeochemistry, 35, 181-226, 10.1007/BF02179827, 1996.

Minas, H. J., Codispoti, L. A., and Dugdale, R. C.: Nutrients and primary production in the upwelling region off Northwest Africa, Rapports et Procès-Verbaux des Réunions, Conseil International pour L'Exploration de la Mer, 180, 148-182, 1982.

Mittelstaedt, E.: The upwelling Area off northwest Africa - a description of phenomena related to coastal upwelling, Progr. Oceanogr., 26, 307-3331, 1983.

Molina, V., Belmar, L., and Ulloa, O.: High diversity of ammonia-oxidizing archaea in permanent and seasonal oxygen-deficient waters of the eastern South Pacific, Env. Microbiol., 12, 2450-2465, DOI 10.1111/j.1462-2920.2010.02218.x, 2010.

Monteiro, F. M., and Follows, M.: Nitrogen fixation and preferential remineralization of phosphorus in the North Atlantic: Model insights, Eos Trans., AGU, 87(36), Ocean Science Meeting OS35A– 06, 2006.

Montoya, J. P., Carpenter, E. J., and Capone, D. G.: Nitrogen fixation and nitrogen isotope abundances in zooplankton of the oligotrophic North Atlantic, Limnology and Oceanography, 47, 1617-1628, 2002.

Montzka, S. A., Dlugokencky, E. J., and Butler, J. H.: Non-CO(2) greenhouse gases and climate change, Nature, 476, 43-50, 10.1038/nature10322, 2011.

Morel, A., Claustre, H., and Gentili, B.: The most oligotrophic subtropical zones of the global ocean: similarities and differences in terms of chlorophyll and yellow substance, Biogeosciences, 7, 3139-3151, 10.5194/bg-7-3139-2010, 2010.

Morell, J. M., Capella, J., Mercado, A., Bauza, J., and Corredor, J. E.: Nitrous oxide fluxes in Caribbean and tropical Atlantic waters: evidence for near surface production, Mar. Chem., 74, 131-143, 2001.

Morin, S., Savarino, J., Frey, M. M., Domine, F., Jacobi, H. W., Kaleschke, L., and Martins, J. M. F.: Comprehensive isotopic composition of atmospheric nitrate in the Atlantic Ocean boundary layer from 65 degrees S to 79 degrees N, Journal of Geophysical Research-Atmospheres, 114, D05303, 10.1029/2008JD010696, 2009.

Naqvi, S. W. A., Jayakumar, D. A., Narveka, P. V., Naik, H., Sarma, V. V. S. S., D'Souza, W., Joseph, S., and George, M. D.: Increased marine production of N_2O due to intensifying anoxia on the Indian continental shelf, Nature, 408, 346-349, 2000.

Naqvi, S. W. A., Bange, H. W., Farias, L., Monteiro, P. M. S., Scranton, M. I., and Zhang, J.: Marine hypoxia/anoxia as a source of CH4 and N2O, Biogeosciences, 7, 2159-2190, 10.5194/bg-7-2159-2010, 2010.

Nevison, C. D., Weiss, R. F., and Erickson, D. J.: Global oceanic emissions of nitrous oxide, Journal of Geophysical Research-Oceans, 100, 15809-15820, 1995.

Nevison, C., Butler, J. H., and Elkins, J. W.: Global distribution of N2O and the Delta N2O-AOU yield in the subsurface ocean, Global Biogeochemical Cycles, 17, 1119 10.1029/2003gb002068, 2003.

Nevison, C. D., Lueker, T. J., and Weiss, R. F.: Quantifying the nitrous oxide source from coastal upwelling, Global Biogeochem. Cycles, 18, GB1018, DOI: 10.1029/2003GB002110, 2004.

Nightingale, P., Malin, G., Law, C. S., Watson, A. J., Liss, P. S., Liddicoat, M. I., Boutin, J., and Upstill-Goddard, R. C.: In situ evaluation of air-sea gas exchange parameterizations using novel conservative and volatile tracers, Global Biogeochem. Cycles, 14, 373-387, 2000.

Oakey, N. S.: Determination of the rate of dissipation of turbulent energy from simultaneous temperature and velocity shear microstructure measurements, J. Phys. Oceanogr., 12, 256-271, 1982.

O'Connor, B. M., Fine, R. A., Maillet, K. A., and Olson, D. B.: Formation rates of subtropical underwater in the Pacific Ocean, Deep-Sea Research Part I-Oceanographic Research Papers, 49, 1571-1590, 10.1016/S0967-0637(02)00087-0, 2002.

Osborn, T. R.: Estimates of the local-rate of vertical diffusion from dissipation measurements, J. Phys. Ocean., 10, 83-89, 1980.

Ostrom, N. E., Russ, M. E., Popp, B., Rust, T. M., and Karl, D. M.: Mechanisms of nitrous oxide production in the subtropical North Pacific based on determinations of the isotopic abundances of nitrous oxide and di-oxygen, Chemosphere - Global Change Science, 2, 281-290, 2000.

Otte, S., Schalk, J., Kuenen, J. G., and Jetten, M. S. M.: Hydroxylamine oxidation and subsequent nitrous oxide production by the heterotrophic ammonia oxidizer *Alcaligenes faecalis*, Applied Microbiology Technology, 51, 255-261, 1999.

Oudot, C., Andrie, C., and Montel, Y.: Nitrous oxide production in the tropical Atlantic Ocean, Deep Sea Research Part A. Oceanographic Research Papers, 37, 183-202, 10.1016/0198-0149(90)90123-D, 1990.

Oudot, C., Jean-Baptiste, P., Fourre, E., Mormiche, C., Guevel, M., Ternon, J. F., and Le Corre, P.: Transatlantic equatorial distribution of nitrous oxide and methane, Deep-Sea Research Part I-Oceanographic Research Papers, 49, 1175-1193, 2002.

Paulmier, A., Ruiz-Pino, D., and Garcon, V.: The oxygen minimum zone (OMZ) off Chile as intense source of CO2 and N2O, Continental Shelf Research, 28, 2746-2756, 10.1016/j.csr.2008.09.012, 2008.

Perrott, J. R., Stedman, G., and Uysal, N.: Kinetic and product stucy of reaction between nitrous acid and hydrazine, Journal of the Chemical Society-Dalton Transactions, 2058-2064, 1976.

Popp, B. N., Westley, M. B., Toyoda, S., Miwa, T., Dore, J. E., Yoshida, N., Rust, T. M., Sansone, F. J., Russ, M. E., Ostrom, N. E., and Ostrom, P. H.: Nitrogen and oxygen isotopomeric constraints on the origins and sea-to-air flux of N2O in the oligotrophic subtropical North Pacific gyre, Global Biogeochemical Cycles, 16, 1064 DOI: 10.1029/2001gb001806, 2002.

Prather, M. J.: Time scales in atmospheric chemistry: Coupled perturbations to N2O, NOy, and O-3, Science, 279, 1339-1341, 10.1126/science.279.5355.1339, 1998.

Prinn, R., Cunnold, D., Rasmussen, R., Simmonds, P., Alyea, F., Crawford, A., Fraser, P., and Rosen, R.: Atmospheric emissions and trends of nitrous-oxide deduced from 10 years of ALE-GAUGE data, J. Geophys. Res.-Atmos., 95, 18369-18385, 1990.

Purkhold, U., Pommerening-Roser, A., Juretschko, S., Schmid, M. C., Koops, H. P., and Wagner, M.: Phylogeny of all recognized species of ammonia oxidizers based on comparative 16S rRNA and amoA sequence analysis: Implications for molecular diversity surveys, Applied and Environmental Microbiology, 66, 5368-5382, 2000.

Qu, T., Gao, S., Fukumori, I., Fine, R. A., and Lindstrom, E. J.: Origin and Pathway of Equatorial 13°C Water in the Pacific Identified by a Simulated Passive Tracer and Its Adjoint, Journal of Physical Oceanography, 39, 1836-1853, 10.1175/2009JPO4045.1, 2009.

Raimbault, P., and Garcia, N.: Evidence for efficient regenerated production and dinitrogen fixation in nitrogen-deficient waters of the South Pacific Ocean: impact on new and export production estimates, Biogeosciences, 5, 323-338, 2008.

Rajendran, A., and Venugopalan, V. K.: Hydroxylamine formation in laboratory experiments on marine nitrification, Mar. Chem., 4, 93-98, 1976.

Ravishankara, A. R., Daniel, J. S., and Portmann, R. W.: Nitrous Oxide (N2O): The Dominant Ozone-Depleting Substance Emitted in the 21st Century, Science, 326, 123-125, 10.1126/science.1176985, 2009.

Reichart, G. J., Lourens, L. J., and Zachariasse, W. J.: Temporal variability in the northern Arabian Sea Oxygen Minimum Zone (OMZ) during the last 225,000 years, Paleoceanography, 13, 607-621, 10.1029/98pa02203, 1998.

Rees, A. P., Brown, I. J., Clark, D. R., and Torres, R.: The Lagrangian progression of nitrous oxide within filaments formed in the Mauritanian upwelling, Geophys. Res. Lett., in press, 10.1029/2011GL049322, 2011.

Rotthauwe, J. H., Witzel, K. P., and Liesack, W.: The ammonia monooxygenase structural gene amoA as a functional marker: Molecular fine-scale analysis of natural ammonia-oxidizing populations, Applied and Environmental Microbiology, 63, 4704-4712, 1997.

Ryabenko, E., Altabet, M. A., and Wallace, D. W. R.: Effect of chloride on the chemical conversion of nitrate to nitrous oxide for $\delta^{15}N$ analysis, Limnology and Oceanography: Methods, 7, 545–552, 2009.

Saitou, N., and Nei, M.: On the Maximum-Likelihood Method for Molecular Phylogeny, Japanese Journal of Genetics, 62, 547-548, 1987.

Santoro, A. E., Casciotti, K. L., and Francis, C. A.: Activity, abundance and diversity of nitrifying archaea and bacteria in the central California Current, Environ. Microbiol., 12, 1989-2006, DOI 10.1111/j.1462-2920.2010.02205.x, 2010.

Santoro, A. E., Buchwald, C., McIlvin, M. R., and Casciotti, K. L.: Isotopic Signature of N(2)O Produced by Marine Ammonia-Oxidizing Archaea, Science, 333, 1282-1285, 10.1126/science.1208239, 2011.

Schafstall, J.: Turbulente Vermischungsprozesse und Zirkulation im Auftriebsgebiet vor Nordwestafrika, PhD, RD1 - Physical Oceanography, Christian-Albrechts-Universität, Kiel, 219 pp., 2010.

Schafstall, J., Dengler, M., Brandt, P., and Bange, H.: Tidal-induced mixing and diapycnal nutrient fluxes in the Mauritanian upwelling region, J. Geophys. Res. - Oceans, 115, C10014, DOI: 10.1029/2009jc005940, 2010.

Schemainda, R., Nehring, D., and Schulz, S.: Ozeanologische Untersuchungen zum Produktionspotential der nordwestafrikanischen Wasserauftriebsregion 1970-1973, Akademie der Wissenschaften der Deutschen Demokratischen Republik, Berlin, 1-88, 1975.

Schepanski, K., Tegen, I., and Macke, A.: Saharan dust transport and deposition towards the tropical northern Atlantic, Atmospheric Chemistry and Physics, 9, 1173-1189, 10.5194/acp-9-1173-2009, 2009.

Schleper, C., Jurgens, G., and Jonuscheit, M.: Genomic studies of uncultivated archaea, Nature Reviews Microbiology, 3, 479-488, 10.1038/nrmicro1159, 2005.

Schleper, C.: Ammonia oxidation: different niches for bacteria and archaea?, Isme Journal, 4, 1092-1094, 10.1038/ismej.2010.111, 2010.

Schott, F. A., McCreary, J. P., and Johnson, G. C.: Shallow overturning circulations of the tropical-subtropical oceans in: Earth Climate: The Ocean-Atmosphere Interaction edited by: Wang, C., Xie, S. P., and Carton, J. A., American Geophysical Union, Washington D.C. , 261–304 2004.

Schmidt, R., and Schneider, B.: The effect of surface films on the air-sea gas exchange in the Baltic Sea, Marine Chemistry, 126, 56-62, 2011.

Schweiger, B., Hansen, H. P., and Bange, H. W.: A time series of hydroxylamine (NH2OH) in the southwestern Baltic Sea, Geophysical Research Letters, 34, L24608,Artnr: l24608, 2007.

Shaw, L. J., Nicol, G. W., Smith, Z., Fear, J., Prosser, J. I., and Baggs, E. M.: Nitrosospira spp. can produce nitrous oxide via a nitrifier denitrification pathway, Environmental Microbiology, 8, 214–222, 2006.

Siedler, G., Zangenberg, N., and Onken, R.: SEASONAL-CHANGES IN THE TROPICAL ATLANTIC CIRCULATION - OBSERVATION AND SIMULATION OF THE GUINEA DOME, Journal of Geophysical Research-Oceans, 97, 703-715, 10.1029/91jc02501, 1992.

Signorini, S. R., Murtugudde, R. G., McClain, C. R., Christian, J. R., Picaut, J., and Busalacchi, A. J.: Biological and physical signatures in the tropical and subtropical Atlantic, J. Geophys. Res. - Oceans, 104, 18367-18382, 1999.

Sigman, D. M., Altabet, M. A., Michener, R., McCorkle, D. C., Fry, B., and Holmes, R. M.: Natural abundance-level measurement of the nitrogen isotopic composition of oceanic nitrate: an adaptation of the ammonia diffusion method, Marine Chemistry, 57, 227-242, 10.1016/S0304-4203(97)00009-1, 1997.

Sigman, D. M., Robinson, R., Knapp, A. N., van Geen, A., McCorkle, D. C., Brandes, J. A., and Thunell, R. C.: Distinguishing between water column and sedimentary denitrification in the Santa Barbara Basin using the stable isotopes of nitrate, Geochem. Geophys. Geosyst., 4(5), 1040, 10.1029/2002gc000384, 2003.

Sigman, D. M., DiFiore, P. J., Hain, M. P., Deutsch, C., Wang, Y., Karl, D. M., Knapp, A. N., Lehmann, M. F., and Pantoja, S.: The dual isotopes of deep nitrate as a constraint on the cycle and budget of oceanic fixed nitrogen, Deep-Sea Research Part I-Oceanographic Research Papers, 56, 1419-1439, 10.1016/j.dsr.2009.04.007, 2009.

Spang, A., Hatzenpichler, R., Brochier-Armanet, C., Rattei, T., Tischler, P., Spieck, E., Streit, W., Stahl, D. A., Wagner, M., and Schleper, C.: Distinct gene set in two different lineages of ammonia-oxidizing archaea supports the phylum Thaumarchaeota, Trends in Microbiology, 18, 331-340, 2010.

Spott, O., Russow, R., and Stange, C. F.: Formation of hybrid N2O and hybrid N2 due to codenitrification: First review of a barely considered process of microbially mediated N-nitrosation, Soil Biology and Biochemistry, 43, 1995-2011, 2011.

Stanbury, D. M.: Oxidation of hydrazine in aqueous solution, in: Progress in Inorganic Chemistry, Vol 47, Progress in Inorganic Chemistry, 511-561, 1998.

Steglich, C., Lindell, D., Futschik, M., Rector, T., Steen, R., and Chisholm, S.: Short RNA half-lives in the slow-growing marine cyanobacterium Prochlorococcus., Genome Biol. , 11, 2010.

Stein, L. Y., and Yung, Y. L.: Production, isotopic composition, and atmospheric fate of biologically produced nitrous oxide, Annual Review of Earth and Planetary Sciences, 31, 329-356, 10.1146/annurev.earth.31.110502.080901, 2003.

Stramma, L., Hüttl, S., and Schafstall, J.: Water masses and currents in the upper tropical northeast Atlantic off northwest Africa, Journal of Geophysical Research, 110, C12006, 10.1029/2005jc002939, 2005.

Stramma, L., Brandt, P., Schafstall, J., Schott, F., Fischer, J., and Kortzinger, A.: Oxygen minimum zone in the North Atlantic south and east of the Cape Verde Islands, J. Geophys. Res. - Oceans, 113, C04014, DOI: 10.1029/2007jc004369, 2008a.

Stramma, L., Johnson, G. C., Sprintall, J., and Mohrholz, V.: Expanding oxygen-minimum zones in the tropical oceans, Science, 320, 655-658, 10.1126/science.1153847, 2008b.

Stramma, L., Johnson, G. C., Firing, E., and Schmidtko, S.: Eastern Pacific oxygen minimum zones: Supply paths and multidecadal changes, Journal of Geophysical Research-Oceans, 115, C09011, DOI: 10.1029/2009jc005976, 2010a.

Stramma, L., Schmidtko, S., Levin, L. A., and Johnson, G. C.: Ocean oxygen minima expansions and their biological impacts, Deep-Sea Research Part I-Oceanographic Research Papers, 57, 587-595, 10.1016/j.dsr.2010.01.005, 2010b.

Suntharalingam, P., and Sarmiento, J. L.: Factors governing the oceanic nitrous oxide distribution: Simulations with an ocean general circulation model, Global Biogeochemical Cycles, 14, 429-454, 10.1029/1999gb900032, 2000.

Suntharalingam, P., Sarmiento, J. L., and Toggweiler, J. R.: Global significance of nitrous-oxide production and transport from oceanic low-oxygen zones: A modeling study, Global Biogeochemical Cycles, 14, 1353-1370, 2000.

Sutka, R. L., Ostrom, N. E., Ostrom, P. H., Gandhi, H., and Breznak, J. A.: Nitrogen isotopomer site preference of N2O produced by Nitrosomonas europaea and Methylococcus capsulatus Bath, Rapid Communications in Mass Spectrometry, 17, 738-745, 10.1002/rcm.968, 2003.

Sutka, R. L., Ostrom, N. E., Ostrom, P. H., Breznak, J. A., Gandhi, H., Pitt, A. J., and Li, F.: Distinguishing nitrous oxide production from nitrification and denitrification on the basis of isotopomer abundances, Appl. Environ. Microbiol., 72, 638-644, 10.1128/aem.72.1.638-644.2006, 2006.

Tanaka, T. Y., and Chiba, M.: A numerical study of the contributions of dust source regions to the global dust budget, Global and Planetary Change, 52, 88-104, 10.1016/j.gloplacha.2006.02.002, 2006.

Thamdrup, B., Dalsgaard, T., Jensen, M. M., Ulloa, O., Farias, L., and Escribano, R.: Anaerobic ammonium oxidation in the oxygen-deficient waters off northern Chile, Limnology and Oceanography, 51, 2145-2156, 10.4319/lo.2006.51.5.2145, 2006.

Toggweiler, J. R., Dixon, K., and Broecker, W. S.: The Peru Upwelling and the Ventilation of the South Pacific Thermocline, J. Geophys. Res., 96, 20467-20497, 10.1029/91jc02063, 1991.

Treusch, A. H., Leininger, S., Kletzin, A., Schuster, S. C., Klenk, H. P., and Schleper, C.: Novel genes for nitrite reductase and Amo-related proteins indicate a role of uncultivated mesophilic crenarchaeota in nitrogen cycling, Environmental Microbiology, 7, 1985-1995, 10.1111/j.1462-2920.2005.00906.x, 2005.

Tsai, W. T., and Liu, K. K.: An assessment of the effect of sea surface surfactant on global atmosphere-ocean CO2 flux, Journal of Geophysical Research-Oceans, 108, 3127, DOI: 10.1029/2000jc000740, 2003a.

Upstill-Goddard, R. C.: Air-sea gas exchange in the coastal zone, Estuar. Coast. Shelf Sci., 70, 388-404, 10.1016/j.ecss.2006.05.043, 2006.

Upstill-Goddard, R. C., Barnes, J., and Owens, N. J. P.: Nitrous oxide and methane during the 1994 SW monsoon in the Arabian Sea/northwestern Indian Ocean, Journal of Geophysical Research-Oceans, 104, 30067-30084, 10.1029/1999jc900232, 1999.

van Cleemput, O.: Subsoils: chemo- and biological denitrification, N2O and N-2 emissions, Nutrient Cycling in Agroecosystems, 52, 187-194, 10.1023/a:1009728125678, 1998.

van de Graaf, A. A., de Bruijn, P., Robertson, L. A., Jetten, M. S. M., and Kuenen, J. G.: Metabolic pathway of anaerobic ammonium oxidation on the basis of 15N studies in a fluidized bed reactor, Microbiology, 143, 2415-2421, 10.1099/00221287-143-7-2415, 1997.

Venter, J. C., Remington, K., Heidelberg, J. F., Halpern, A. L., Rusch, D., Eisen, J. A., Wu, D. Y., Paulsen, I., Nelson, K. E., Nelson, W., Fouts, D. E., Levy, S., Knap, A. H., Lomas, M. W., Nealson, K., White, O., Peterson, J., Hoffman, J., Parsons, R., Baden-Tillson, H., Pfannkoch, C., Rogers, Y. H., and Smith, H. O.: Environmental genome shotgun sequencing of the Sargasso Sea, Science, 304, 66-74, 10.1126/science.1093857, 2004.

Von Breymann, M. T., De Angelis, M. A., and Gordon, L. I.: Gas chromatography with electron capture detection for determination of hydroxylamine in seawater, Anal. Chem., 54, 1209-1210, 1982.

Voss, M., Dippner, J. W., and Montoya, J. P.: Nitrogen isotope patterns in the oxygen-deficient waters of the Eastern Tropical North Pacific Ocean, Deep-Sea Research Part I-Oceanographic Research Papers, 48, 1905-1921, 10.1016/S0967-0637(00)00110-2, 2001.

Voss, M., and Montoya, J. P.: NITROGEN CYCLE Oceans apart, Nature, 461, 49-50, 10.1038/461049a, 2009.

Walker, C. B., de la Torre, J. R., Klotz, M. G., Urakawa, H., Pinel, N., Arp, D. J., Brochier-Armanet, C., Chain, P. S. G., Chan, P. P., Gollabgir, A., Hemp, J., Hugler, M., Karr, E. A., Konneke, M., Shin, M., Lawton, T. J., Lowe, T., Martens-Habbena, W., Sayavedra-Soto, L. A., Lang, D., Sievert, S. M., Rosenzweig, A. C., Manning, G., and Stahl, D. A.: Nitrosopumilus maritimus genome reveals unique

mechanisms for nitrification and autotrophy in globally distributed marine crenarchaea, Proceedings of the National Academy of Sciences of the United States of America, 107, 8818-8823, 10.1073/pnas.0913533107, 2010.

Walter, S., Bange, H. W., and Wallace, D. W. R.: Nitrous oxide in the surface layer of the tropical North Atlantic Ocean along a west to east transect, Geophys. Res. Lett., 31, L23s07 Artn l23s07, 2004.

Walter, S., Breitenbach, U., Bange, H. W., Nausch, G., and Wallace, D. W. R.: Distribution of N2O in the Baltic Sea during transition from anoxic to oxic conditions, Biogeosciences, 3, 557-570, 2006a.

Walter, S., Bange, H. W., Breitenbach, U., and Wallace, D. W. R.: Nitrous oxide in the North Atlantic Ocean, Biogeosciences, 3, 607-619, 10.5194/bg-3-607-2006, 2006b.

Wankel, S. D., Kendall, C., Pennington, J. T., Chavez, F. P., and Paytan, A.: Nitrification in the euphotic zone as evidenced by nitrate dual isotopic composition: Observations from Monterey Bay, California, Global Biogeochemical Cycles, 21, GB2009, 10.1029/2006gb002723, 2007.

Wankel, S. D., Chen, Y., Kendall, C., Post, A. F., and Paytan, A.: Sources of aerosol nitrate to the Gulf of Aqaba: Evidence from delta N-15 and delta O-18 of nitrate and trace metal chemistry, Marine Chemistry, 120, 90-99, 10.1016/j.marchem.2009.01.013, 2010.

Wannicke, N., Liskow, I., and Voss, M.: Impact of diazotrophy on N stable isotope signatures of nitrate and particulate organic nitrogen: case studies in the north-eastern tropical Atlantic Ocean, Isot. Environ. Health Stud., 46, 337-354, 10.1080/10256016.2010.505687, 2010.

Wanninkhof, R.: Relationship between wind speed and gas exchange over the ocean, J. Geophys. Res. - Oceans, 97, 7373-7382, 1992.

Wanninkhof, R., Asher, W. E., Ho, D. T., Sweeney, C., and McGillis, W. R.: Advances in Quantifying Air-Sea Gas Exchange and Environmental Forcing, Annu. Rev. Mar. Sci., 1, 213-244, 10.1146/annurev.marine.010908.163742, 2009.

Ward, B. B.: Nitrification in marine systems, in: Nitrogen in the marine environment, edited by: Capone, D. G., Bronk, D. A., Mulholland, M. R., and Carpenter, E. J., Academic Press/Elsevier, 199-262, 2008.

Ward, B. B., Devol, A. H., Rich, J. J., Chang, B. X., Bulow, S. E., Naik, H., Pratihary, A., and Jayakumar, A.: Denitrification as the dominant nitrogen loss process in the Arabian Sea, Nature, 461, 78-U77, 10.1038/nature08276, 2009.

Weiss, R. F.: The solubility of nitrogen, oxygen and argon in water and seawater, Deep-Sea Res., 17, 721-735, 1970.

Weiss, R. F., and Price, B. A.: Nitrous oxide solubility in water and seawater, Mar. Chem., 8, 347-359, 1980.

Wittke, F., Kock, A., and Bange, H. W.: Nitrous oxide emissions from the upwelling area off Mauritania (NW Africa), Geophys. Res. Lett., 37, L12601 10.1029/2010gl042442, 2010.

Wrage, N., Velthof, G. L., van Beusichem, M. L., and Oenema, O.: Role of nitrifier denitrification in the production of nitrous oxide, Soil Biology and Biochemistry, 33, 1723-1732, 2001.

Wuchter, C., Abbas, B., Coolen, M. J. L., Herfort, L., van Bleijswijk, J., Timmers, P., Strous, M., Teira, E., Herndl, G. J., Middelburg, J. J., Schouten, S., and Damste, J. S. S.: Archaeal nitrification in the ocean, Proc. Natl. Acad. Sci. U.S.A 103, 12317-12322, 10.1073/pnas.0600756103, 2006.

Wurl, O., Wurl, E., Miller, L., Johnson, K., and Vagle, S.: Formation and global distribution of sea-surface microlayers, Biogeosciences, 8, 121-135, 10.5194/bg-8-121-2011, 2011.

Yamagishi, H., Westley, M. B., Popp, B. N., Toyoda, S., Yoshida, N., Watanabe, S., Koba, K., and Yamanaka, Y.: Role of nitrification and denitrification on the nitrous oxide cycle in the eastern tropical North Pacific and Gulf of California, Journal of Geophysical Research-Biogeosciences, 112, G02015, DOI: 10.1029/2006jg000227, 2007.

Yool, A., Martin, A. P., Fernandez, C., and Clark, D. R.: The significance of nitrification for oceanic new production, Nature, 447, 999-1002, 10.1038/nature05885, 2007.

Yordy, D. M., and Ruoff, K. L.: Dissimilatory nitrate reduction to ammonia, in: Denitrification, nitrification, and atmospheric nitrous oxide, edited by: Delwiche, C. C., J. Wiley and Sons, New York, 171-190, 1981.

Yoshida, N., Morimoto, H., Hirano, M., Koike, I., Matsuo, S., Wada, E., Saino, T., and Hattori, A.: Nitrification rates and N-15 abundances of N_2O and NO_3^- in the western North Pacific, Nature, 342, 895-897, 10.1038/342895a0, 1989.

Yoshinari, T.: Nitrous oxide in the sea, Mar. Chem., 4, 189-202, 1976.

Danksagung

Allen voran möchte ich Dr. Hermann Bange danken, dafür, dass er mir diese Arbeit ermöglicht hat, für sein Vertrauen in meine Arbeit und seine vielen guten Ideen und Ratschläge, wenn ich wieder einmal an meinen Ergebnissen zu verzweifeln drohte. Ein Gespräch mit Hermann wirkt da Wunder.

Carolin Löscher und Alina Freing möchte ich für viele gute Diskussionen über N_2O danken, die mich immer ein ganzes Stück weitergebracht haben, und für ihre Einblicke in die biologische sowie die „mathematische“ Sichtweise auf dieses Thema. Jens Werbing, Tim Fischer, Marcus Dengler und Peter Brandt möchte ich in diesem Zusammenhang für ihre Erläuterungen der physikalischen Transportprozesse von N_2O im Ozean danken.

Marita Krumbholz, Maya Beyer und Tina Baustian möchte ich für die viele Arbeit danken, die sie mir abgenommen haben – ohne euch wäre ich noch lange nicht fertig geworden. Das gleiche gilt auch für die vielen Hiwis, die mich beim Messen fleißig unterstützt haben.

Ich danke meinen Kollegen in der chemischen Ozeanographie für die gute Zusammenarbeit in einem netten Arbeitsklima. Besonders bedanken möchte ich mich bei den „Mädels“ aus der HPA, für ihre Hilfe bei Matlab-Problemen, Labor-Problemen, Schreibblockaden und anderen Katastrophen und natürlich für jedes anständige Gelächter in unserem Büro.

Nicht zuletzt danke ich meiner Familie und Jakob für ihre Unterstützung, ihr offenes Ohr für langeweilige Themen, und ihr Verständnis, wenn ich wieder einmal viel zu wenig Zeit für sie hatte.

Diese Arbeit wurde vom Bundesministerium für Bildung und Forschung (BMBF, Bonn) im Rahmen des Verbundprojektes „Surface Ocean Processes in the Anthropocene“ (SOPRAN, www.sopran.pangaea.de, FKZ 03F0462A) gefördert. Einige der hier vorgestellten Arbeiten wurden weiterhin im Rahmen des Sonderforschungsbereichs 754 der Deutschen Forschungsgemeinschaft ausgeführt.

Appendix

Data of discrete N_2O measurements from all six cruises are included in the MEMENTO database (see Bange et al. (2009)) for details.

Appendix A. Diapycnal and sea-to-air fluxes of N_2O in the Mauritanian upwelling

Table A1: Discrete sea-to-air and diapycnal fluxes from the Mauritanian upwelling. Missing values are marked as -999.

Cruise	Station	Lat [°N]	Lon [°E]	SST [°C]	SST_{An} [°C]	Bottom depth [m]	Wind speed [m s^{-1}]	Surface N_2O [nmol L^{-1}]	Sea-to-air flux LM86 [nmol m^{-2} s^{-1}]	Sea-to-air flux W92 [nmol m^{-2} s^{-1}]	Sea-to-air flux N2000 [nmol m^{-2} s^{-1}]	Sea-to-air flux TL2003 [nmol m^{-2} s^{-1}]	Diapycnal flux [nmol m^{-2} s^{-1}]
P347	113	18.00	-17.50	19.96	-0.56	2509	7.29	7.8	0.020	0.050	0.042	0.009	0.0020
P347	114	18.00	-17.24	20.12	-0.40	2146	5.50	7.3	0.039	0.067	0.060	0.017	0.0001
P347	115	18.00	-17.00	19.67	-0.85	1716	4.56	10.0	0.048	0.080	0.050	0.021	0.0050
P347	119	18.00	-16.58	19.68	-0.84	457	9.94	7.0	0.009	0.032	0.040	0.004	0.0000
P347	120	18.00	-16.50	18.68	-1.84	189	9.49	12.9	0.035	0.099	0.070	0.016	0.0446
P347	121	18.00	-16.42	18.69	-1.83	104	3.69	11.4	0.034	0.098	0.100	0.016	0.0182
P347	122	18.00	-16.34	18.06	-2.46	75	6.84	14.8	0.040	0.123	0.110	0.018	0.0159
P347	123	18.00	-16.27	17.41	-3.11	33	7.68	20.8	0.155	0.255	0.200	0.068	0.0073
P347	124	18.17	-16.25	17.91	-2.63	33	5.95	14.8	0.106	0.184	0.130	0.048	0.0102
P347	141	18.50	-16.50	17.46	-3.02	92	5.50	17.2	0.041	0.093	0.080	0.019	-999
P347	144	18.50	-16.75	19.41	-1.07	683	3.23	9.4	0.023	0.046	0.060	0.010	-999
P347	146	18.50	-17.00	19.42	-1.06	1615	8.62	9.6	0.000	0.002	0.003	0.000	-999
P347	148	18.54	-17.26	20.07	-0.37	2191	8.18	6.8	0.084	0.145	0.070	0.037	0.0002
P347	150	18.50	-17.50	19.09	-1.39	2399	6.84	8.7	-0.004	-0.007	-0.005	-0.002	0.1060
P347	156	17.52	-17.50	20.71	0.16	2415	8.93	8.3	-0.001	-0.002	-0.002	-0.001	0.0044
P347	160	17.50	-17.00	20.76	0.26	1594	5.43	7.2	-0.010	-0.010	-0.009	-0.003	0.0019
P347	162	17.50	-16.75	18.86	-1.65	878	4.35	13.8	0.030	0.060	0.073	0.013	0.0009
P347	164	17.50	-16.59	18.45	-2.06	186	3.89	15.2	0.008	0.053	0.050	0.004	-999
P347	165	17.50	-16.50	18.58	-1.93	125	5.10	10.3	0.016	0.096	0.090	0.008	0.0422
P347	166	17.50	-16.42	18.39	-2.10	94	5.35	17.0	0.010	0.080	0.070	0.005	0.0073
P347	167	17.50	-16.33	18.41	-2.08	62	5.50	10.6	0.072	0.134	0.130	0.054	0.0428
P348	227	17.60	-24.30	22.67	-999	3599	6.28	6.68	-0.003	-0.005	-0.005	-0.001	0.0003
P348	228	18.00	-23.00	22.26	-999	3489	6.64	7.1	0.004	0.006	0.010	0.001	0.0074
P348	230	18.00	-21.00	21.97	-999	3067	5.59	6.7	0.012	0.019	0.020	0.005	0.0029
P348	232	18.00	-19.00	20.72	-999	3137	6.28	7.1	0.062	0.115	0.090	0.025	0.0014
P348	233	18.00	-18.00	20.35	-0.17	2795	6.64	7.5	0.037	0.060	0.050	0.016	0.0003
P348	234	18.00	-17.50	20.30	-0.22	2513	7.24	8.7	0.022	0.036	0.030	0.009	0.0026

Cruise	Station	Lat [°N]	Lon [°E]	SST [°C]	SST_{An} [°C]	Bottom depth [m]	Wind speed [m s^{-1}]	Surface N_2O [nmol L^{-1}]	Sea-to-air flux LM86 [nmol m^{-2} s^{-1}]	Sea-to-air flux W92 [nmol m^{-2} s^{-1}]	Sea-to-air flux N2000 [nmol m^{-2} s^{-1}]	Sea-to-air flux TL2003 [nmol m^{-2} s^{-1}]	Diapycnal flux [nmol m^{-2} s^{-1}]
P348	235	18.00	-17.00	20.34	-0.18	1721	10.97	8.4	0.038	0.065	0.050	0.016	0.0074
P348	236	18.00	-16.50	17.84	-2.68	191	3.55	12.7	0.168	0.276	0.230	0.073	-999
P348	238	18.50	-17.00	18.83	-1.65	1616	5.05	9.1	0.141	0.244	0.180	0.059	0.0038
P348	240	19.00	-17.79	19.06	-1.32	2459	6.84	8.3	0.044	0.077	0.060	0.019	0.0015
P348	241	19.00	-17.50	18.77	-1.61	2212	5.11	9.6	0.132	0.232	0.180	0.055	0.0005
P348	242	19.00	-17.00	18.13	-2.25	1163	3.23	9.5	0.217	0.379	0.300	0.091	0.0032
P348	243	19.00	-16.55	17.01	-3.37	57	5.88	14.3	0.370	0.610	0.500	0.159	0.0115
ATA3	2	16.17	-16.67	20.23	-0.99	55	7.18	14.3	0.188	0.310	0.260	0.082	0.0047
ATA3	5	16.17	-17.07	21.65	0.32	1258	4.60	10.0	0.104	0.175	0.140	0.044	0.0129
ATA3	8	16.17	-19.00	22.66	-999	3361	8.03	8.0	0.003	0.005	0.004	0.001	0.0002
ATA3	12	17.00	-18.00	21.43	0.42	2831	6.84	7.0	-0.011	-0.018	-0.010	-0.005	0.0045
ATA3	15	17.00	-16.80	20.25	-0.39	584	9.25	11.0	0.032	0.053	0.040	0.014	0.0013
ATA3	16	16.99	-16.65	20.49	-0.08	92	3.40	7.8	0.008	0.013	0.010	0.003	-999
ATA3	18	19.00	-16.48	18.59	-1.79	32	5.95	14.0	0.040	0.072	0.060	0.018	0.0054
ATA3	19	18.99	-16.65	19.11	-1.27	95	7.13	7.5	0.003	0.044	0.040	0.001	0.3220
ATA3	20	19.00	-16.85	19.28	-1.10	488	4.14	11.5	0.003	0.018	0.020	0.001	-999
ATA3	20	19.00	-16.85	19.82	-0.56	445	9.44	8.7	0.003	0.018	0.020	0.001	0.0014
ATA3	21	18.99	-17.42	19.61	-0.77	2129	9.66	10.6	0.074	0.128	0.110	0.033	0.0372
ATA3	23	18.99	-19.01	20.41	-999	3011	5.89	12.1	0.012	0.020	0.020	0.005	0.0044
ATA3	25	19.49	-19.00	20.42	-999	2983	6.33	7.0	-0.001	-0.002	-0.002	-0.001	0.0064
ATA3	26	19.99	-18.00	19.52	-0.81	1848	6.26	9.9	0.019	0.045	0.040	0.009	0.0048
ATA3	27	20.14	-17.69	18.99	-1.40	339	4.14	10.6	0.016	0.057	0.050	0.007	0.0035
ATA3	27	20.14	-17.69	19.07	-1.32	449	5.95	11.7	0.012	0.044	0.040	0.006	-999
ATA3	28	20.17	-17.55	19.11	-1.31	109	5.95	7.8	0.009	0.019	0.020	0.007	0.0009
ATA3	29	18.00	-16.28	18.00	-2.52	41	4.73	13.1	0.075	0.180	0.160	0.034	-999
ATA3	30	17.92	-16.38	18.67	-1.84	100	4.28	15.8	0.134	0.243	0.210	0.060	0.0073
ATA3	31	17.83	-16.56	18.83	-1.63	260	3.55	15.3	0.125	0.216	0.180	0.056	0.0015
ATA3	31	17.83	-16.56	19.10	-1.36	327	4.38	13.8	0.112	0.193	0.170	0.050	0.1270
ATA3	33	18.00	-17.50	20.35	-0.17	2534	4.19	9.6	0.023	0.037	0.030	0.010	0.0024
ATA3	34	18.00	-18.00	20.68	0.16	2788	5.97	9.6	-0.015	-0.027	-0.020	-0.006	0.0029

Appendix B. Data from laboratory experiments in Chapter 6

Table A2: Data from Exp. 2.1.1; background N_2O production from nitrite

Medium	NH_2OH [nmol L^{-1}]	NO_2^- [µmol L^{-1}]	FAS [µmol L^{-1}]	Reaction Time [h]	N_2O [nmol L^{-1}]	N_2O stdev. [nmol L^{-1}]	Remarks
MilliQ	-	0.504	-	0.1	10.8	0.6	
MilliQ	-	0.504	-	6.3	11.4	0.6	
MilliQ	-	0.504	-	14.4	12.7	0.5	
MilliQ	-	0.504	-	27.7	16.4	0.5	samples with different bacgkground N_2O concentrations
MilliQ	-	0.504	-	49.3	12.3	-999	
MilliQ	-	0.504	-	71.7	15.4	0.4	
MilliQ	-	0.504	-	96	13.5	0.1	
MilliQ	-	0.504	-	168	13.9	0.6	
MilliQ	-	0.504	-	336	13.4	0.5	
MiliQ	-	9.54	-	0	11.0	0.9	
MiliQ	-	9.54	-	6	12.3	0.4	
MiliQ	-	9.54	-	15	15.2	1.0	
MiliQ	-	9.54	-	28	21.5	1.1	samples with different bacgkground N_2O concentrations
MiliQ	-	9.54	-	50	19.6	0.6	
MiliQ	-	9.54	-	72	20.6	0.4	
MiliQ	-	9.54	-	96	16.2	0.8	
MiliQ	-	9.54	-	168	18.7	0.8	
MiliQ	-	9.54	-	336	18.5	0.1	
BE water	-	0.504	-	0	12.8	0.4	
BE water	-	0.504	-	6	13.1	0.5	
BE water	-	0.504	-	12	12.4	0.3	
BE water	-	0.504	-	24	14.8	0.2	
BE water	-	0.504	-	48	17.8	0.3	
BE water	-	0.504	-	72	19.0	0.2	
BE water	-	0.504	-	96	18.8	0.2	
BE water	-	0.504	-	168	22.5	1.2	
BE water	-	9.54	-	0	13.2	0.2	
BE water	-	9.54	-	6	15.3	0.8	
BE water	-	9.54	-	12	14.8	0.8	
BE water	-	9.54	-	24	21.2	0.8	
BE water	-	9.54	-	48	29.8	2.2	

Medium	NH_2OH [nmol L^{-1}]	NO_2^- [µmol L^{-1}]	FAS [µmol L^{-1}]	Reaction Time [h]	N_2O [nmol L^{-1}]	N_2O stdev. [nmol L^{-1}]	Remarks
BE water	-	9.54	-	72	49.8	3.2	
BE water	-	9.54	-	96	53.6	3.0	
BE water	-	9.54	-	168	74.4	0.4	

Table A3: Data from Exp. 2.1.2; background N_2O production from nitrite, purged

Medium	NH_2OH [nmol L^{-1}]	NO_2^- [µmol L^{-1}]	FAS [µmol L^{-1}]	Reaction Time [h]	N_2O [nmol L^{-1}]	N_2O stdev. [nmol L^{-1}]	Remarks
BE water	-	0	-	0	0.6	0.4	purged with N_2
BE water	-	0	-	12	1.0	0.4	purged with N_2
BE water	-	0	-	24	4.0	1.0	purged with N_2
BE water	-	0	-	48	1.5	0.3	purged with N_2
BE water	-	0	-	168	3.0	0.2	purged with N_2
BE water	-	0.504	-	0	1.3	0.4	purged with N_2
BE water	-	0.504	-	12	4.3	0.3	purged with N_2
BE water	-	0.504	-	24	10.3	0.5	purged with N_2
BE water	-	0.504	-	48	11.6	0.6	purged with N_2
BE water	-	0.504	-	168	19.0	0.9	purged with N_2
BE water	-	9.54	-	0	1.7	0.6	purged with N_2
BE water	-	9.54	-	12	10.8	0.5	purged with N_2
BE water	-	9.54	-	24	19.5	1.3	purged with N_2
BE water	-	9.54	-	48	37.0	1.5	purged with N_2
BE water	-	9.54	-	168	75.5	2.6	purged with N_2

Table A4: Data from Exp. 2.1.3; background N_2O production from nitrite, abortion by NaOH addition

Medium	HA Conc. [nmol L^{-1}]	Nitrite [µmol L^{-1}]	FAS [µmol L^{-1}]	T (NaOH addition)	T (N_2O analysis)	N2O [nmol L^{-1}]	N2O Stdev. [nmol L^{-1}]	Remarks
MilliQ	-	1	-	-	23	17.4	2.6	acidified with HCl
MilliQ	-	1	-	-	47	20.0	0.2	acidified with HCl
MilliQ	-	1	-	-	73	20.1	0.3	acidified with HCl
MilliQ	-	1	-	-	247	24.9	0.9	acidified with HCl
MilliQ	-	10	-	-	23	29.8	0.3	acidified with HCl
MilliQ	-	10	-	-	47	29.6	0.7	acidified with HCl
MilliQ	-	10	-	-	73	33.3	1.1	acidified with HCl
MilliQ	-	10	-	-	247	49.0	5.0	acidified with HCl
MilliQ	-	10	-	-	23	36.52	2.1	acidified with HCl
MilliQ	-	10	-	-	47	55.01	13.2	acidified with HCl
MilliQ	-	10	-	-	72	118.91	70.2	acidified with HCl
MilliQ	-	10	-	-	246	115.21	10.0	acidified with HCl
MilliQ	-	10	-	23	191	26.9	0.72	acidified with HCl
MilliQ	-	10	-	47	215	29.7	1.39	acidified with HCl
MilliQ	-	10	-	73	241	38.2	2.32	acidified with HCl
MilliQ	-	10	-	247	415	40.3	0.97	acidified with HCl

Table A5: Data from Exp. 2.2.1; N_2O production from the reaction between hydroxylamine and nitrite

Medium	NH_2OH [nmol L^{-1}]	NO_2^- [µmol L^{-1}]	FAS [µmol L^{-1}]	Reaction Time [h]	N_2O [nmol L^{-1}]	N_2O stdev. [nmol L^{-1}]	Remarks
MilliQ	0	3.54	-	24	15.4	1.2	
MilliQ	0	2.14	-	24	14.7	0.6	
MilliQ	0	1.07	-	24	14.6	1.0	
MilliQ	0	0.54	-	24	14.6	0.6	
MilliQ	0	0.23	-	24	13.2	0.3	
MilliQ	49.4	3.54	-	24	63.4	3.1	
MilliQ	49.4	2.14	-	24	60.5	2.6	
MilliQ	49.4	1.07	-	24	64.3	4.7	
MilliQ	49.4	0.54	-	24	61.8	4.7	
MilliQ	49.4	0.23	-	24	60.9	2.7	

Table A6: Data from Exp. 2.2.2; N_2O production from the reaction between hydroxylamine and nitrite, BE water

Medium	NH_2OH [nmol L^{-1}]	NO_2^- [µmol L^{-1}]	FAS [µmol L^{-1}]	Reaction Time [h]	N_2O [nmol L^{-1}]	N_2O stdev. [nmol L^{-1}]	Remarks
BE water	0	0	-	72	10.4	0.4	
BE water	14.2	0	-	72	10.7	0.3	
BE water	70.8	0	-	72	11.1	0.8	
BE water	0	0.151	-	72	10.8	0.3	
BE water	14.2	0.151	-	72	15.4	1.9	
BE water	70.8	0.151	-	72	20.5	0.8	
BE water	0	0.739	-	72	17.3	0.6	
BE water	14.2	0.739	-	72	17.8	2.2	
BE water	70.8	0.739	-	72	25.9	1.4	

Table A7: Data from Exp. 2.2.3; reaction of hydroxylamine with FAS in presence of nitrite

Medium	NH_2OH [nmol L^{-1}]	NO_2^- [µmol L^{-1}]	FAS [µmol L^{-1}]	Reaction Time [h]	N_2O [nmol L^{-1}]	N_2O Stdev. [nmol L^{-1}]	Remarks
MilliQ	0	2.695	120	23	22.2	1.2	Background production aborted by NaOH addition
MilliQ	14.5	2.695	120	23	27.8	0.5	Background production aborted by NaOH addition
MilliQ	28.9	2.695	120	23	35.6	0.7	Background production aborted by NaOH addition
MilliQ	57.8	2.695	120	23	42.4	0.6	Background production aborted by NaOH addition
MilliQ	0	0.539	120	23	16.6	0.6	Background production aborted by NaOH addition
MilliQ	14.5	0.539	120	23	21.8	0.2	Background production aborted by NaOH addition
MilliQ	28.9	0.539	120	23	23.4	1.3	Background production aborted by NaOH addition
MilliQ	57.8	0.539	120	23	28.4	1.9	Background production aborted by NaOH addition
MilliQ	0	0	120	23	11.4	1.0	Background production aborted by NaOH addition
MilliQ	14.5	0	120	23	13.4	0.6	Background production aborted by NaOH addition
MilliQ	28.9	0	120	23	18.5	0.7	Background production aborted by NaOH addition
MilliQ	57.8	0	120	23	23.7	0.2	Background production aborted by NaOH addition

Table A8: Data from Exp. 2.3.1; nitrite removal by ascorbic acid

Medium	NH_2OH [nmol L^{-1}]	NO_2^- addition [µmol L^{-1}]	Ascorbic acid [µmol L^{-1}]	FAS [µmol L^{-1}]	Reaction time [h]	NO_2^- measured [µmol L^{-1}]	Remarks
MilliQ	-	6.41	10000	-	0	0	continuously purged with N_2
MilliQ	-	6.41	10000	-	4	0	continuously purged with N_2
MilliQ	-	6.41	10000	-	8	0	continuously purged with N_2
MilliQ	-	6.41	10000	-	12	0	continuously purged with N_2

Table A9: Data from Exp. 2.3.2; FAS conversion of hydroxylamine in presence of ascorbic acid

Medium	NH_2OH [nmol L^{-1}]	Ascorbic acid [µmol L^{-1}]	Time of FAS addition [h]	Time of N_2O analysis [h]	N_2O [nmol L^{-1}]	N_2O Stdev. [nmol L^{-1}]	Remarks
MilliQ	39.5	10000	0	18	7.2	0.9	purged with N_2
MilliQ	78.8	10000	0	18	8.2	0.9	purged with N_2
MilliQ	158	10000	0	18	8.7	1.3	purged with N_2
MilliQ	39.5	10000	4	12	8.4	0.3	purged with N_2
MilliQ	78.8	10000	4	12	8.6	0.9	purged with N_2
MilliQ	158	10000	4	12	7.7	0.4	purged with N_2
MilliQ	39.5	-	4	14	17.4	0.5	purged with N_2
MilliQ	78.8	-	4	14	27.4	1.0	purged with N_2
MilliQ	158	-	4	14	49.4	0.3	purged with N_2

Table A10: Data from Exp. 2.3.3; FAS conversion in presence of nitrite in samples with and without sulfanilamide addition

Medium	NH_2OH [nmol L^{-1}]	NO_2^- [µmol L^{-1}]	FAS [µmol L^{-1}]	Sulfanilamide [µmol L^{-1}]	N_2O [µmol L^{-1}]	N_2O stdev. [nmol L^{-1}]	Remarks
MilliQ	0	0.873	120	100	2.4	0.2	purged with N_2
MilliQ	18.6	0.873	120	100	7.1	0.6	purged with N_2
MilliQ	37.0	0.873	120	100	16.0	0.5	purged with N_2
MilliQ	0	0.873	120	-	2.4	0.3	purged with N_2
MilliQ	18.6	0.873	120	-	6.9	0.1	purged with N_2
MilliQ	37.0	0.873	120	-	16.0	0.4	purged with N_2
MilliQ	0	4.37	120	100	3.6	0.6	purged with N_2
MilliQ	18.6	4.37	120	100	9.9	2.7	purged with N_2
MilliQ	37.0	4.37	120	100	14.2	0.4	purged with N_2
MilliQ	0	4.37	120	-	5.8	0.7	purged with N_2
MilliQ	18.6	4.37	120	-	12.7	0.5	purged with N_2
MilliQ	37.0	4.37	120	-	16.7	0.5	purged with N_2
filtered Seawater	0	0.873	120	100	2.7	0.6	purged with N_2
filtered Seawater	18.6	0.873	120	100	5.1	0.2	purged with N_2
filtered Seawater	37.0	0.873	120	100	12.4	0.7	purged with N_2
filtered Seawater	77.2	0.873	120	100	28.1	0.6	purged with N_2
filtered Seawater	0	0.873	120	-	5.9	0.3	purged with N_2
filtered Seawater	18.6	0.873	120	-	10.6	0.4	purged with N_2
filtered Seawater	37.0	0.873	120	-	20.0	0.3	purged with N_2
filtered Seawater	77.2	0.873	120	-	36.8	1.1	purged with N_2
filtered Seawater	0	4.37	120	100	2.4	0.3	purged with N_2
filtered Seawater	18.6	4.37	120	100	5.7	0.7	purged with N_2
filtered Seawater	37.0	4.37	120	100	13.9	0.1	purged with N_2
filtered	77.2	4.37	120	100	29.2	0.6	purged with N_2

Medium	NH_2OH [nmol L^{-1}]	NO_2^- [µmol L^{-1}]	FAS [µmol L^{-1}]	Sulfanilamide [µmol L^{-1}]	N_2O [µmol L^{-1}]	N_2O stdev. [nmol L^{-1}]	Remarks
Seawater							
filtered Seawater	0	4.37	120	-	34.1	2.5	purged with N_2
filtered Seawater	18.6	4.37	120	-	40.9	2.1	purged with N_2
filtered Seawater	37.0	4.37	120	-	59.9	3.9	purged with N_2
filtered Seawater	77.2	4.37	120	-	83.3	1.1	purged with N_2

Appendix C. Data from field measurements of hydroxylamine

Table A11: standard additions from Boknis Eck Time Series Measurements

Date	Sampling depth [m]	NH_2OH Standard addition [nmol L^{-1}]	N_2O (NH_2OH Std-add) [nmol L^{-1}]	N_2O stdev. [nmol L^{-1}]
2011-02-18	15	6.79	19.3	0.7
2011-02-18	15	13.58	20.4	0.9
2011-02-18	15	27.14	26.7	3.2
2011-02-18	15	54.22	33.4	0.4
2011-03-08	15	6.53	19.4	1.0
2011-03-08	15	13.06	20.3	0.7
2011-03-08	15	26.11	23.0	0.5
2011-03-08	15	52.16	32.0	0.5
2011-04-19	15	6.7	16.7	1.8
2011-04-19	15	13.4	18.8	1.0
2011-04-19	15	26.78	24.2	1.7
2011-04-19	15	53.5	33.3	0.4
2011-06-21	15	6.65	16.0	-999
2011-06-21	15	13.30	20.5	-999
2011-06-21	15	26.59	31.1	-999
2011-06-21	15	53.13	35.9	-999
2011-08-01	15	9.35	12.3	0.7
2011-08-01	15	18.68	16.7	0.2
2011-08-01	15	33.35	20.9	0.3
2011-08-01	15	66.61	33.1	1.0
2011-09-21	15	9.1	15.1	0.7
2011-09-21	15	18.1	16.1	2.5
2011-09-21	15	36.3	23.0	0.9
2011-09-21	15	72.5	34.4	1.9

Table A12: depth profiles from the Boknis Eck Time Series Station

Date	Sampling depth [m]	N_2O BG [nmol L^{-1}]	N_2O (NH_2OH) [nmol L^{-1}]	Recovery factor	NH_2OH [nmol L^{-1}]	NH_2OH uncertainty [nmol L^{-1}]
2011-02-18	1	17.4	18.3	0.64	1.4	1.5
2011-02-18	5	17.9	20.0	0.64	3.3	4.6

Date	Sampling depth [m]	N_2O BG [nmol L^{-1}]	N_2O (NH_2OH) [nmol L^{-1}]	Recovery factor	NH_2OH [nmol L^{-1}]	NH_2OH uncertainty [nmol L^{-1}]
2011-02-18	10	18.5	18.9	0.64	0.6	1.3
2011-02-18	15	12.6	19.1	0.64	10.3	3.0
2011-02-18	20	13.2	18.5	0.64	8.3	4.1
2011-02-18	25	14.1	20.1	0.64	9.4	4.1
2011-03-08	1	15.2	21.2	0.58	10.3	2.5
2011-03-08	5	16.9	19.2	0.58	4.0	0.7
2011-03-08	10	12.5	19.7	0.58	12.4	2.7
2011-03-08	15	13.8	19.3	0.58	9.5	2.2
2011-03-08	20	18.4	18.7	0.58	0.6	3.5
2011-03-08	25	-999	19.1	0.58	-999	-999
2011-04-19	1	16.3	16.3	0.74	2.1	1.1
2011-04-19	5	14.2	14.2	0.74	4.9	1.4
2011-04-19	10	13.3	13.3	0.74	3.2	2.1
2011-04-19	15	13.8	13.8	0.74	1.0	2.1
2011-04-19	20	11.2	11.2	0.74	3.6	2.8
2011-04-19	25	11.6	11.6	0.74	0.2	2.1
2011-06-21	1	9.1	10.7	0.42	3.9	0.5
2011-06-21	5	9.4	12.1	0.42	6.3	3.4
2011-06-21	10	9.9	14.0	0.42	9.9	1.1
2011-06-21	15	11.5	15.1	0.42	8.5	2.1
2011-06-21	20	13.9	17.9	0.42	9.7	2.4
2011-06-21	25	15.3	20.6	0.42	12.7	3.6
2011-08-01	1	8.5	9.5	0.60	1.7	3.8
2011-08-01	5	8.6	11.7	0.60	5.2	1.2
2011-08-01	10	9.3	11.7	0.60	4.0	3.8
2011-08-01	15	9.7	11.8	0.60	3.6	2.3
2011-08-01	20	13.9	14.2	0.60	0.5	1.9
2011-08-01	25	13.9	14.8	0.60	1.5	1.7
2011-09-21	1	10.0	1.8	0.66	3.4	1.5
2011-09-21	5	10.0	2.3	0.66	3.4	0.5
2011-09-21	10	9.6	3.1	0.66	3.6	0.6
2011-09-21	15	9.8	3.4	0.66	4.7	0.7
2011-09-21	20	8.8	2.4	0.66	3.5	0.9
2011-09-21	25	7.6	3.4	0.66	4.9	0.8

Table A13: standard additions from MSM 18-2

Station	Sampling depth [m]	NH_2OH Standard addition [nmol L^{-1}]	N_2O (NH_2OH Std-add) [nmol L^{-1}]	N_2O stdev. [nmol L^{-1}]
38	200	15.11	29.98	0.31
38	200	30.19	35.62	0.69
38	200	60.23	48.2	0.39
38	200	119.89	75.38	0.31
51	198	15.11	32.81	0.4
51	198	30.19	37.33	0.54
51	198	60.23	51.37	0.71
51	198	119.89	75.68	0.94
56	199	15.11	27.43	0.77
56	199	30.19	34.45	1.28
56	199	60.23	45.94	1.49
56	199	119.89	70.27	2.08
66	200	15.11	28.37	0.86
66	200	30.19	33.37	0.92
66	200	60.23	44.44	2.03
66	200	119.89	69.08	1.02

Table A14: depth profiles from MSM 18-2

Station	Lat [°N]	Lon [°E]	Depth	N_2O BG [nmol L^{-1}]	N_2O (NH_2OH) [nmol L^{-1}]	Recovery factor	NH_2OH [nmol L^{-1}]	NH_2OH uncertainty [nmol L^{-1}]
38	-5	-23	200	26.91	25.12	0.84	-2.11	0.87
38	-5	-23	97	19.49	21.32	0.84	2.16	1.13
38	-5	-23	75	12.41	12.52	0.84	0.12	1.13
38	-5	-23	68	9.13	9.46	0.84	0.38	0.17
38	-5	-23	59	7.5	8.33	0.84	0.98	0.38
38	-5	-23	30	5.61	6.33	0.84	0.85	0.28
38	-5	-23	9	6.37	6.66	0.84	0.35	1.52
51	-1	-23	198	26.24	28.06	0.80	2.25	1.36
51	-1	-23	97	14.01	14.69	0.80	0.84	0.85
51	-1	-23	80	11.96	12.82	0.80	1.06	0.33
51	-1	-23	70	10.21	10.49	0.80	0.34	0.19
51	-1	-23	59	9.24	9.64	0.80	0.49	0.42
51	-1	-23	49	7.63	8.35	0.80	0.88	0.26
51	-1	-23	28	6.22	7.35	0.80	1.39	0.38
51	-1	-23	11	6.4	7.26	0.80	1.06	0.25
56	0	-23	199	23.39	24.91	0.78	1.95	2.07
56	0	-23	100	13.95	16.41	0.78	3.16	0.29
56	0	-23	78	12.87	13.24	0.78	0.47	0.58
56	0	-23	60	10.31	11.37	0.78	1.36	0.53
56	0	-23	49	8.92	10.81	0.78	2.42	1.9
56	0	-23	45	9.74	10.65	0.78	1.18	1.46
56	0	-23	39	8.47	9.52	0.78	1.35	1.2
56	0	-23	29	6.22	7.83	0.78	2.07	1.39
56	0	-23	9	6.11	6.99	0.78	1.14	0.61
66	4	-23	200	23.84	23.9	0.76	0.07	1.54
66	4	-23	98	22.95	22.7	0.76	-0.33	2.55
66	4	-23	80	16.74	16.74	0.76	-0.01	0.92
66	4	-23	60	5.88	8.08	0.76	2.89	1.08
66	4	-23	49	5.55	6.45	0.76	1.17	0.96
66	4	-23	39	5.35	6.35	0.76	1.32	0.39
66	4	-23	29	5.51	6.07	0.76	0.74	0.33
66	4	-23	10	5.53	7.22	0.76	2.22	0.8